

2017

H_∞ ROBUST CONTROLLER FOR WIND TURBINE POWER BOOSTING

Group members:

Ali Debes

(adebes15@student.aau.dk)

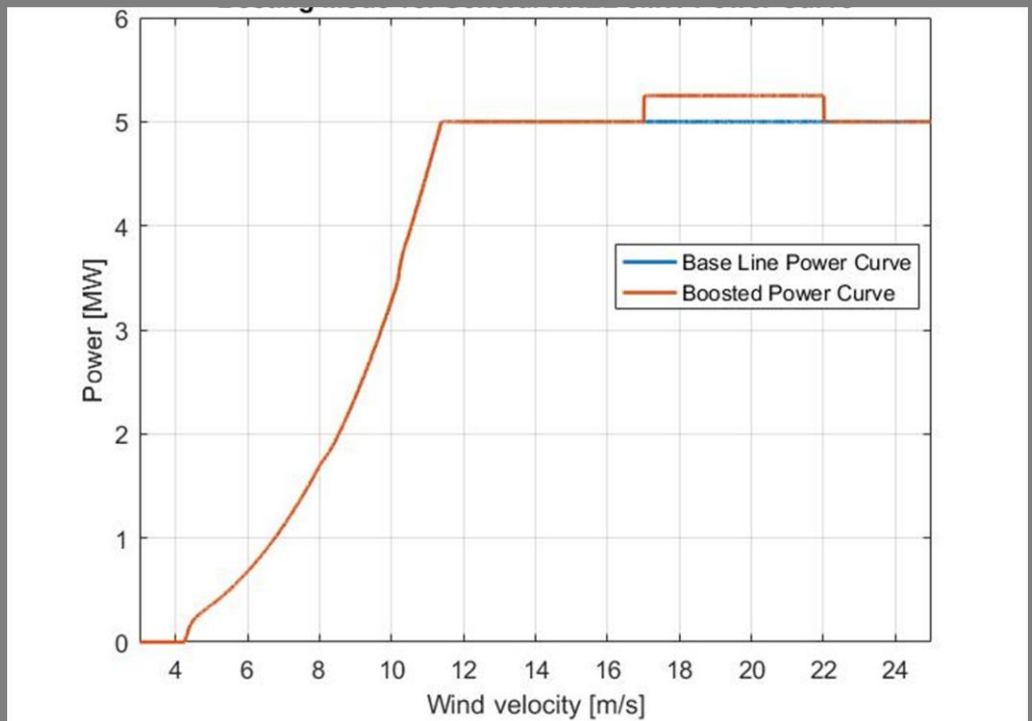
Dorin Bordeasu

(dborde15@student.aau.dk)

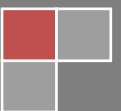
Supervisor

Assoc. Prof. Mohsen Soltani

(sms@et.aau.dk)



AALBORG UNIVERSITY
DENMARK



Title Sheet

Title: H-infinity robust controller for wind turbine power boosting

Authors: Ali Debes (adebes15@student.aau.dk)
Dorin Bordeasu (dborde15@student.aau.dk)

AAU Supervisor: Assoc. Prof. Mohsen Soltani (sms@et.aau.dk)

Date: 8.05.2017

University: Aalborg University Esbjerg

Department: Energy Department

Master Programme: Sustainable Energy, Specialization in Offshore Energy Systems



AALBORG UNIVERSITY
DENMARK

Abstract

A power boosting controller is a controller which increases the generator torque in order to increase the wind turbine's nominal output power by up to 5%. This increase in power production can lead to an increase in the wind turbine's AEP (annual energy production) by up to 2%.

The current master thesis, starts with the development of a 5 MW NREL wind turbine nonlinear mathematical model which is linearized twice, once for being used in the design of the H_∞ standard robust controller, and once for being used in the design of the H_∞ power booster robust controller. Next, the parametric uncertainties are added to the LTI (linear time invariant)/ss (state space) model and then reconstructed for the control design purposes. Two H_∞ optimal controllers are obtained for operating the wind turbine in two modes: standard and the power boosting mode. The logic for the boosting mode was built to switch between the controllers when certain wind speeds are reached. A pre-analysis for determining the stability, performance and robustness was executed on the open loops and gain loops bode diagrams and pole-zero maps.

The response, robustness and performance of the H_∞ robust controllers with and without the power booster are compared with the gain scheduled PI controller (base line). It is discovered that the pitch angle of the baseline controller varies more than the other controllers and there is not a significant difference in pitch angle between power booster and standard H-infinity controllers. On the other hand, the generator speed and torque of the base line controller oscillates less than the other controllers. The insignificant difference between boost and standard H-infinite controllers is kept just for the generator speed, while for the generator torque the difference becomes more clearly. This fact can be explained by the significant difference between linearization and operation points associated with the generator torque. From the analysis, it can be also seen that the generator speeds of the two H-infinity robust controllers is decreasing in higher speeds whereas the generator torque increases dramatically.

By analyzing the output power response of the different controllers, the H-infinity robust controller with power booster, boosts without any difficulties the power from 5 MW to 5.25 MW when the defined conditions (the wind speed lays between 15 and 22 m/s) are meet.

The visual analysis of the tower and blade moments is also confirmed by the fatigue analysis with the DELs (damage equivalent loads) calculated based on the standard deviation of the bending moments. Finally, it can be concluded, that by adding a power booster to h-infinity controller increases the tower fatigue loads just 1.2% and the blades fatigue loads just 1.07%.

Key words: H-infinity controller, robust controller, wind turbine, power booster, uncertainty model, Wind turbine model, damage equivalent loads, state space, LTI.

Standard pages: 88 pages and 111 349 number of characters including spaces.

Acknowledgements:

First and foremost, we would like to express our greatest gratitude to our supervisor Assoc. Prof. Mohsen Soltani for his unconditional assistance, guidance and supervision from beginning until the end of the master thesis.

Special thanks to Ph.D Yunlong Wang for kind help and valuable assistance in debugging the model..

Last but not least, we would like to expand our deepest gratitude to our parents, colleagues and friends, who have directly and indirectly supported and gave us valuable suggestions during the project development.

Table of Contents

1.	Introduction	13
1.1.	Background	13
1.2.	Problem Formulation	14
1.3.	Objectives and scopes.....	14
1.4.	Delimitations.....	15
1.5.	Organization of the thesis.....	16
2.	Wind turbine modelling.....	17
2.1.	Wind turbine description.....	17
2.2.	Nonlinear model	19
2.2.1.	Aerodynamics	19
2.2.2.	Drive train	20
2.2.3.	Generator.....	21
2.2.4.	Tower	22
2.2.5.	Blade	22
2.2.6.	Pitch actuator.....	22
2.3.	Linearized model.....	23
2.3.1.	Tip speed ratio linearization	23
2.3.2.	Power coefficient linearization	24
2.3.3.	Rotor torque linearization.....	27
2.3.4.	Rotor torque reference linearization	29
2.3.5.	Gross output power linearization	30
2.3.6.	Summary of the linearized model.....	32
2.3.7.	State-space model	33
2.3.8.	Linearized model vs. nonlinear model.....	38
2.4.	Linearized model with uncertainties	39
2.4.1.	Defining uncertainties.....	39
2.4.2.	Summary of the linearized model with uncertainties	42
2.4.3.	State-space linearized model with uncertainties.....	46
2.4.4.	Linearized model with uncertainties vs. Linearized model vs. Nonlinear model	54
3.	Robust controller for wind turbine	56
3.1.	Uncertainty model for robust controller	56
3.2.	H-inf Robust Controller	57



3.3.	Control Plan & Implementation	59
3.4.	Results	63
4.	Power boosting mode	65
5.	Robust controller for wind turbine power booster	67
5.1.	Operating and linearization points for wind turbine power booster controller	67
5.1.1.	Tip speed ratio linearization for power booster	67
5.1.2.	Power coefficient linearization for power booster	68
5.1.3.	Rotor torque linearization for power booster	69
5.1.4.	Rotor torque reference linearization for power booster	70
5.1.5.	Gross output power linearization for power booster	71
5.1.6.	Summary of the power booster linearized model	72
5.1.7.	State-space for power booster linearized model	72
5.1.8.	Linearized power booster model vs. nonlinear power booster model	73
5.2.	Uncertainty model for wind turbine power booster robust controller	74
5.3.	Power booster logic	78
5.4.	Results	81
6.	Fatigue Analysis	83
7.	Further Developments and discussions	84
8.	Conclusion	85

Table of Figures

Figure 1. Horizontal-axis wind turbine	17
Figure 2. Rotor nacelle assembly components	18
Diagram. 1. Mechanical equivalent for drive train	20
Diagram. 2. Block diagram of the linearized model.....	32
Diagram. 3. Bode diagram of the open loop: pitch angle to generator angular velocity relation	34
Diagram. 4. Pole-zero map of the open loop: pitch angle to generator angular velocity relation.....	35
Diagram. 5. Step response of the open loop: pitch angle to generator angular velocity relation	35
Diagram. 6. Bode diagram of the open loop: pitch angle to output power relation.....	36
Diagram. 7. Pole-zero map of the open loop: pitch angle to output power relation.....	37
Diagram. 8. Step response of the open loop: pitch angle to output power relation	37
Diagram. 9. Block diagram of the rotor inertia with uncertainty	42
Diagram. 10. Block diagram of the main shaft spring constant with uncertainty	42
Diagram. 11. Block diagram of the main shaft viscous friction with uncertainty.....	43
Diagram. 12. Block diagram of the generator inertia with uncertainty.....	43
Diagram. 13. Block diagram of the Mrot's vrot coefficient with uncertainty.....	43
Diagram. 14. Block diagram of the Mrot's Ω coefficient with uncertainty.....	44
Diagram. 15. Block diagram of the Mrot's β coefficient with uncertainty	44
Diagram. 16. Block diagram of the linearized model with uncertainties	46
Diagram. 17. Bode diagram of the open loop with uncertainties: pitch angle to generator angular velocity relation	49
Diagram. 18. Pole-zero map of the open loop with uncertainties: pitch angle to generator angular velocity relation	49
Diagram. 19. Step response of the open loop with uncertainties: pitch angle to generator angular velocity relation	50
Diagram. 20. Bode diagram of the open loop with uncertainties: pitch angle to output power relation .	51
Diagram. 21. Pole-zero map of the open loop with uncertainties: pitch angle to output power relation	51
Diagram. 22. Step response of the open loop with uncertainties: pitch angle to output power relation .	52
Diagram. 23. Input/output block diagram of the linearized model with uncertainties	53
Diagram. 24. LFT representation of the linearized model with uncertainties.....	53
Diagram. 25. Simplified LFT representation of the linearized model with uncertainties.....	53
Diagram. 26. Simplified LFT representation of the linearized model with uncertainties for robust controller.....	57
Diagram. 27. LFT representation of the linearized model with uncertainties with H infinity controller ...	59
Diagram. 28. Bode diagram of the loop gain with uncertainties.....	60
Diagram. 29. Pole-zero map of the loop gain with uncertainties: pitch angle to output power relation ..	61
Diagram. 30. Step Response of the Loop gain with uncertainties.....	62
Diagram. 31. Bode diagram of the power booster Open- loop.....	75
Diagram. 32. Pole-zero map of the power booster open loop with uncertainties: pitch angle to output power relation	76
Diagram. 33. Step Response of the power booster open loop with uncertainties	77
Diagram. 34. Logic to switch from standard h-infinity controller to h-infinity power booster controller .	78



Diagram. 35. Bode diagram of the power booster controller loop gain 79

Diagram. 36. Pole zero map of the power booster controller loop gain 80

Diagram. 37. Step Response of the power booster loop gain with uncertainties 81

Graph 1. Tip speed ratio nonlinear vs. linearized equation..... 24

Graph 2. Graphical representation of the CP table 24

Graph 3. Reduced graphical representation of the CP table 25

Graph 4. CP look up table vs. linearized equation 26

Graph 5. Rotor torque nonlinear vs. linearized equation 28

Graph 6. Rotor torque reference nonlinear vs. linearized equation 30

Graph 7. Gross output power nonlinear vs. linearized equation 31

Graph 8. Generator angular velocity response of the nonlinear vs. linearized model..... 38

Graph 9. Output power response of the nonlinear vs. linearized model 38

Graph 10. Generator angular velocity response of the nonlinear vs. linearized model with uncertainties
..... 54

Graph 11. Output power response of the nonlinear vs. linearized model with uncertainties..... 55

Graph 12. Singular values for h-infinity controller 58

Graph 13. Wind speed(m/s)..... 63

Graph 14. H-infinity results, pitch angle, generator speed and generator torque..... 63

Graph 15. Simulation results power output, tower and blade moments 64

Graph 16. 5 MW NREL wind turbine generator speed, pitch angle, electrical power..... 65

Graph 18. 5 MW NREL boosted wind turbine generator speed, pitch angle, electrical power 66

Graph 20. Tip speed ratio nonlinear vs. linearized power booster equation 68

Graph 21. CP look up table vs. linearized power booster equation 69

Graph 22. Rotor torque nonlinear vs. linearized power booster equation 70

Graph 23. Rotor torque reference nonlinear vs. linearized power booster equation 71

Graph 24. Gross output power nonlinear vs. linearized power booster equation..... 72

Graph 25. Generator angular velocity response of the nonlinear vs. linearized power booster models .. 73

Graph 26. Output power response of the nonlinear vs. linearized power booster models..... 73

Graph 27. Generator angular velocity response of the nonlinear power booster model vs. linearized
power booster model with uncertainties 74

Graph 28. Output power response of the nonlinear power booster model vs. linearized power booster
model with uncertainties..... 75

Graph 30. Wind speed(m/s)..... 81

Graph 31. H-infinity with booster results, pitch angle, generator speed and generator torque 82

Graph 32. H-infinity with booster results, power output, tower and blade moments 82

Graph 33. Wind speed(m/s)..... 85

Graph 34. Base line, H-infinity robust controller with and without booster results, pitch angle, generator
speed and generator torque 85

Graph 35. Base line, H-infinity robust controller with and without booster results, power output, tower
and blade moments 86

Table of Tables

Table 1. NREL 5 MW wind turbine's characteristics [13] 18

Acronyms, symbols and abbreviations

Short form	Full form
WT	Wind turbine
HAWT	horizontal axis wind turbine
RNA	Rotor-nacelle-assembly
LHP	Left half plane
LFT	Linear fraction transformation
SISO	Single input - single output
MIMO	Multiple input - multiple output
MISO	Multiple input - single output
SIMO	Single input - multiple output
CP	Power coefficient
PI	Proportional Integrative
DEL	Damage equivalent loads
FEM	Finite element method
LTI	Linear time invariant
SS	State-space
RHP	Right half plane
NCON	Number of outputs of the controller
NMEAS	Number of measurements provided to the controller

Variables

Variable	Variable name	Unit
P_{rot}	Rotor power	[kW]
v_{rot}	Average wind speed over the rotor	[m/s]
Ω	Rotor angular velocity	[rad/s]
ρ	Air density	[kg/m ³]
R	Rotor radius	[m]
C_p	Power coefficient	[-]
λ	Tip speed ratio	[-]
β	Pitch angle of the blades	[deg]
F_{rot}	Rotor thrust force	[N]
C_T	Thrust coefficient	[-]
M_{rot}	Rotor torque	[N·m]
I_{rot}	Moment of inertia of the rotor	[kg·m ²]
I_{gen}	Moment of inertia of the generator	[kg·m ²]
K_{shaft}	Torsion spring constant of the drive train	[N·m/rad]
B_{shaft}	Viscous friction constant of the drive train	[N·m·s]
N	Gearbox gear ratio	[-]
Φ	Drive train shaft torsion angle	[rad]
P_{rated}	Rated Power of the wind turbine	[kW]
P_{ref}	Power reference signal	[kW]
ω	Generator angular velocity	[rad/s]



M_{gen}	Generator torque	[N·m]
$M_{gen.ref}$	Generator torque reference	[N·m]
τ_{gen}	Generator time constant	[s]
z	Position of the tower deflection	[m]
K_{tow}	Tower spring constant	[N/m]
B_{tow}	Tower damping constant	[N·s/m]
\dot{z}	Velocity of the nacelle	[m/s]
\ddot{z}	Acceleration of the nacelle	[m/s ²]
m_{tow}	Tower mass	[kg]
M_{blade}	Blade moment	[N·m]
K_{beta}	Constant of the proportional regulator	[-]
$\dot{\beta}$	Rate of the pitch angle	[deg/s]
τ_B	Time constant of the pitch actuator	[s]
P_{out}	Output Power	[kw]
e_λ	Error in tip speed ratio linearization	[-]
e_{CP}	Error in power coefficient linearization	[-]
$e_{\omega_{gen}}$	Error in generator angular velocity	[rad/s]
$e_{P_{out}}$	Error in output power	[kW]
Δ	Uncertainty matrix	[-]
$TF1_{\beta\omega_{gen}}$	Linearized model transfer function from pitch angle β to generator angular velocity ω	[1/s]
$TF1_{\beta P_{out}}$	Linearized model transfer function from pitch angle β to output power P_{out}	[1/s]
$TF2_{\beta\omega_{gen}}$	Linearized model with uncertainties transfer function from pitch angle β to generator angular velocity ω	[1/s]
$error_{\Delta 1}$	Error in generator angular velocity with uncertainty matrix $\Delta = \text{diag}(0)$	[rad/s]
$error_{\Delta 2}$	Error in generator angular velocity with uncertainty matrix $\Delta = \text{diag}(-1)$	[rad/s]
$error_{\Delta 3}$	Error in generator angular velocity with uncertainty matrix $\Delta = \text{diag}(1)$	[rad/s]
$error_{\Delta 4}$	Error in output power with uncertainty matrix $\Delta = \text{diag}(0)$	[kW]
$error_{\Delta 5}$	Error in output power with uncertainty matrix $\Delta = \text{diag}(-1)$	[kW]
$error_{\Delta 6}$	Error in output power with uncertainty matrix $\Delta = \text{diag}(1)$	[kW]
\bar{I}_{rot}	Nominal rotor moment of inertia	[kg·m ²]
K_{shaft}	Nominal main shaft spring constant	[N·m/rad]
\bar{B}_{shaft}	Nominal main shaft viscous friction	[N·m·s]
\bar{I}_{gen}	Nominal generator moment of inertia	[kg·m ²]
G_{eff}	Nominal generator efficiency	[%]
\bar{N}	Nominal gear ratio	[-]
\bar{a}	Nominal mrot's v_{rot} coefficient	[-]
\bar{b}	Nominal mrot's Ω coefficient	[-]
\bar{c}	Nominal mrot's β coefficient	[-]
\bar{a}_1	Nominal $M_{gen.ref}$'s ω coefficient	[-]
\bar{a}_2	Nominal $P_{outgross}$'s M_{gen} coefficient	[-]
\bar{b}_2	Nominal $P_{outgross}$'s ω coefficient	[-]
P_{Irot}	uncertainty in the rotor moment of inertia	[%]
P_{Kshaft}	uncertainty in the main shaft spring constant	[%]
P_{Bshaft}	uncertainty in the main shaft viscous friction	[%]



P_N	uncertainty in gear ratio	[%]
$P_{I_{gen}}$	uncertainty in the generator moment of inertia	[%]
P_{Geff}	uncertainty in the generator efficiency	[%]
P_a	uncertainty in Mrot's vrot coefficient	[%]
P_b	uncertainty in Mrot's Ω coefficient	[%]
P_c	uncertainty in Mrot's β coefficient	[%]
δ_{Irot}	perturbation in the rotor moment of inertia	[-]
δ_{Kshaft}	perturbation in the main shaft spring constant	[-]
δ_{Bshaft}	perturbation in the main shaft viscous friction	[-]
δ_N	perturbation in gear ratio	[-]
δ_{Igen}	perturbation in the generator moment of inertia	[-]
δ_{Geff}	perturbation in the generator efficiency	[-]
δ_a	perturbation in Mrot's vrot coefficient	[-]
δ_b	perturbation in Mrot's Ω coefficient	[-]
δ_c	perturbation in Mrot's β coefficient	[-]
$e_{\lambda.PB}$	Error in tip speed ratio linearization for power booster model	[-]
$e_{CP.PB}$	Error in power coefficient linearization for power booster model	[-]
$e_{Mrot.PB}$	Error in rotor torque linearization for power booster model	[-]
$e_{\omega_{gen.PB}}$	Error in generator angular velocity linearization for power booster model	[-]
$e_{Pout.PB}$	Error in output power linearization for power booster model	[-]
$error_{\Delta 7}$	Error in power booster's generator angular velocity with uncertainty matrix $\Delta = \text{diag}(0)$	[rad/s]
$error_{\Delta 8}$	Error in power booster's generator angular velocity with uncertainty matrix $\Delta = \text{diag}(-1)$	[rad/s]
$error_{\Delta 9}$	Error in power booster's generator angular velocity with uncertainty matrix $\Delta = \text{diag}(1)$	[rad/s]
$error_{\Delta 10}$	Error in power booster's output power with uncertainty matrix $\Delta = \text{diag}(0)$	[kW]
$error_{\Delta 11}$	Error in power booster's output power with uncertainty matrix $\Delta = \text{diag}(-1)$	[kW]
$error_{\Delta 12}$	Error in power booster's output power with uncertainty matrix $\Delta = \text{diag}(1)$	[kW]
\bar{a}_{PB}	Nominal power booster's mrot's vrot coefficient	[-]
\bar{b}_{PB}	Nominal power booster's mrot's Ω coefficient	[-]
\bar{c}_{PB}	Nominal power booster's mrot's β coefficient	[-]
\bar{a}_{1PB}	Nominal power booster's M_{genref} 's ω coefficient	[-]
\bar{a}_{2PB}	Nominal power booster's $P_{outgross}$'s M_{gen} coefficient	[-]
\bar{b}_{2PB}	Nominal power booster's $P_{outgross}$'s ω coefficient	[-]
m_{t0}	zeroth spectral tower bending moment of quantity used	[-]
Γ	gamma function	[-]
m_t	is the inverse slope of the tower steel S-N-curve	[-]
$DEL_{tow.BL}$	Tower Damage equivalent loads using the base line controller	[kNm]
$DEL_{tow.Hinf}$	Tower Damage equivalent loads using the h-infinity controller	[kNm]
$DEL_{tow.Hinf.PB}$	Tower Damage equivalent loads using the h-infinity controller with power booster	[kNm]

1. Introduction

This chapter gives a brief introduction to worldwide, European Union and Danish wind energy and the trends in its costs reduction.

1.1. Background

Worldwide, at the end of 2015 there were 860 GW of installed wind power capacity from which 15% (126 GW) was installed just in this year [1]. While in the European Union, there were 142 GW of wind power installations (131 GW onshore and 11 GW offshore), with 9% (13 GW) installed just in 2015 [1], [2]. Focusing on Denmark, at the end of the same specified year, there were 5.1 GW of wind power installations, with 4% (217 MW) installed just this year [2].

Taking into account that Renewable energy sources produced the most electrical energy worldwide (23.7%) [1] and within the European Union (28.8%) in 2015 [2], with wind accounting 5.6% worldwide and 9.6% within the European Union [3]. While In Denmark, the renewable energy covered 56% of electricity production with wind accounting 42%, breaking the world record for wind power generation in 2015 [4]. Taking into account the European Union 2020 (2030) energy strategy which aims to reduce its greenhouse gas emissions by at least 20% (40%), increase the share of renewable energy to at least 20% (27%) of consumption, achieve energy savings of 20% (27%) or more until 2020 (2030) [5], plus focusing on Danish energy strategy which aims to increase the share of wind energy to at least 50% (60%) of consumption by 2020 (2025)[4], further cost reduction into wind energy must be achieved.

In the last 15 years, the cost reduction in the wind energy consisted mainly in upscaling the wind turbines by increasing enormously the rotor diameters and hub heights [6]. However, this naturally creates the wind share and tower shadow exacerbates the difference of wind speed distribution in the rotor rotation plane, which causes the fluctuations of aerodynamic load and ripples the aerodynamic torque and output power [6], [7]. The aerodynamic load fluctuation is the main reason of rotor unbalance load and fatigue damage [7], therefore, technology breakthroughs are prerequisites for reducing and balancing the wind turbine components loads and fatigue damage, as well as further upscaling in a cost-efficient way [8], [9].

An effective way in suppressing the fluctuations, alleviating and balancing the wind turbine loads is by separately tiny adjusting the pitch angle of each blade on the basis of collective pitch control in order to modify the angle-of-attack, lift coefficient and corresponding lift force generated by the blade, resulting in reducing the fluctuations of the blade bending moment [10], aerodynamic load, torque and output power [7] and determine how the wind turbine captures the wind power [7]. By doing so, either the wind turbine lifetime, either the wind turbine annual energy production (AEP) can be slightly increased [11], [8].

1.2. Problem Formulation

As mentioned above, for achieving European Union's and Danish wind energy goals, this wind energy has to become economically competitive to the conventional power production without taking into consideration any environmental costs. Although in the past years, a significant progress was made in making wind energy more cost effective by increasing the wind turbine size, further cost reduction must be achieved. As we can see in other developments[11], one way to achieve this is by increasing the wind farm revenue and improve cash flow considerably through the increase in AEP of the wind turbines with the help of a power boosting controller[12].

1.3. Objectives and scopes

The goal of the current master thesis is to develop a new controller for the wind turbine power boost mode that increases the power production of a wind turbine by increasing the wind turbine's nominal power output by up to 5% [12]. This can be achieved through the increase in generator torque when wind speed is within certain limits. In other words, depending on wind distribution, the new power boosting controller will increase the wind turbine nominal power output by up to 5%, which can lead to an increase in AEP by up to 2%.

This master thesis explains in detail the development, validation and simulation with MATLAB and Simulink software, of a h-infinity robust controller which boosts the wind turbine power by slightly pitching the blades and increasing the generator torque of the wind turbine rotor while minimizing load impact [12]. For achieving this goal, the following tasks had to be accomplished:

- Develop a nonlinear mathematical model of a 5 MW NREL wind turbine;
- Linearize the mathematical model;
- Define and develop a linearized mathematical model with uncertainties;
- Validate the wind turbine models;
- Develop a h-infinity robust controller for normal operation of the wind turbine and compare it with the base controller, a gain scheduled PI (Proportional Integrative) controller;
- Develop a h-infinity robust controller for power boosting mode of the wind turbine and compare it with the base controller;
- Simulate the response of the h-infinity robust controller wind turbine with and without the power boosting mode and compare it with the base controller.

1.4. Delimitations

This master thesis contains a rather simple wind turbine model with two degrees of freedom and takes into consideration just the following aspects:

- The wind is evenly distributed through the rotor;
- The rotor is homogenous, no imperfections in the rotor symmetry;
- The same deflections with the same accelerations and velocities occurs at the same time for all the three blades;
- The power coefficient and thrust coefficient are obtained from a look up table in the nonlinear model, and from linearized fitted curve to the look up table in the linearized model;
- The blades are directly connected to the pitch actuator ignoring the bearing and other components;
- The blades are pitched in the same time with the same pitching angle;
- The drive train is modeled based on the rotational moments of inertia of rotor and generator shafts connected to a gearbox with torsion and viscous friction;
- The generator is modeled as a first-order equation between the requested and the actual generator torque;
- The tower is modeled as a spring-damper system which approximates the tower deflection, velocity and acceleration;
- The blades bending moments are equally of all the three blades and they are approximated based on the thrust force (evenly distributed to all three blades) acting on the rotor;
- The model is linearized with the help of Taylor series expansion;
- The uncertainties for the linearized model are defined based on the common sense without any pre-analysis on data collected from a real wind turbine;
- Simple approach to tower and blades fatigue loads;

All the aspects of the wind turbine which were not mentioned above are neglected (for example the ambient temperature, component temperature and grid voltage etc.).

The highest increase in the wind turbine nominal power output (which is by up to 5%) or the highest increase in AEP (which is by up to 2%) is guaranteed to be achieved in an offshore site, but is not guaranteed to be achieved in an onshore site, due to the reason that in an offshore site the reference wind velocity is higher while the wind turbulences are lower [12].

Finally, note that this robust controller for boosting the wind turbine power was just simulated, in MATLAB and Simulink, on a NREL 5MW wind turbine model, but was not test on any real wind turbine.

1.5. Organization of the thesis

The thesis is divided in 9 chapters. A summary of each chapter is briefly present hereafter.

Chapter one gives a general introduction to the worldwide current situation in wind energy. Here are also presented the problem formulation, delimitations, objectives and scopes of the current thesis.

Chapter two starts with a short description of the 5 MW NREL wind turbine followed by the development of a nonlinear mathematical model of the wind turbine. Next part of this chapter focuses on the linearization and its comparison with the nonlinear model. The last section of this chapter contains the definition of the uncertainties which were used for developing the linearized mathematical model with uncertainties and its comparisons with the linear and nonlinear models.

In the third chapter, are presented the uncertainty modelling, design and implementation of the h-infinity robust controller for the standard operation of the wind turbine.

In chapter four, the wind turbine is defined as a control object including the discussion regarding the optimal equilibrium points and defining the operating modes of the wind turbine with and without the power boosting mode.

Chapter five presents the uncertainty modelling, design and implementation of the h-infinity robust controller of the wind turbine including the power booster mode and the comparison with the uncertainty modelling, design and implementation of the h-infinity robust controller for the standard operation of the wind turbine.

In chapter six, is evaluated the performance of the robust controller with and without the power booster regarding the blades and tower increase in fatigue loads.

Chapter seven presents the further developments which can be implemented in the upcoming future but were not covered in this thesis due to time limitation. Also in this chapter, are included the discussions and authors reflections on the project itself.

Finally, chapter eight, provides the conclusion of the thesis.

2. Wind turbine modelling

This chapter starts with a short description of the 5 MW NREL wind turbine followed by the nonlinear mathematical model of the wind turbine based on the model presented in [13] together with the linearization points where the nonlinear model has been linearized. Next section of the chapter consists in a summary of the linear model and its comparison with the nonlinear model. The last section of this chapter contains the definition of the uncertainties which were used for developing the linear mathematical model with uncertainties and its comparisons with the linear and nonlinear model.

Note that in the wind turbine model all notations and symbols were kept the same as in [13].

2.1. Wind turbine description

Firstly, the main components of a horizontal axis wind turbine (HAWT) will be introduced. The HAWT is basically a rotor-nacelle-assembly (RNA) mounted on a tower.

A HAWT consists of several components, see figure. 1. The most important components are shortly described below [14]:

- The nacelle houses the main shaft, generator, gearbox, mechanical brakes, hydraulic cooling devices, transformer, anemometers, frame of the nacelle, yaw driving device, power converter and electrical control, protection and disconnection devices. At the intersection between nacelle and tower, a yawing system can be found, which has the main role to turn the RNA against the wind. figure. 2 shows the different components which are located in the nacelle.
- The rotor consists of the hub and the blades. The blades are connected through blade supports to the hub, which transmits the rotational energy to the gearbox via the main shaft. The blade support contains also bearings in order to allow the blades to rotate around their own axis. The blade angle is called pitch angle and it is controlled by pitch angle actuators. The wind acting on the rotor will exert a torque, M_{rot} , which is transferred to the generator via the drive train. The drive train consists of two shafts, one low-speed shaft which connects

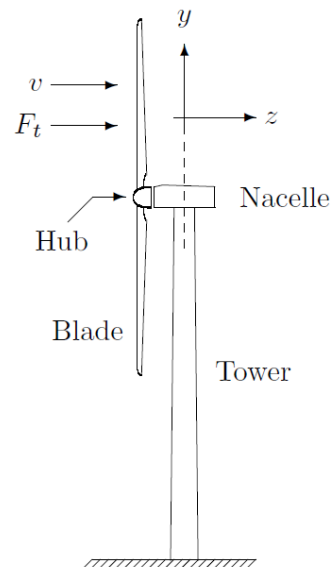


Figure 1. Horizontal-axis wind turbine [14]

the hub to the gearbox, and a high-speed shaft which connects the gearbox to the generator [14].

Beside acting on the rotor, the wind acts also on the tower and exerts a thrust force, F_{rot} , which causes a deflection z of the tower structure.

Due to this reason, the real wind speed v_{rot} acting on the rotor plane is equal with the incoming wind speed v less the nacelle velocity \dot{z} resulted from the tower deflection [14]:

$$v_{rot} = v - \dot{z}$$

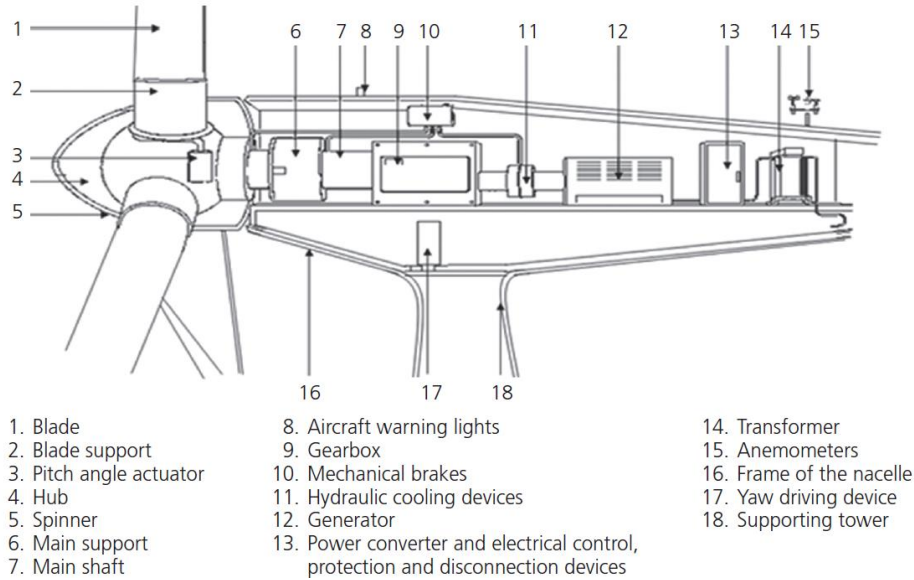


Figure 2. Rotor nacelle assembly components [15]

- The tower supports to the RNA. The tower is a standard steel tubular structure made out of several sections. The tower helps the turbine to capture winds at heights far above the terrain or water’s surface, where the wind resource is generally more energetic and less turbulent [15].

The wind turbine considered in this master thesis is a 5 MW NREL offshore wind turbine with the main properties presented in the following table [13]:

Rated power	5MW
Configuration	Upwind, 3 Blades
Control	Variable speed, collective pitch
Wind	
Cut-in	3 m/s
Rated	11.4 m/s
Cut-out	25 m/s
Rotor	
Cut-in	6.9 rpm
Rated	12.1 rpm
Diameter	126 rpm
Hub	
Diameter	3 m
Height	90 m

Table 1. NREL 5 MW wind turbine's characteristics [13]

2.2. Nonlinear model

In the current subchapter is presented the nonlinear mathematical model of 5 MW NREL wind turbine.

2.2.1. Aerodynamics

When wind passes the wind turbine rotor plane, some of the kinetic energy in the wind is transferred to the rotor. The power P_{rot} obtained by the rotor is given by the following equation [14]:

$$P_{rot} = \frac{1}{2} \cdot v_{rot}^3 \cdot \rho \cdot \pi \cdot R^2 \cdot C_P(\lambda, \beta) \quad \text{Eq. 1 [14]}$$

where

P_{rot} is the rotor power;

v_{rot} is the average wind speed over the rotor;

Ω is the rotor angular velocity;

$\rho=1.2$ [kg/m³] is the air density;

$R=63$ [m] is the rotor radius;

C_P is the power coefficient;

λ is the tip speed ratio;

and

β is the pitch angle.

The power coefficient C_P is a look-up table derived from the geometry of the blades with inputs tip speed ratio ($\lambda = \frac{R \cdot \Omega}{v_{rot}}$) and pitch angle β . C_P has a maximum limit of 0.59, known as Betz limit. Betz limit represents the maximum energy, approximative 59 %, which can be extracted by a turbine from the total wind energy in ideal conditions [14].

$$F_{rot} = \frac{1}{2} \cdot v_{rot}^2 \cdot \rho \cdot \pi \cdot R^2 \cdot C_T(\lambda, \beta) \quad \text{Eq. 2 [14]}$$

where

F_{rot} is the rotor thrust force;

v_{rot} is the average wind speed over the rotor;

Ω is the rotor angular velocity;

ρ is the air density;

R is the rotor radius;

C_T is the thrust coefficient;

λ is the tip speed ratio;

and

β is the pitch angle.

Similar to the power coefficient C_P , the thrust coefficient C_T is a look-up table derived from the geometry of the blades with tip speed ratio λ and pitch angle β as the inputs.

The rotor torque M_{rot} results from the ratio between the rotor power P_{rot} and the rotor angular speed Ω [14]:

$$M_{rot} = \frac{P_{rot}}{\Omega} \quad \text{Eq. 3 [14]}$$

Finally substituting the rotor power P_{rot} in eq.3, results:

$$M_{rot} = \frac{1}{2} \cdot v_{rot}^3 \cdot \rho \cdot \pi \cdot R^2 \cdot C_{p,l} \cdot \Omega^{-1} \quad \text{Eq. 4}$$

where

M_{rot} is the rotor torque;

v_{rot} is the average wind speed over the rotor;

Ω is the rotor angular velocity;

ρ is the air density;

R is the rotor radius;

C_p is the power coefficient;

λ is the tip speed ratio;

and

β is the pitch angle.

2.2.2. Drive train

The modelled drive train is the same as the one in [13], where the structural model is presented in the following figure:

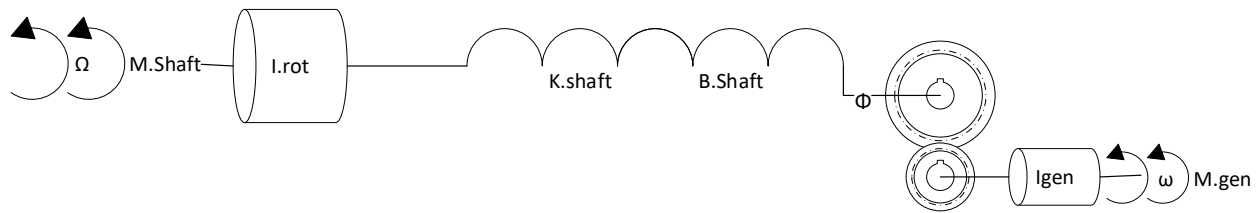


Diagram. 1. Mechanical equivalent for drive train

As you can see depicted in the figure above, the drive train is model based on the moments of inertia of rotating shafts, I_{rot} representing the combined moments of inertia of the rotor and low-speed shaft and I_{gen} representing the combined moments of inertia of the gearbox, generator and high-speed shaft. The two rotating shafts are connected through a gearbox with torsion spring constant K_{shaft} , viscous friction B_{shaft} , and gear ratio N . Φ represents the shaft torsion angle.

$$\dot{\Omega} = \frac{1}{I_{rot}} \cdot (M_{rot} - \Phi \cdot K_{shaft} - \dot{\Phi} \cdot B_{shaft}) \quad \text{Eq. 5 [13]}$$

$$\dot{\omega} = \frac{1}{I_{gen}} \cdot \left(-M_{gen} + \frac{1}{N} \cdot (\Phi \cdot K_{shaft} - \dot{\Phi} \cdot B_{shaft}) \right) \quad \text{Eq. 6 [13]}$$

$$\dot{\Phi} = \Omega - \frac{1}{N} \cdot \omega \quad \text{Eq. 7 [13]}$$

With the following constants:

$$I_{rot} = 3.544e+7 \quad [\text{kg}\cdot\text{m}^2]$$

$$I_{gen} = 534.116 \quad [\text{kg}\cdot\text{m}^2]$$

$$K_{shaft} = 8.676e+8 \quad [\text{N}\cdot\text{m}/\text{rad}]$$

$$B_{shaft} = 6.215e+6 \quad [\text{N}\cdot\text{m}\cdot\text{s}]$$

$$N = 97 \quad [-]$$

In the above system, the inputs are the rotor torque M_{rot} and generator torque M_{gen} . The outputs are rotor Ω and generator ω angular speeds.

The drive train state space representation is based on the differential system of equations (eq. 5-6), and can be described as:

$$\begin{pmatrix} \dot{\Omega} \\ \dot{\omega} \\ \dot{\Phi} \end{pmatrix} = \begin{pmatrix} -\frac{B_{shaft}}{I_{rot}} & \frac{B_{shaft}}{N \cdot I_{rot}} & \frac{K_{shaft}}{I_{rot}} \\ \frac{B_{shaft}}{N \cdot I_{gen}} & \frac{B_{shaft}}{N^2 \cdot I_{gen}} & \frac{K_{shaft}}{N \cdot I_{rot}} \\ 1 & -\frac{1}{N} & 0 \end{pmatrix} \cdot \begin{pmatrix} \Omega \\ \omega \\ \Phi \end{pmatrix} + \begin{pmatrix} \frac{M_{rot}}{I_{rot}} \\ -\frac{M_{gen}}{I_{gen}} \\ 0 \end{pmatrix} \quad \text{Eq. 8}$$

2.2.3. Generator

The generator is considered as a device that generates the electrical power P_{rated} according to the power reference signal P_{ref} . The generated power is controlled by adapting the rotor current, which in turn, governs the torque exerted by the generator to the high-speed shaft. It is also considered an ideal generator without any losses, meaning that the electrical power equals the product between the generator speed and the generator torque:

$$P_{rated} = \omega \cdot M_{gen} \quad \text{Eq. 9}$$

Due to the reason that in practice, the generators cannot change the torque instantaneously [14], the generator will be modeled as a first-order equation between the requested and the actual generator torque:

$$\dot{M}_{gen} = \frac{1}{\tau_{gen}} \cdot (M_{gen.ref} - M_{gen}) \quad \text{Eq. 10 [13]}$$

In the above equation, the requested generator torque can be substituted with $M_{gen.ref} = \frac{P_{ref}}{\omega}$ Eq. 11.

Finally, the 1st order MIMO (multiple input - multiple output) system is obtained:

$$\dot{M}_{gen} = \frac{1}{\tau_{gen}} \cdot \left(\frac{P_{ref}}{\omega} - M_{gen} \right) \quad \text{Eq. 12}$$

With power reference P_{ref} and time constant τ_{gen} as inputs and with M_{gen} and P_{rated} as outputs:

Notice, that instead of a torque reference as in [10], a power reference is used.

The generator model presented above does not include a time delay because pure time delays cannot be described by finite dimensional, continuous-time models. This happens due to the reason that when considering discrete-time models for contemporary, discrete-time controller design, the inclusion of time delays in the model does not pose any problems, as time delays are already implemented as delay states in a linear discrete-time model [14]. As this master thesis concentrates on developing a new controller for operating a wind turbine in boosting mode while taking into consideration just the turbines components fatigue damages, the mathematical results needed for this analysis are all based on continuous-time descriptions.

2.2.4. Tower

The wind creates a thrust force acting on the rotor which deflects the tubular steel tower. The following spring-damper system approximates the tower deflection, z , with spring constant K_{tow} and damping constant B_{tow} :

$$\ddot{z} = \frac{1}{m_{tow}} \cdot (F_{tow} - K_{tow} \cdot z - B_{tow} \cdot \dot{z}) \quad \text{Eq. 13}$$

With the following constants:

$$\begin{aligned} m_{tow} &= 3.474e+5 \quad [\text{kg}] \\ K_{tow} &= 0.08 \quad [\text{N/m}] \\ B_{tow} &= 3.58e+04 \quad [\text{N}\cdot\text{s/m}] \end{aligned}$$

Where z represents the position, \dot{z} the velocity, and \ddot{z} the acceleration of the nacelle.

The state space representation of the above equation is:

$$\begin{pmatrix} \dot{z} \\ \ddot{z} \end{pmatrix} = \begin{pmatrix} 0 & 1 \\ -\frac{K_{tow}}{m_{tow}} & -\frac{B_{tow}}{m_{tow}} \end{pmatrix} \begin{pmatrix} z \\ \dot{z} \end{pmatrix} + \begin{pmatrix} 0 \\ \frac{F_{tow}}{m_{tow}} \end{pmatrix} \quad \text{Eq. 14}$$

2.2.5. Blade

The wind creates a thrust force acting on the rotor which creates a bending moment on the wind turbine blades. The following equation approximates the blade moment:

$$M_{blade} = \frac{1}{3} \cdot 2 \cdot R \cdot F_{rot} \quad \text{Eq. 15}$$

Where R represents the rotor radius, F_{rot} the rotor thrust force, and M_{blade} the blade moment.

2.2.6. Pitch actuator

The system controlling blade pitch angle consists of electrical motors, gears, and controlling unit. Instead of using the NREL model which is a spring-damper system, a second order system with a time constant of τ_β , and input delay λ (from input u_β to pitch rate $\dot{\beta}$) as in [13], is considered.

The actuator is controlled by a proportional regulator with constant K_{beta} resulting in a pitch servo

$$\ddot{\beta} = \frac{1}{\tau_\beta} \cdot (u_\beta^\lambda - \dot{\beta}) \quad \text{Eq. 16 [13]}$$

$$u_\beta = K_\beta \cdot (\beta_{ref} - \beta_{meas}) \quad \text{Eq. 17 [13]}$$

From the previous equations (eq.16 and eq.17), is obtained the following state space representation

$$\begin{pmatrix} \dot{\beta} \\ \ddot{\beta} \end{pmatrix} = \begin{pmatrix} 0 & 1 \\ 0 & \frac{-1}{\tau_\beta} \end{pmatrix} \begin{pmatrix} \beta \\ \dot{\beta} \end{pmatrix} + \begin{pmatrix} 0 \\ \frac{u_\beta^\lambda}{\tau_\beta} \end{pmatrix} \quad \text{Eq. 18}$$

2.3. Linearized model

In the present subchapter, the nonlinear parts from the nonlinear mathematical model ([subchapter 2.2. Nonlinear model](#)) are linearized at the linearization points. The summary of the linearized mathematical model, its state-space and a comparison with the nonlinear model are also presented.

All the nonlinear parts of the nonlinear model will be linearized using Taylor expansion approximation at a wind speed in front of the rotor of 18 [m/s].

2.3.1. Tip speed ratio linearization

The first equation which is linearized is the tip speed ratio ($\lambda = \frac{R \cdot \Omega}{v_{rot}}$) and first step in executing the linearization is to calculate, using the equations ($\lambda = \frac{R \cdot \Omega}{v_{rot}}$) from the nonlinear model, the wind speed at the rotor v_{rot0} , rotor angular velocity Ω_0 and the tip speed ratio λ_0 at a wind speed in front of the rotor of 18 [m/s]

$$\Omega_0 = 1.274$$

$$v_{rot0} = 17.981$$

$$\lambda_0 = \lambda(\Omega_0, v_{rot0}) = 4.463$$

The linearization will be done using Taylor expansion approximation:

$$\lambda_l(\Omega, v_{rot}) = \lambda(\Omega_0, v_{rot0}) + \left. \frac{\partial \lambda}{\partial \Omega} \right|_{(\Omega_0, v_{rot0})} \cdot \Delta \Omega + \left. \frac{\partial \lambda}{\partial v_{rot}} \right|_{(\Omega_0, v_{rot0})} \cdot \Delta v_{rot} \quad \text{Eq. 19}$$

In the above equation, $\lambda(\Omega_0, v_{rot0})$ is substituted with λ_0 and $\lambda_l(\Omega, v_{rot})$ with λ and the following equation was obtained:

$$\lambda_l - \lambda_0 = \left. \frac{\partial \lambda}{\partial \Omega} \right|_{(\Omega_0, v_{rot0})} \cdot \Delta \Omega + \left. \frac{\partial \lambda}{\partial v_{rot}} \right|_{(\Omega_0, v_{rot0})} \cdot \Delta v_{rot} \quad \text{Eq. 20}$$

Where the differences in tip speed ratio, in wind speed at rotor and in angular velocity of the rotor can be expressed by Δ :

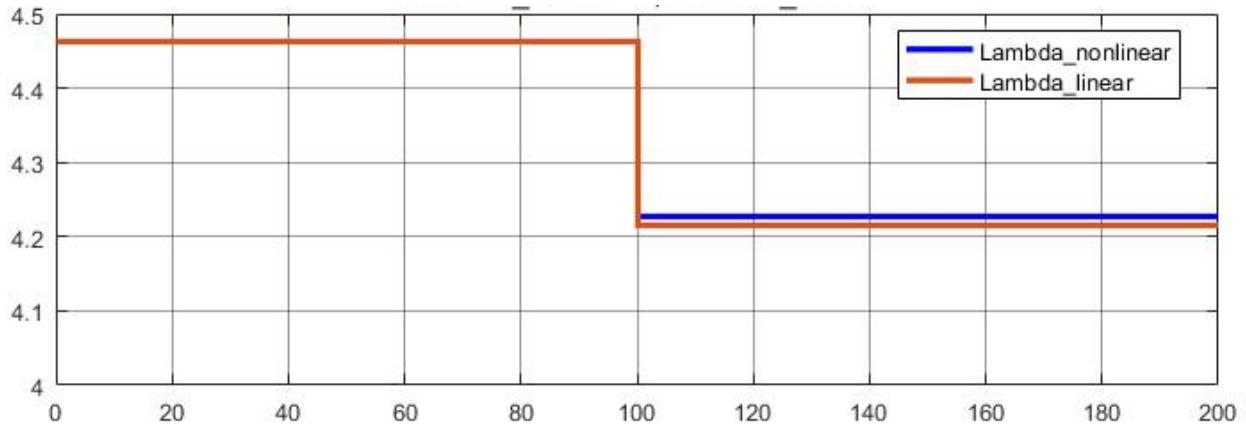
$$\Delta \lambda = \left. \frac{\partial \lambda}{\partial \Omega} \right|_{(\Omega_0, v_{rot0})} \cdot \Delta \Omega + \left. \frac{\partial \lambda}{\partial v_{rot}} \right|_{(\Omega_0, v_{rot0})} \cdot \Delta v_{rot} \quad \text{Eq. 21}$$

Finally, the slopes in the angular velocity and wind speed at rotor which contributes to the change in tip speed ratio are calculated:

$$\left. \frac{\partial \lambda}{\partial \Omega} \right|_{(\Omega_0, v_{rot0})} = \frac{R}{v_{rot0}} = 3.503 \quad \text{Eq. 22}$$

$$\left. \frac{\partial \lambda}{\partial v_{rot}} \right|_{(\Omega_0, v_{rot0})} = -\frac{R \cdot \Omega_0}{v_{rot0}^2} = -0.248 \quad \text{Eq. 23}$$

The following graph represents the comparison between the nonlinear and linearized equations of the tip speed ratio:



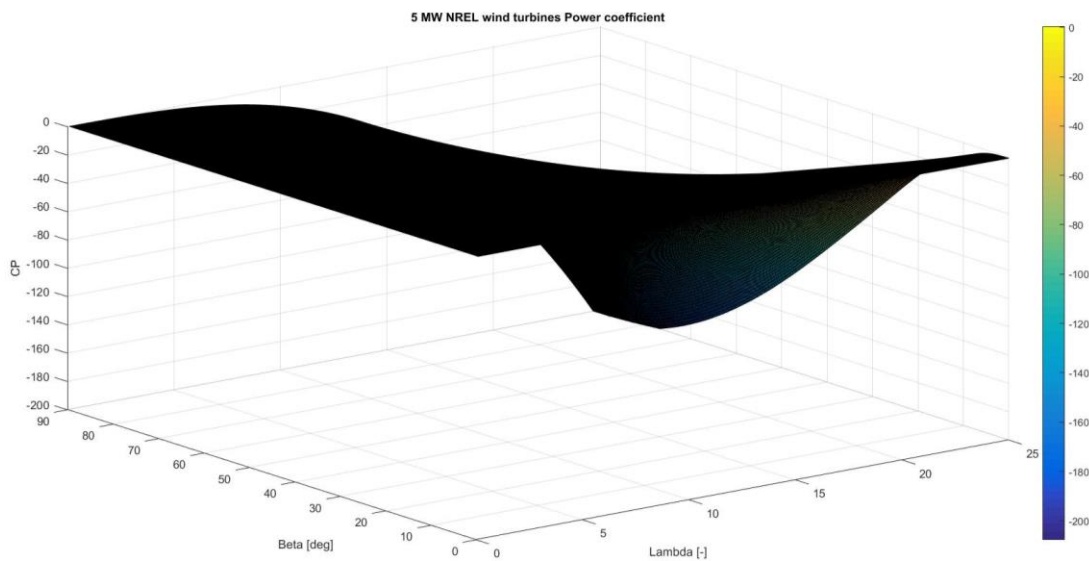
Graph 1. Tip speed ratio nonlinear vs. linearized equation

From the above graph, it can be seen that there is small difference between the outputs of the nonlinear and linear equations due to the error ($e_\lambda=0.0131$) occurred using the Taylor series approximation for linearizing the equation.

2.3.2. Power coefficient linearization

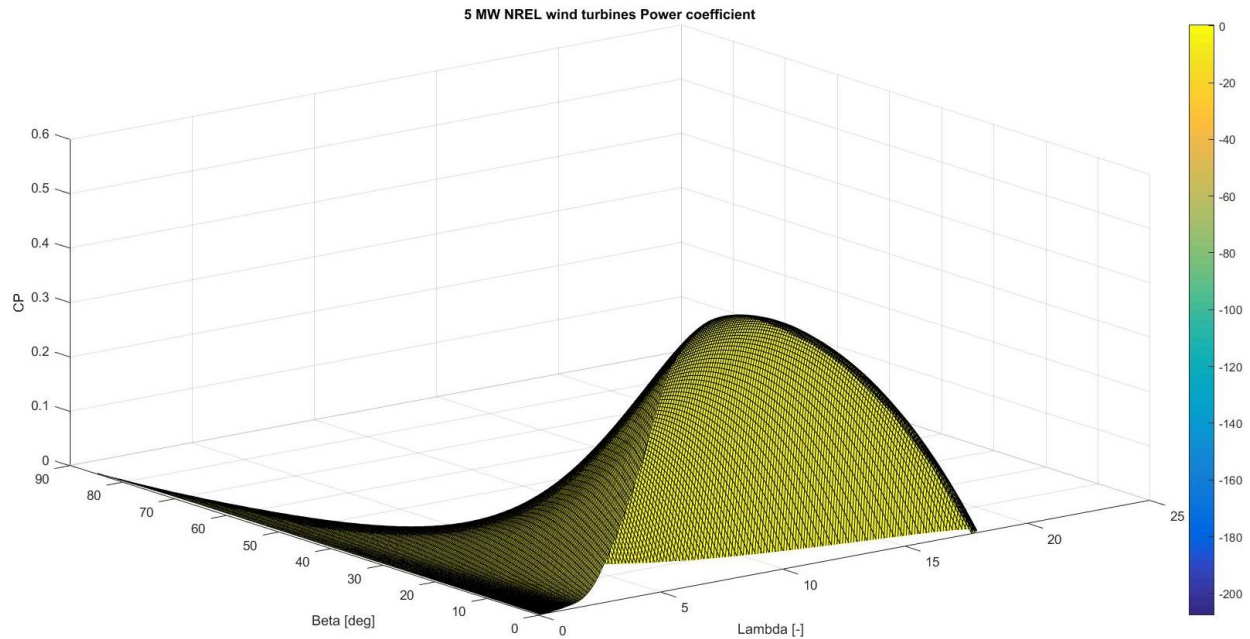
The second equation which is linearized is the power coefficient and first step in executing the linearization is approximate the power coefficient equation from the look up table using curve fitting tool (cftool) from matlab.

In the following graph, it can be seen the graphical representation of the entire power coefficient (CP) look up table.



Graph 2. Graphical representation of the CP table

In the following diagram it can be seen the graphical representation of the power coefficient look up table limited to the NREL 5 MW wind turbine operating range (pitch angle β from 0° to 90° , tips speed ratio from 0 to 25 and the power coefficient from 0 to Betz limit 0.59).



Graph 3. Reduced graphical representation of the CP table

By inserting the power coefficient look up table as an input to the curve fitting tool (cftool) in MATLAB, the following nonlinear power coefficient equation was obtained:

$$C_p(\beta, \lambda) = p_{00} + p_{10} \cdot \beta + p_{01} \cdot \lambda + p_{20} \cdot \beta^2 + p_{11} \cdot \beta \cdot \lambda + p_{02} \cdot \lambda^2 + p_{30} \cdot \beta^3 + p_{21} \cdot \beta^2 \cdot \lambda + p_{12} \cdot \beta \cdot \lambda^2 + p_{03} \cdot \lambda^3 + p_{40} \cdot \beta^4 + p_{31} \cdot \beta^3 \cdot \lambda + p_{22} \cdot \beta^2 \cdot \lambda^2 + p_{13} \cdot \beta \cdot \lambda^3 + p_{04} \cdot \lambda^4 + p_{50} \cdot \beta^5 + p_{41} \cdot \beta^4 \cdot \lambda + p_{32} \cdot \beta^3 \cdot \lambda^2 + p_{23} \cdot \beta^2 \cdot \lambda^3 + p_{14} \cdot \beta \cdot \lambda^4 + p_{05} \cdot \lambda^5 \quad \text{Eq. 24}$$

With the following parameters:

$p_{00} = -0.9401$	$p_{21} = 0.0007099$	$p_{04} = 8.464e - 05$
$p_{10} = 0.06098$	$p_{12} = 0.001433$	$p_{50} = -2.87e - 07$
$p_{01} = 0.4706$	$p_{03} = 0.001068$	$p_{41} = -8.289e - 07$
$p_{20} = 0.002549$	$p_{40} = 2.151e - 05$	$p_{32} = 4.013e - 06$
$p_{11} = -0.02382$	$p_{31} = 8.71e - 06$	$p_{23} = -4.293e - 06$
$p_{02} = -0.04861$	$p_{22} = -0.000153$	$p_{14} = -7.17e - 06$
$p_{30} = -0.0004969$	$p_{13} = 0.0001294$	$p_{05} = -3.799e - 06$

Next step in executing the linearization is by using the wind speed at the rotor v_{rot0} , the pitch angle β_0 , the tip speed ratio λ_0 and at a wind speed in front of the rotor of 18 [m/s], and the above equation (Eq.24) to calculate the power coefficient C_{p0} at the same linearization speed:

$$v_{R0} = 17.981$$

$$\beta_0 = 14.81$$

$$\lambda_0 = 4.463$$

$$C_{P0} = 0.119$$

The linearization will be done using Taylor expansion approximation:

$$C_{PI}(\beta, \lambda) = CP(\beta_0, \lambda_0) + \left. \frac{\partial CP}{\partial \beta} \right|_{(\beta_0, \lambda_0)} \cdot (\beta - \beta_0) + \left. \frac{\partial CP}{\partial \lambda} \right|_{(\beta_0, \lambda_0)} \cdot (\lambda - \lambda_0) \quad \text{Eq. 25}$$

By substituting in the above equation, $CP(\beta_0, \lambda_0)$ is substituted with C_{P0} and $C_{PI}(\beta, \lambda)$ with C_{PI} , the following equation is obtained:

$$C_{PI} - C_{P0} = \left. \frac{\partial CP}{\partial \beta} \right|_{(\beta_0, \lambda_0)} \cdot \Delta\beta + \left. \frac{\partial CP}{\partial \lambda} \right|_{(\beta_0, \lambda_0)} \cdot \Delta\lambda \quad \text{Eq. 26}$$

The differences in power coefficient, in pitch angle and in tip speed ratio can be expressed by Δ :

$$\Delta CP = \left. \frac{\partial CP}{\partial \beta} \right|_{(\beta_0, \lambda_0)} \cdot \Delta\beta + \left. \frac{\partial CP}{\partial \lambda} \right|_{(\beta_0, \lambda_0)} \cdot \Delta\lambda \quad \text{Eq. 27}$$

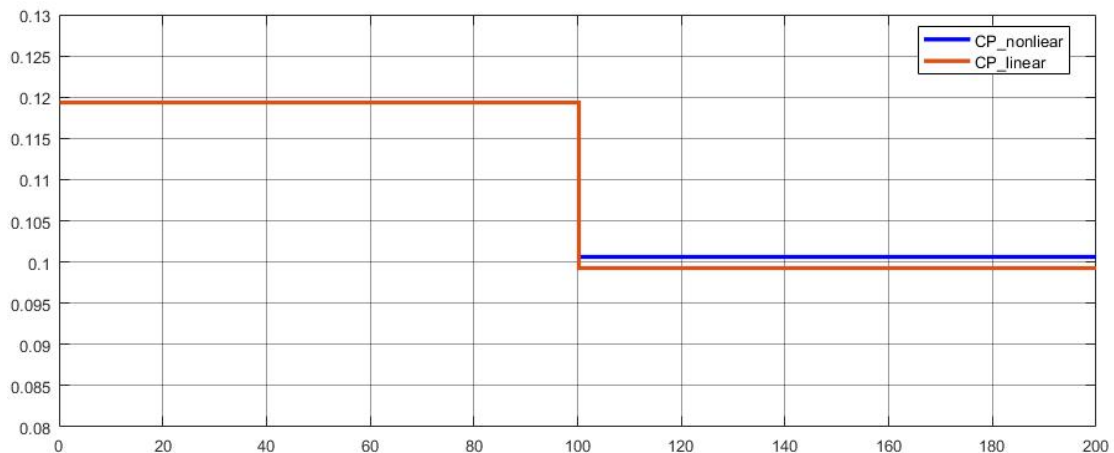
Deriving the equation (Eq. 24) results in:

$$\begin{aligned} \Delta CP = & (p_{10} + 2 \cdot p_{20} \cdot \beta_0 + p_{11} \cdot \lambda_0 + 3 \cdot p_{30} \cdot \beta_0^2 + p_{21} \cdot 2 \cdot \beta_0 \cdot \lambda_0 + p_{12} \cdot \lambda_0^2 + 4 \cdot p_{40} \cdot \beta_0^3 + 3 \cdot p_{31} \cdot \\ & \beta_0^2 \cdot \lambda_0 + 2 \cdot p_{22} \cdot \beta_0 \cdot \lambda_0^2 + p_{13} \cdot \lambda_0^3 + 5 \cdot p_{50} \cdot \beta_0^4 + 4 \cdot p_{41} \cdot \beta_0^3 \cdot \lambda_0 + 3 \cdot p_{32} \cdot \beta_0^2 \cdot \lambda_0^2 + 2 \cdot p_{23} \cdot \beta_0 \cdot \\ & \lambda_0^3 + p_{14} \cdot \lambda_0^4) \cdot \Delta\beta + (p_{01} + p_{11} \cdot \beta_0 + 2 \cdot p_{02} \cdot \lambda_0 + p_{21} \cdot \beta_0^2 + 2 \cdot p_{12} \cdot \beta_0 \cdot \lambda_0 + 3 \cdot p_{03} \cdot \lambda_0^2 + p_{31} \cdot \\ & \beta_0^3 + 2 \cdot p_{22} \cdot \beta_0^2 \cdot \lambda_0 + 3 \cdot p_{13} \cdot \beta_0 \cdot \lambda_0^2 + 4 \cdot p_{04} \cdot \lambda_0^3 + p_{41} \cdot \beta_0^4 + 2 \cdot p_{32} \cdot \beta_0^3 \cdot \lambda_0 + 3 \cdot p_{23} \cdot \beta_0^2 \cdot \lambda_0^2 + 4 \cdot \\ & p_{14} \cdot \beta_0 \cdot \lambda_0^3 + 5 \cdot p_{05} \cdot \lambda_0^4) \cdot \Delta\lambda \quad \text{Eq. 28} \end{aligned}$$

Finally, the slopes of the pitch angle and tip speed which contributes to the change in power coefficient are calculated:

$$\left. \frac{\partial CP}{\partial \beta} \right|_{(\beta_0, \lambda_0)} = -0.027 \quad \text{Eq. 29} \quad \left. \frac{\partial CP}{\partial \lambda} \right|_{(\beta_0, \lambda_0)} = -0.059 \quad \text{Eq. 30}$$

The following graph represents the comparison between the look up table and linear equations of the power coefficient:



Graph 4. CP look up table vs. linearized equation

From graph 4, it can be seen that there is small difference between the outputs of the look up table and linear equation due to the error ($e_{CP}=0.001472$) occurred while fitting the look up table curve and using the Taylor series approximation for linearizing the fitted curve.

2.3.3. Rotor torque linearization

Next equation which is linearized, is the rotor torque (eq. 4). The first step in executing the linearization is by using the wind speed at the rotor v_{rot0} , rotor angular velocity Ω_0 and the power coefficient C_{p0} at a wind speed in front of the rotor of 18 [m/s] and using the equation (eq. 4) from the nonlinear model to calculate the M_{rot0} at the same linearization point.

$$v_{R_0} = 18$$

$$v_{rot0} = 17.981$$

$$C_{p0} = 0.119$$

$$\Omega_0 = 1.274$$

$$M_{rot0} = 4.157e + 6$$

The linearization will be done using Taylor expansion approximation:

$$M_{rotl}(v_{rot}, C_P, \Omega) = M_{rot}(v_{rot0}, C_{P0}, \Omega_0) + \left. \frac{\partial M_{rot}}{\partial v_{rot}} \right|_{(v_{rot0}, C_{P0}, \Omega_0)} \cdot \Delta v_{rot} + \left. \frac{\partial M_{rot}}{\partial C_P} \right|_{(v_{rot0}, C_{P0}, \Omega_0)} \cdot \Delta C_P + \left. \frac{\partial M_{rot}}{\partial \Omega} \right|_{(v_{rot0}, C_{P0}, \Omega_0)} \cdot \Delta \Omega \quad \text{Eq. 31}$$

In the above equation, $M_{rot}(v_{rot0}, C_{P0}, \Omega_0)$ is substituted with M_{rot0} and $M_{rotl}(v_{rot}, C_P, \Omega)$ with M_{rotl} and the following equation was obtained:

$$M_{rotl} - M_{rot0} = \left. \frac{\partial M_{rot}}{\partial v_{rot}} \right|_{(v_{rot0}, C_{P0}, \Omega_0)} \cdot \Delta v_{rot} + \left. \frac{\partial M_{rot}}{\partial C_P} \right|_{(v_{rot0}, C_{P0}, \Omega_0)} \cdot \Delta C_P + \left. \frac{\partial M_{rot}}{\partial \Omega} \right|_{(v_{rot0}, C_{P0}, \Omega_0)} \cdot \Delta \Omega \quad \text{Eq. 32}$$

In the above equation, the slope of the power coefficient is substituted using Eq. 29 and the slope of the angular velocity of the rotor is substituted using Eq. 30 and the following equation is obtained:

$$M_{rotl} - M_{rot0} = \left. \frac{\partial M_{rot}}{\partial v_{rot}} \right|_{(v_{rot0}, C_{P0}, \Omega_0)} \cdot \Delta v_{rot} + \left. \frac{\partial M_{rot}}{\partial C_P} \right|_{(v_{rot0}, C_{P0}, \Omega_0)} \cdot \left. \frac{\partial C_P}{\partial \beta} \right|_{(\beta_0, \Omega_0, v_{rot0})} \cdot \Delta \beta + \left. \frac{\partial M_{rot}}{\partial C_P} \right|_{(v_{rot0}, C_{P0}, \Omega_0)} \cdot \left. \frac{\partial C_P}{\partial \Omega} \right|_{(\beta_0, \Omega_0, v_{rot0})} \cdot \Delta \Omega + \left. \frac{\partial M_{rot}}{\partial C_P} \right|_{(v_{rot0}, C_{P0}, \Omega_0)} \cdot \left. \frac{\partial C_P}{\partial v_{rot}} \right|_{(\beta_0, \Omega_0, v_{rot0})} \cdot \Delta v_{rot} + \left. \frac{\partial M_{rot}}{\partial \Omega} \right|_{(v_{rot0}, C_{P0}, \Omega_0)} \cdot \Delta \Omega \quad \text{Eq. 33}$$

Simplifying the above equation results in:

$$M_{rotl} - M_{rot0} = \left. \frac{\partial M_{rot}}{\partial v_{rot}} \right|_{(v_{rot0}, \Omega_0, \beta_0)} \cdot \Delta v_{rot} + \left. \frac{\partial M_{rot}}{\partial \beta} \right|_{(v_{rot0}, \Omega_0, \beta_0)} \cdot \Delta \beta + \left. \frac{\partial M_{rot}}{\partial \Omega} \right|_{(v_{rot0}, \Omega_0, \beta_0)} \cdot \Delta \Omega + \left. \frac{\partial M_{rot}}{\partial v_{rot}} \right|_{(v_{rot0}, \Omega_0, \beta_0)} \cdot \left. \frac{\partial M_{rot}}{\partial \Omega} \right|_{(v_{rot0}, \Omega_0, \beta_0)} \cdot \Delta \Omega \quad \text{Eq. 34}$$



Substituting the difference in rotor torque with Δ

$$\Delta M_{rot} = \left. \frac{\partial M_{rot}}{\partial v_{rot}} \right|_{(v_{rot0}, \Omega_0, \beta_0)} \cdot \Delta v_{rot} + \left. \frac{\partial M_{rot}}{\partial \Omega} \right|_{(v_{rot0}, \Omega_0, \beta_0)} \cdot \Delta \Omega + \left. \frac{\partial M_{rot}}{\partial \beta} \right|_{(v_{rot0}, \Omega_0, \beta_0)} \cdot \Delta \beta \quad \text{Eq. 35}$$

The change in rotor torque M_{rot} in respect to wind speed at rotor v_{rot} is derived from the eq. 4.

$$\left. \frac{\partial M_{rot}}{\partial v_{rot}} \right|_{(v_{rot0}, \Omega_0, \beta_0)} = \frac{1}{2} \cdot \pi \cdot \rho \cdot R^2 \cdot \frac{1}{\Omega_0} \cdot \left(3 \cdot v_{rot}^2 \cdot CP_0 - v_{rot0}^2 \cdot \lambda_0 \cdot \frac{\partial CP(\lambda_0, \beta_0)}{\partial \lambda_0} \right) = 1.202e + 06 \quad \text{Eq. 36}$$

The change in rotor torque M_{rot} in respect to rotor angular velocity Ω is derived from the eq. 4.

$$\left. \frac{\partial M_{rot}}{\partial \Omega} \right|_{(v_{rot0}, \Omega_0, \beta_0)} = \frac{1}{2} \cdot \pi \cdot \rho \cdot R^2 \cdot v_{rot0}^3 \cdot \left(-\frac{1}{\Omega_0^2} \cdot CP_0 + \frac{1}{\Omega_0} \cdot \frac{R}{v_{rot0}} \cdot \frac{\partial CP(\lambda_0, \beta_0)}{\partial \lambda_0} \right) = -1.044e + 07 \quad \text{Eq. 37}$$

The change in rotor torque M_{rot} in respect to pitch angle β is derived from the eq. 4.

$$\left. \frac{\partial M_{rot}}{\partial \beta} \right|_{(v_{rot0}, \Omega_0, \beta_0)} = \frac{1}{2} \cdot \pi \cdot \rho \cdot R^2 \cdot v_{rot0}^3 \cdot \frac{1}{\Omega_0} \cdot \left(\frac{\partial CP(\lambda_0, \beta_0)}{\partial \beta_0} \right) = -9.313e + 05 \quad \text{Eq. 38}$$

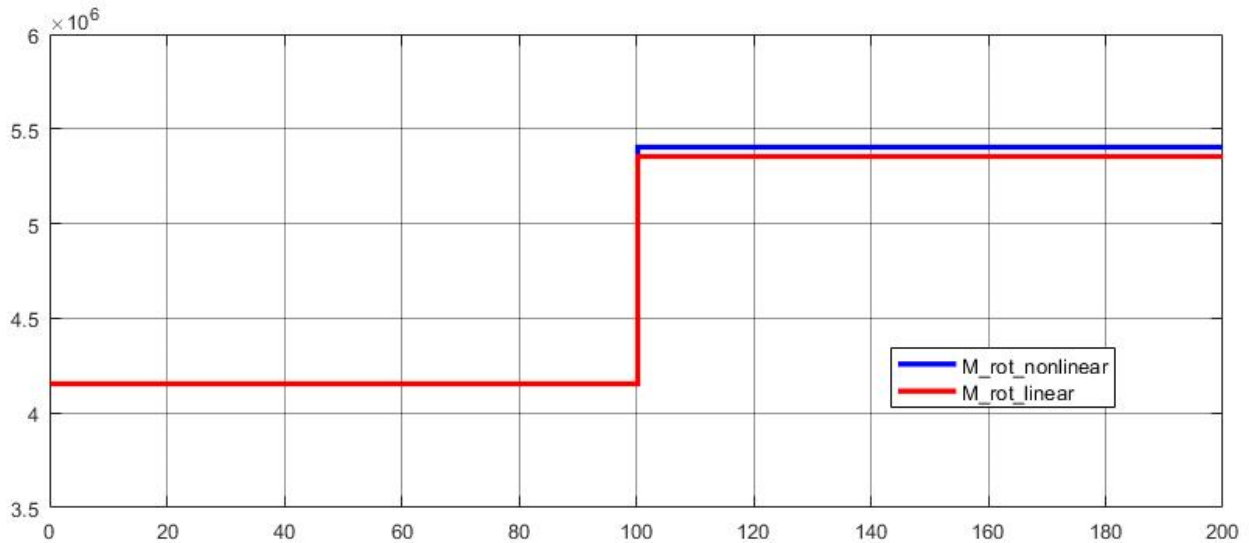
The final form of the equation for calculating the change in rotor torque can be written in the following form:

$$\Delta M_{rot} = a \cdot \Delta v_{rot} + b \cdot \Delta \Omega + c \cdot \Delta \beta \quad \text{Eq. 39}$$

Where:

$$a = 1.202e + 06 \quad b = -1.044e + 07 \quad c = -9.313e + 05$$

The following graph represents the comparison between the nonlinear and linear equations of the rotor torque:



Graph 5. Rotor torque nonlinear vs. linearized equation

From graph 5, it can be seen that there is small difference between the outputs of the nonlinear and linear equations due to the error ($e_{M_{rot}}=5.087e+4$) occurred by using Taylor series approximation for linearizing the equation.

2.3.4. Rotor torque reference linearization

Next equation which is linearized, is the generator torque reference (eq. 11) The first step in executing the linearization is by using the wind speed at the rotor v_{rot0} , generator angular velocity ω_0 and the power reference P_{ref0} at a wind speed in front of the rotor of 18 [m/s] and using the equation (eq. 11) from the nonlinear model to calculate the generator torque reference M_{genref} at the same linearization point.

$$v_{R0} = 17.981$$

$$P_{ref0} = 5.297e + 06$$

$$\omega_0 = 123.575$$

$$M_{genref0} = 4.286e + 04$$

The linearization will be done using Taylor expansion approximation:

$$M_{genrefl}(P_{ref}, \omega) = M_{genref}(P_{ref0}, \omega_0) + \left. \frac{\partial M_{genref}}{\partial P_{ref}} \right|_{(P_{ref0}, \omega_0)} \cdot (P_{ref} - P_{ref0}) + \left. \frac{\partial M_{genref}}{\partial \omega} \right|_{(P_{ref0}, \omega_0)} \cdot (\omega - \omega_0) \quad \text{Eq. 40}$$

In the above equation, $M_{genref}(P_{ref0}, \omega_0)$ is substituted with $M_{genref0}$ and $M_{genrefl}(P_{ref}, \omega)$ with M_{genref} and the following equation was obtained:

$$M_{genrefl} - M_{genref0} = \left. \frac{\partial M_{genref}}{\partial P_{ref}} \right|_{(P_{ref0}, \omega_0)} \cdot (P_{ref} - P_{ref0}) + \left. \frac{\partial M_{genref}}{\partial \omega} \right|_{(P_{ref0}, \omega_0)} \cdot (\omega - \omega_0) \quad \text{Eq. 41}$$

In the above equation, the change in power reference, generator angular velocity and generator torque reference are substitute with Δ :

$$\Delta M_{genref} = \left. \frac{\partial M_{genref}}{\partial P_{ref}} \right|_{(P_{ref0}, \omega_0)} \cdot \Delta P_{ref} + \left. \frac{\partial M_{genref}}{\partial \omega} \right|_{(P_{ref0}, \omega_0)} \cdot \Delta \omega \quad \text{Eq. 42}$$

Finally, the slopes of the power reference and generator angular velocity which contributes to the change in generator torque reference are calculated:

$$\left. \frac{\partial M_{genref}}{\partial P_{ref}} \right|_{(P_{ref0}, \omega_0)} = 0.008 \quad \text{Eq. 43} \quad \left. \frac{\partial M_{genref}}{\partial \omega} \right|_{(P_{ref0}, \omega_0)} = -346.847 \quad \text{Eq. 44}$$

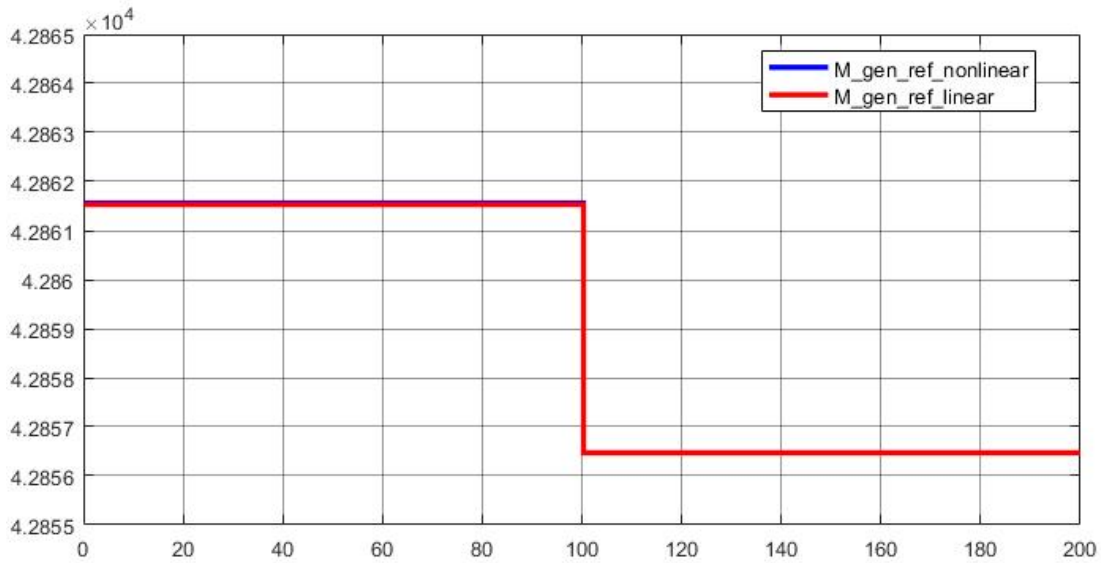
Due to the reason that the power reference is constant, its change is 0:

$$\Delta P_{ref} = 0$$

This statement reduces Eq. 44 to the following equation:

$$\Delta M_{genref} = a_1 \cdot \Delta \omega \quad \text{Where } a_1 = -346.847 \quad \text{Eq. 45}$$

In the following graph, it can be seen the accuracy of the linearization:



Graph 6. Rotor torque reference nonlinear vs. linearized equation

2.3.5. Gross output power linearization

The final equation which is linearized, is the gross output power (eq. 9). The first step in executing the linearization is by using the wind speed at the rotor v_{rot0} , generator angular velocity ω_0 and the generator torque M_{gen0} at a wind speed in front of the rotor of 18 [m/s] and using the equation (eq. 9) from the nonlinear model to calculate the gross output power $P_{out.gross}$ at the same linearization point.

$$v_{R0} = 18$$

$$\omega_0 = 123.574$$

$$M_{gen0} = 42861.556$$

$$P_{out.gross0} = 5.297e + 06$$

The linearization will be done using Taylor expansion approximation:

$$\begin{aligned}
 P_{out.gross}(M_{gen}, \omega) = & P_{out.gross}(M_{gen0}, \omega_0) + \left. \frac{\partial P_{out.gross}}{\partial M_{gen}} \right|_{(M_{gen0}, \omega_0)} \cdot (M_{gen} - M_{gen0}) + \\
 & \left. \frac{\partial P_{out.gross}}{\partial \omega} \right|_{(M_{gen0}, \omega_0)} \cdot (\omega - \omega_0) \quad \text{Eq. 46}
 \end{aligned}$$

In eq. 46, $P_{out.gross}(M_{gen0}, \omega_0)$ is substituted with $P_{out.gross0}$ and $P_{out.gross}(M_{gen}, \omega)$ with $P_{out.gross}$ and the following equation was obtained:

$$P_{out.gross} - P_{out.gross0} = \left. \frac{\partial P_{out.gross}}{\partial M_{gen}} \right|_{(M_{gen0}, \omega_0)} \cdot (M_{gen} - M_{gen0}) + \left. \frac{\partial P_{out.gross}}{\partial \omega} \right|_{(M_{gen0}, \omega_0)} \cdot (\omega - \omega_0)$$

Eq. 47

In the above equation, the change in generator torque, generator angular velocity and gross output power are substitute with Δ :

$$\Delta P_{out.gross} = \left. \frac{\partial P_{out.gross}}{\partial M_{gen}} \right|_{(M_{gen0}, \omega_0)} \cdot \Delta M_{gen} + \left. \frac{\partial P_{out.gross}}{\partial \omega} \right|_{(M_{gen0}, \omega_0)} \cdot \Delta \omega$$

Eq. 48

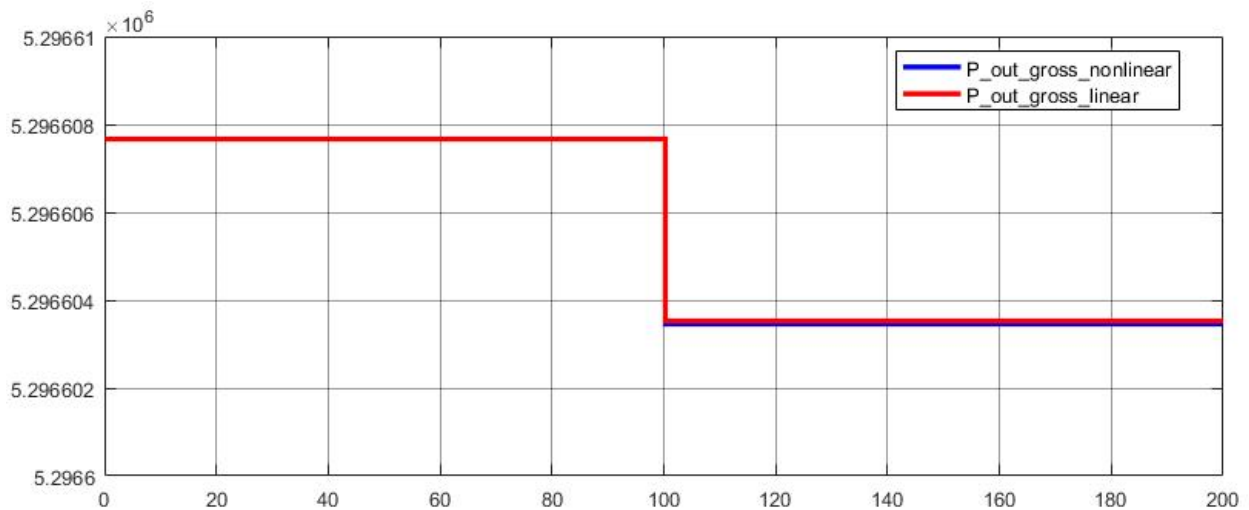
$$\Delta P_{out.gross} = a_2 \cdot \Delta M_{gen} + b_2 \cdot \Delta \omega$$

Eq. 49

Finally, the slopes of the generator torque and generator angular velocity which contributes to the change in gross output power are calculated:

$$a_2 = \left. \frac{\partial P_{out.gross}}{\partial M_{gen}} \right|_{(M_{gen0}, \omega_0)} = 123.575 \quad \text{Eq. 50} \quad b_2 = \left. \frac{\partial P_{out.gross}}{\partial \omega} \right|_{(M_{gen0}, \omega_0)} = 4.286e + 04 \quad \text{Eq. 51}$$

In the following graph, it can be seen the accuracy of the gross output power linearization:



Graph 7. Gross output power nonlinear vs. linearized equation

2.3.6. Summary of the linearized model

All the nonlinear equations which has been linearized, are combined with the linear equations from the nonlinear model into a system of equations which represents the linear model.

$$\dot{\Omega} = \frac{1}{I_{rot}} \cdot (a \cdot v_{rot} + b \cdot \Omega + c \cdot \beta - \Phi \cdot K_{shaft} - \dot{\Phi} \cdot B_{shaft}) \quad \text{Eq. 52}$$

$$\dot{\omega} = \frac{1}{I_{gen}} \cdot \left(-M_{gen} + \frac{1}{N} \cdot (\Phi \cdot K_{shaft} + \dot{\Phi} \cdot B_{shaft}) \right) \quad \text{Eq. 53}$$

$$\dot{\Phi} = \Omega - \frac{1}{N} \cdot \omega \quad \text{Eq. 54}$$

$$\dot{M}_{gen} = \frac{1}{\tau_{gen}} \cdot (a_1 \cdot \omega - M_{gen}) \quad \text{Eq. 55}$$

$$P_{out} = Gen_{eff} \cdot (a_2 \cdot M_{gen} + b_2 \cdot \omega) \quad \text{Eq. 56}$$

The diagram below represents the graphical representation of the linear model.

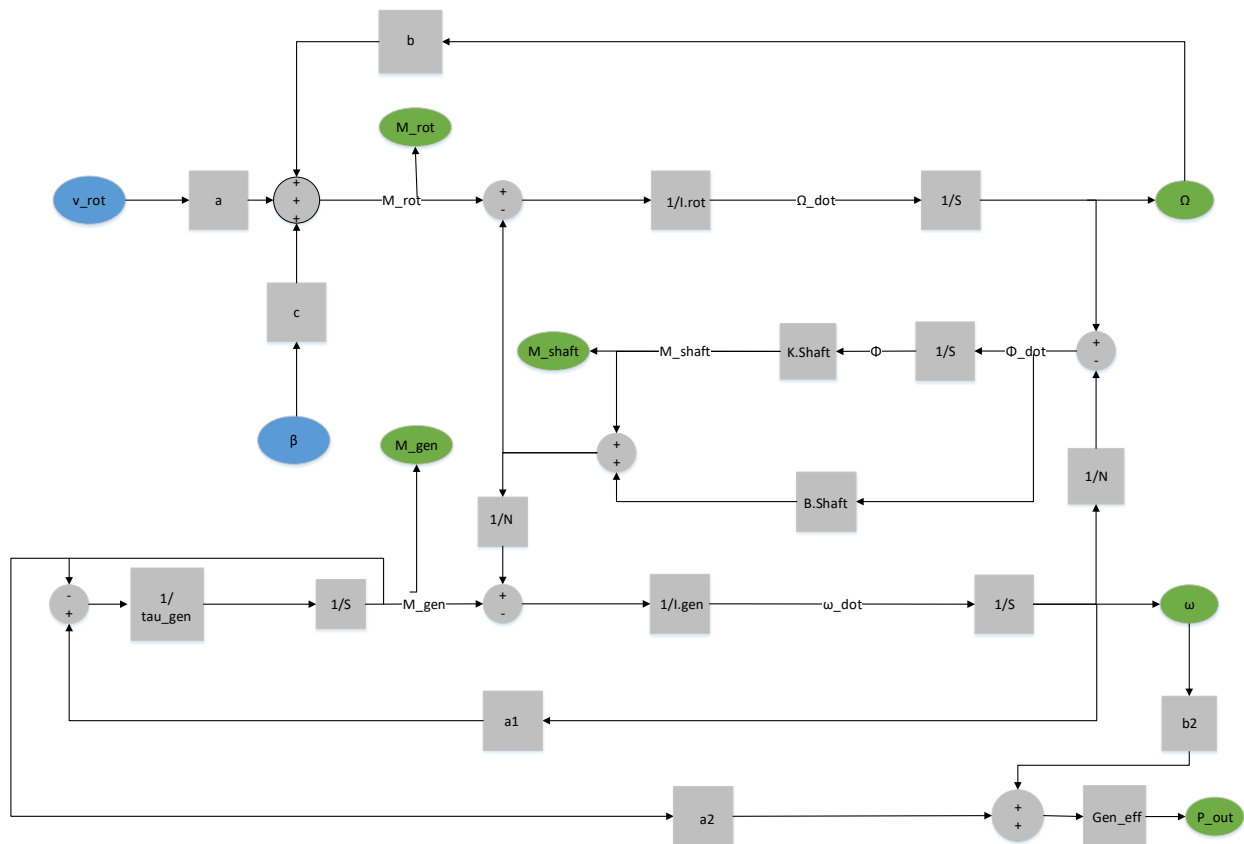


Diagram. 2. Block diagram of the linearized model

Finally, the above 5 equations (eq. 52 – eq. 56) can be expanded to the following equations:

$$\dot{\Omega} = \frac{1}{I_{rot}} \cdot a \cdot v_{rot} + \frac{1}{I_{rot}} \cdot b \cdot \Omega + \frac{1}{I_{rot}} \cdot c \cdot \beta - \frac{1}{I_{rot}} \cdot \Phi \cdot K_{shaft} - \frac{1}{I_{rot}} \cdot \Omega \cdot B_{shaft} + \frac{1}{I_{rot}} \cdot \frac{1}{N} \cdot \omega \cdot B_{shaft} \quad \text{Eq. 57}$$

$$\dot{\omega} = -\frac{1}{I_{gen}} \cdot M_{gen} + \frac{1}{I_{gen}} \cdot \frac{1}{N} \cdot \Phi \cdot K_{shaft} + \frac{1}{I_{gen}} \cdot \frac{1}{N} \cdot \Omega \cdot B_{shaft} - \frac{1}{I_{gen}} \cdot \frac{1}{N} \cdot \omega \cdot B_{shaft} \quad \text{Eq. 58}$$

$$\dot{\Phi} = \Omega - \frac{1}{N} \cdot \omega \quad \text{Eq. 59}$$

$$\dot{M}_{gen} = \frac{1}{\tau_{gen}} \cdot a_1 \cdot \omega - \frac{1}{\tau_{gen}} \cdot M_{gen} \quad \text{Eq. 60}$$

$$P_{out} = Gen_{eff} \cdot a_2 \cdot M_{gen} + Gen_{eff} \cdot b_2 \cdot \omega \quad \text{Eq. 61}$$

2.3.7. State-space model

Before writing the above equations into state space representation, the state vector x with 4 states, the input vector u with 2 inputs, and the output vector y with 2 outputs are defined as below:

State vector	Input vector	Output vector
$x = \begin{bmatrix} x_1 \\ x_2 \\ x_3 \\ x_4 \end{bmatrix} = \begin{bmatrix} \Omega \\ \omega \\ \Phi \\ M_{gen} \end{bmatrix}$	$u = \begin{bmatrix} v_{rot} \\ \beta \end{bmatrix}$	$y = \begin{bmatrix} \omega \\ P_{outnet} \end{bmatrix}$

The linearized model is described by the following state-space model with 2 outputs, 2 inputs, and 4 states.:

State space equations

$$\begin{cases} \dot{x} = A \cdot x + B \cdot u \\ y = C \cdot x + D \cdot u \end{cases} \quad \text{Eq. 62}$$

State-space matrix representation

$$\begin{bmatrix} \dot{x} \\ y \end{bmatrix} = \begin{bmatrix} A & B \\ C & D \end{bmatrix} \cdot \begin{bmatrix} x \\ u \end{bmatrix} \quad \text{Eq. 63}$$

For the above equation, the states matrix A is identified as:

$$A = \begin{bmatrix} \frac{1}{I_{rot}} \cdot b - \frac{1}{I_{rot}} \cdot B_{shaft} & \frac{1}{I_{rot}} \cdot \frac{1}{N} \cdot B_{shaft} & -\frac{1}{I_{rot}} \cdot K_{shaft} & 0 \\ \frac{1}{I_{gen}} \cdot \frac{1}{N} \cdot B_{shaft} & -\frac{1}{I_{gen}} \cdot \frac{1}{N^2} \cdot B_{shaft} & \frac{1}{I_{gen}} \cdot \frac{1}{N} \cdot K_{shaft} & -\frac{1}{I_{gen}} \\ 1 & -\frac{1}{N} & 0 & 0 \\ 0 & \frac{1}{\tau_{gen}} \cdot a_1 & 0 & -\frac{1}{\tau_{gen}} \end{bmatrix} \quad \text{Eq. 64}$$

For equation eq. 63 the input matrix B, is identified as:

$$B = \begin{bmatrix} \frac{1}{I_{rot}} \cdot a_{I_{rot}} \cdot c \\ 0 & 0 \\ 0 & 0 \\ 0 & 0 \end{bmatrix} \quad \text{Eq. 65}$$

The state-space's output matrices C and D are identified as:

$$C = \begin{bmatrix} 0 & 1 & 0 & 0 \\ 0 & Gen_{eff} \cdot b_2 & 0 & Gen_{eff} \cdot a_2 \end{bmatrix} \quad \text{Eq. 66}$$

$$D = \begin{bmatrix} 0 & 0 \\ 0 & 0 \end{bmatrix} \quad \text{Eq. 67}$$

The following transfer function represents the transfer function from the pitch angle β to generator angular velocity ω :

$$TF1_{\beta\omega_{gen}} = \frac{-3.152 \cdot s^2 - 471.6 \cdot s - 4400}{s^4 + 11.71 \cdot s^3 + 208.1 \cdot s^2 + 2023 \cdot s + 349.4} \quad \text{Eq. 68}$$

In the figure below it can be seen the bode diagram of the linear model transfer function from the pitch angle β to generator angular velocity ω :

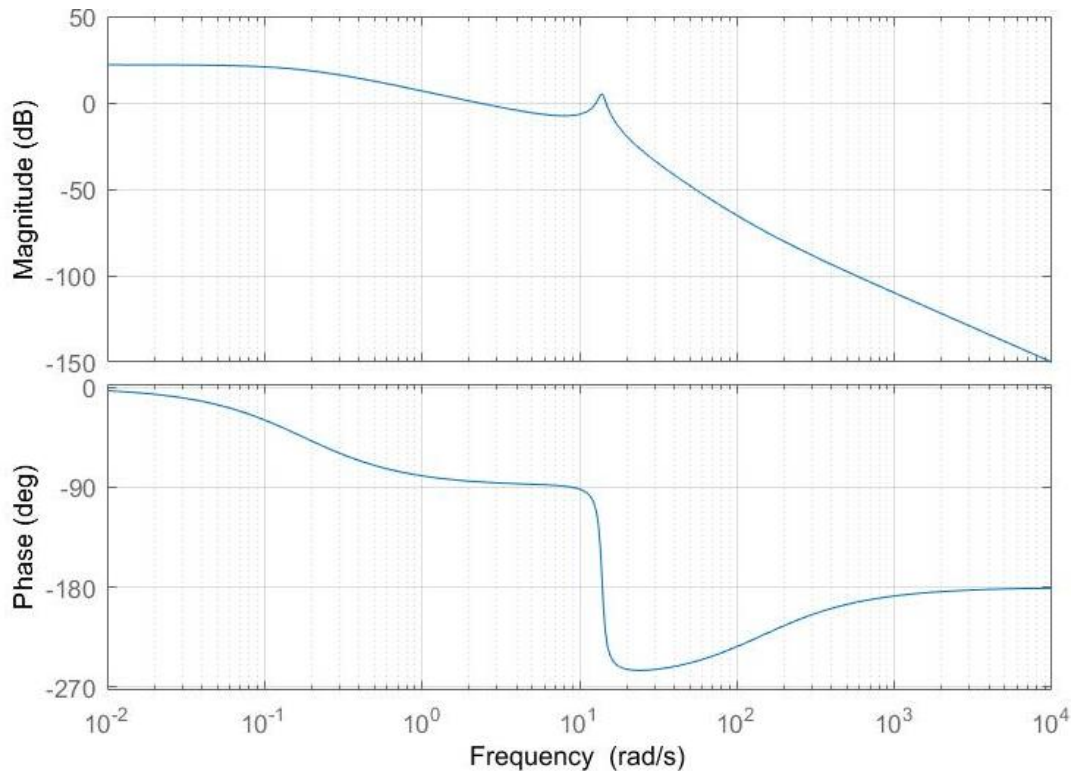


Diagram. 3. Bode diagram of the open loop: pitch angle to generator angular velocity relation

From above diagram, it can be seen that the minimum stability gain margin is -5.01 dB at 14 [rad/s] and the minimum stability phase margin is -44.5 deg at 14.7 [rad/s].



Below it can be seen the pole-zero map of the linear model transfer function from the pitch angle β to generator angular velocity ω :

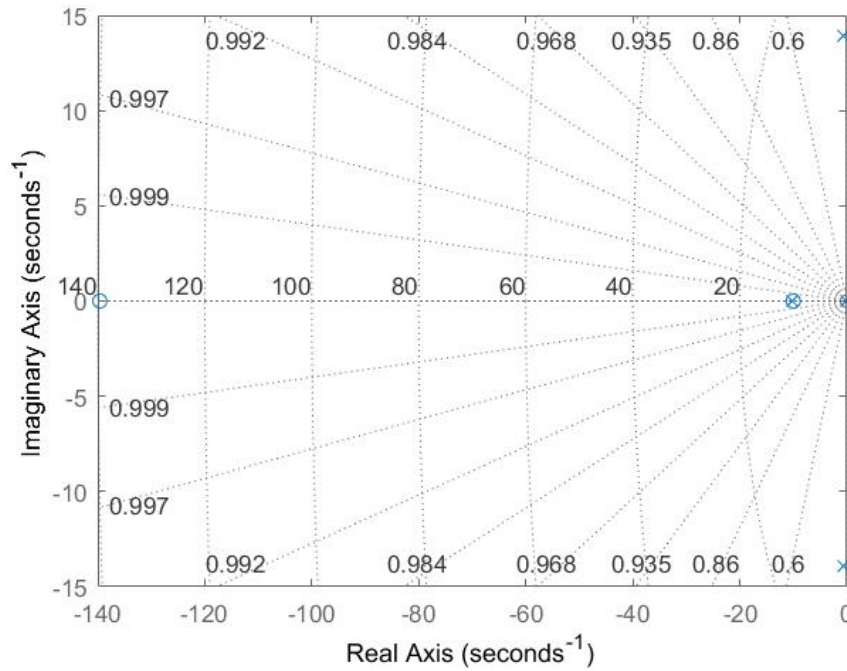


Diagram. 4. Pole-zero map of the open loop: pitch angle to generator angular velocity relation

<p>Poles:</p> <ul style="list-style-type: none"> -0.6243 +13.8855i -0.6243 -13.8855i -10.2821 -0.1759 	<p>From the above diagram, it can be seen that the all the poles are in Left Half Plane (LHP) showing that the model is stable</p>	<p>Also in the above figure, the zero of the system can be identified</p>	<p>Zeros:</p> <ul style="list-style-type: none"> -139.6037 -10.0000
---	--	---	---

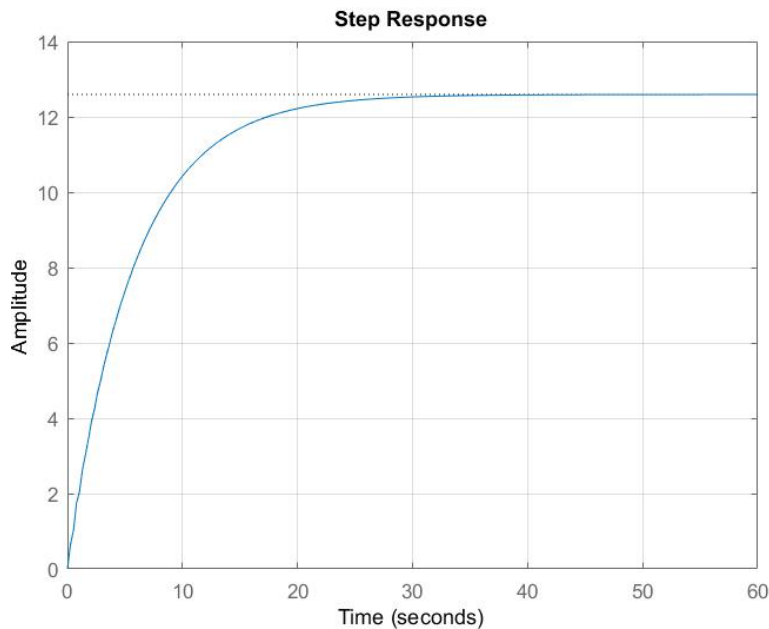


Diagram. 5. Step response of the open loop: pitch angle to generator angular velocity relation

The following transfer function represents the transfer function from the pitch angle β to output power P_{out} :

$$TF1_{\beta P_{out}} = \frac{-1.275e05 \cdot s^2 - 1.78e07 \cdot s + 77.43}{s^4 + 11.71 \cdot s^3 + 208.1 \cdot s^2 + 2023 \cdot s + 349.4} \quad \text{Eq. 69}$$

In the figure below it can be seen the bode diagram of the linear model transfer function from the pitch angle β to output power P_{out} :

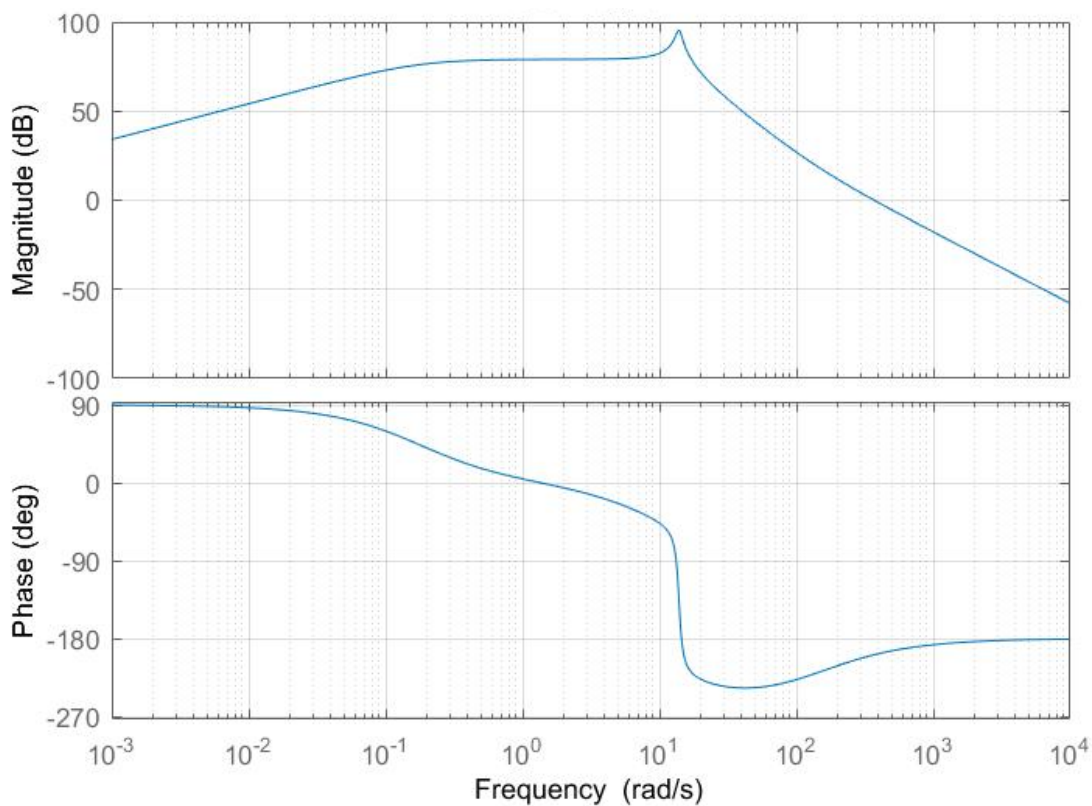


Diagram. 6. Bode diagram of the open loop: pitch angle to output power relation

From above figure, it can be seen that the gain margin is -92.3 dB at 14.5 [rad/s] and the minimum stability phase margin is -18.9 deg at 370 [rad/s].

Below it can be seen the pole-zero map of the linear model transfer function from the pitch angle β to output power P_{out} :

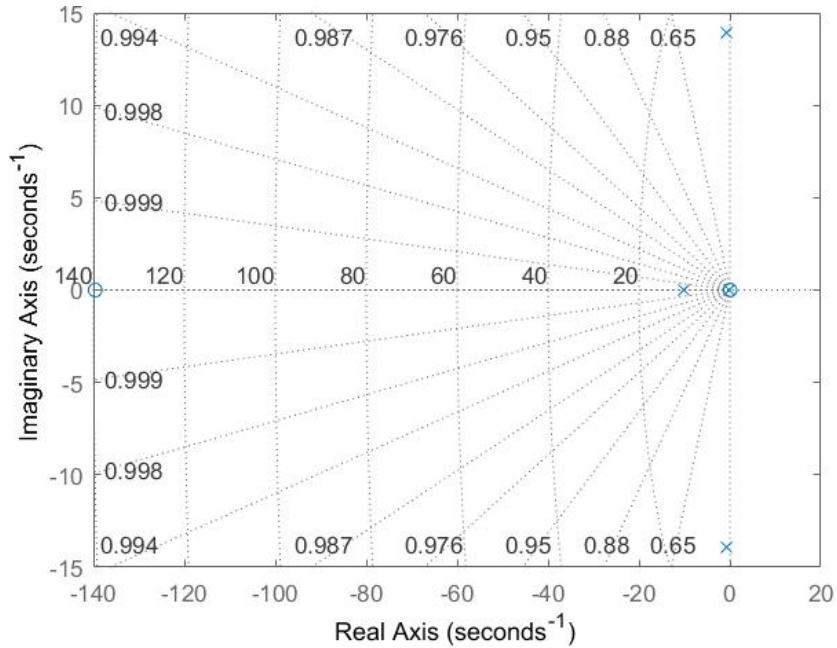


Diagram. 7. Pole-zero map of the open loop: pitch angle to output power relation

Poles:

- 0.6243 +13.8855i
- 0.6243 -13.8855i
- 10.2821
- 0.1759

From the diagram 8, it can be seen that the all the poles are in Left Half Plane (LHP) showing that the model is stable

Also in the diagram 8, the zero of the system can be identified

- Zeros:
- 139.6037
 - 4.349e-6

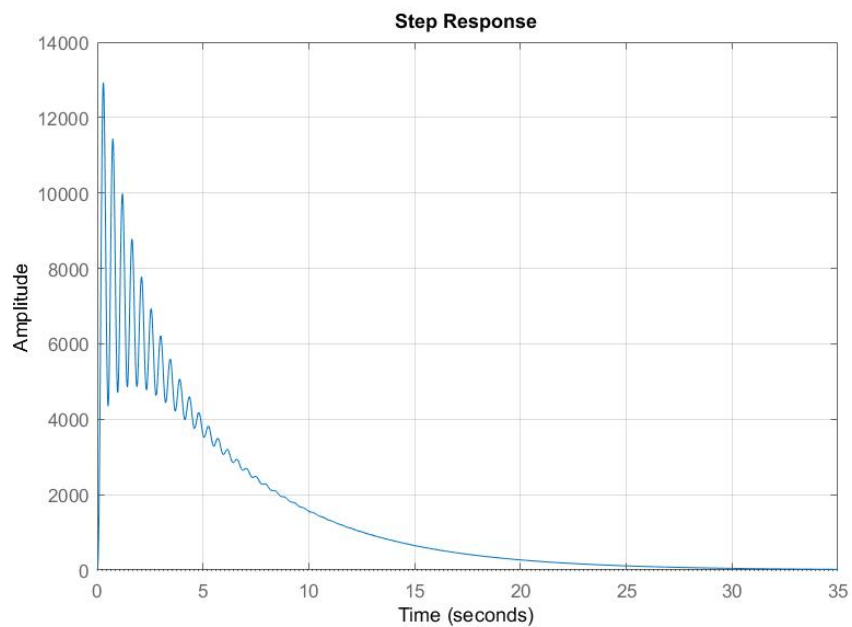
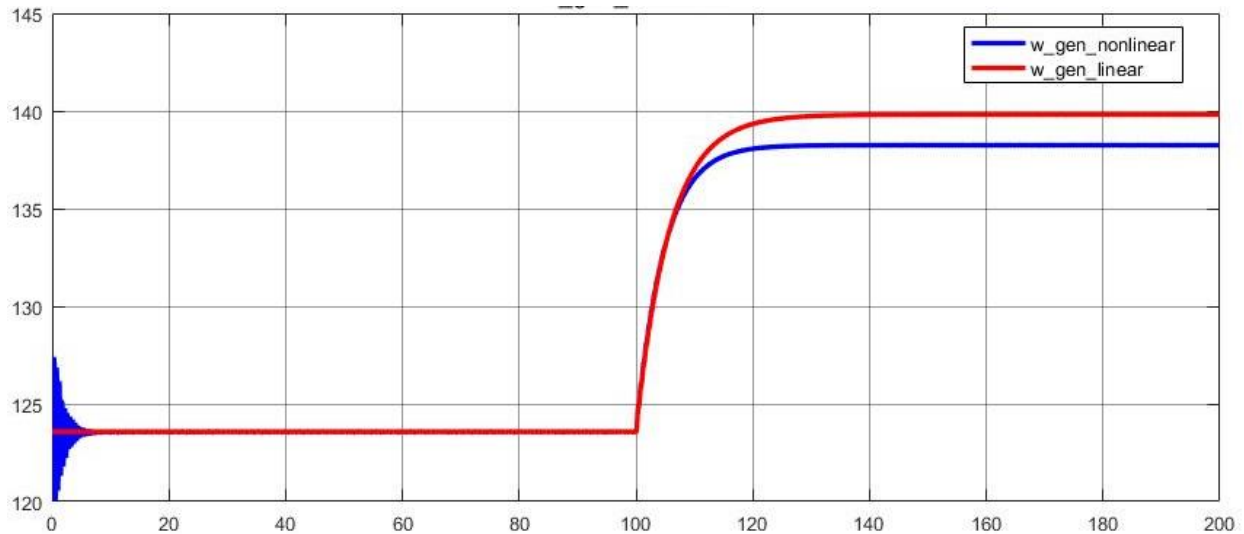


Diagram. 8. Step response of the open loop: pitch angle to output power relation

2.3.8. Linearized model vs. nonlinear model

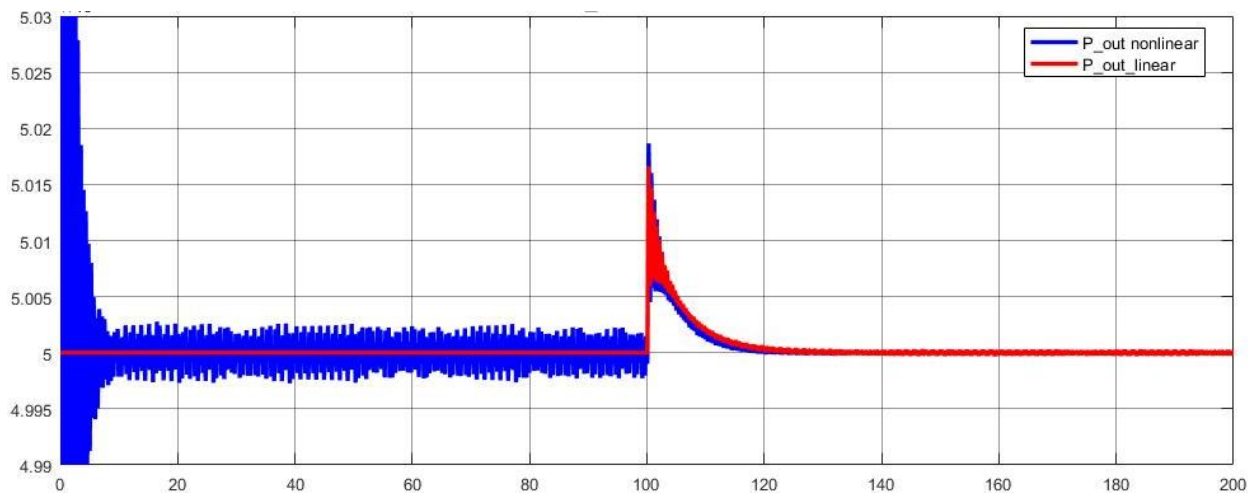
In the figure below it can be seen the comparison between the generator angular velocity ω obtained from the nonlinear model and the one obtained from the linearized model:



Graph 8. Generator angular velocity response of the nonlinear vs. linearized model

From the above graph, it can be seen that there is an acceptable difference between the outputs of the nonlinear and linearized model due to the errors ($e_{\omega_{gen}}=-1.574$) occurred using the Taylor series approximation for linearizing the nonlinear equations.

In the figure below it can be seen the comparison between the output power P_{out} obtained from the nonlinear model and the one obtained from the linearized model:



Graph 9. Output power response of the nonlinear vs. linearized model

From the above graph, it can be seen the high accuracy between the nonlinear and linearize output power ($e_{P_{out}}=-109.6$ [kW]).

2.4. Linearized model with uncertainties

In the current subchapter are added the uncertainties to the most uncertain parameters. The summary of the linearized mathematical model with uncertainties, its state-space representation and a comparison with the nonlinear model are also presented [16] [17].

2.4.1. Defining uncertainties

First step in defining the uncertainties consists in identifying the most uncertain parameters and their nominal values:

$\bar{I}_{rot} = 3.544e + 8$	Rotor moment of inertia	$\bar{N} = 97$	Gear ratio
$\bar{K}_{shaft} = 8.676e + 8$	Main shaft spring constant	$\bar{a} = 1.202e + 6$	M_{rot} 's v_{rot} coefficient
$\bar{B}_{shaft} = 6.215e + 6$	Main shaft viscous friction	$\bar{b} = -1.044e + 07$	M_{rot} 's Ω coefficient
$\bar{I}_{gen} = 534.116$	Generator Moment of inertia	$\bar{c} = -9.313e + 05$	M_{rot} 's β coefficient
$\bar{G}_{eff} = 0.944$	Generator efficiency		

Second step in developing a linearized model with uncertainties is to define the uncertainty intervals within the parameters are ensured they variate:

$$\frac{1}{I_{rot}} = \frac{1}{\bar{I}_{rot} \cdot (1 + P_{Irot} \cdot \delta_{Irot})} \quad \text{Eq. 70}$$

$$K_{shaft} = \bar{K}_{shaft} \cdot (1 + P_{Kshaft} \cdot \delta_{Kshaft}) \quad \text{Eq. 71}$$

$$B_{shaft} = \bar{B}_{shaft} \cdot (1 + P_{Bshaft} \cdot \delta_{Bshaft}) \quad \text{Eq. 72}$$

$$\frac{1}{I_{gen}} = \frac{1}{\bar{I}_{gen} \cdot (1 + P_{Igen} \cdot \delta_{Igen})} \quad \text{Eq. 73}$$

$$G_{eff} = \bar{G}_{eff} \cdot (1 + P_{Geff} \cdot \delta_{Geff}) \quad \text{Eq. 74}$$

$$a = \bar{a} \cdot (1 + P_a \cdot \delta_a) \quad \text{Eq. 75}$$

$$b = \bar{b} \cdot (1 + P_b \cdot \delta_b) \quad \text{Eq. 76}$$

$$c = \bar{c} \cdot (1 + P_c \cdot \delta_c) \quad \text{Eq. 77}$$

Where

$P_{Irot} = 10\%$ represents the uncertainty in the rotor moment of inertia;

$P_{Kshaft} = 30\%$ represents the uncertainty in the main shaft spring constant;



$P_{Bshaft} = 20\%$ represents the uncertainty in the main shaft viscous friction;

$P_N = 10\%$ represents the uncertainty in gear ratio;

$P_{Igen} = 10\%$ represents the uncertainty in the generator moment of inertia;

$P_{Geff} = 10\%$ represents the uncertainty in the generator efficiency;

$P_a = 30\%$ represents the uncertainty in Mrot's v_{rot} coefficient;

$P_b = 30\%$ represents the uncertainty in Mrot's Ω coefficient;

$P_c = 30\%$ represents the uncertainty in Mrot's β coefficient;

$\delta_{Irot}, \delta_{Kshaft}, \delta_{Bshaft}, \delta_{Igen}, \delta_{Geff}, \delta_a, \delta_b, \delta_c$ represents the relative perturbations from the nominal values presented in the beginning of the current section which can vary between ± 1 :

$$-1 \leq \delta_{Irot}, \delta_{Kshaft}, \delta_{Bshaft}, \delta_{Igen}, \delta_{Rot}, \delta_{Geff}, \delta_a, \delta_b, \delta_c \leq 1$$

Next step in modeling the state space together with the uncertainty parameters consists in replacing the block parameters $I_{rot}, K_{shaft}, B_{shaft}, I_{gen}, G_{eff}, a, b, c$ by $\bar{I}_{rot}, \bar{K}_{shaft}, \bar{B}_{shaft}, \bar{I}_{gen}, \bar{c}_{gen}, \bar{G}_{eff}, \bar{a}, \bar{b}, \bar{c}, P_{Irot}, P_{Kshaft}, P_{Bshaft}, P_{Igen}, P_{Geff}, P_a, P_b, P_c, \delta_{Irot}, \delta_{Kshaft}, \delta_{Bshaft}, \delta_{Igen}, \delta_a, \delta_b, \delta_c$ in a unified approach with the Linear Fractional Transformation (LFT) in $\delta_{Irot}, \delta_{Kshaft}, \delta_{Bshaft}, \delta_{Igen}, \delta_{Geff}, \delta_a, \delta_b, \delta_c, \delta_{a1}, \delta_{a2}, \delta_{b2}$

In the following equation $\frac{1}{I_{rot}}$ is represented as LFT in δ_{rot}

$$\begin{aligned} \frac{1}{I_{rot}} &= \frac{1}{\bar{I}_{rot} \cdot (1 + P_{Irot} \cdot \delta_{Irot})} = \frac{1 + P_{Irot} \cdot \delta_{Irot} - P_{Irot} \cdot \delta_{Irot}}{\bar{I}_{rot} \cdot (1 + P_{Irot} \cdot \delta_{Irot})} = \\ &= \frac{1 + P_{Irot} \cdot \delta_{Irot}}{\bar{I}_{rot} \cdot (1 + P_{Irot} \cdot \delta_{Irot})} - \frac{P_{Irot} \cdot \delta_{Irot}}{\bar{I}_{rot} \cdot (1 + P_{Irot} \cdot \delta_{Irot})} = \\ &= \frac{1}{\bar{I}_{rot}} - \frac{P_{Irot}}{\bar{I}_{rot}} \cdot \delta_{Irot} \cdot (\bar{I}_{rot} + P_{Irot} \cdot \delta_{Irot})^{-1} = F_u(M_{Irot}, \delta_{Irot}) \end{aligned} \quad \text{Eq. 78}$$

Where in general $F_u(M, \delta)$ represents the upper LFT:

$$F_u(M, \delta) = M_{22} + M_{21} \cdot \delta \cdot (I - M_{11} \cdot \delta)^{-1} \cdot M_{12} \quad \text{Eq. 79}$$

In the above equations, the matrix M_{Irot} was identified as:

$$M_{Irot} = \begin{bmatrix} -P_{Irot} & \frac{1}{\bar{I}_{rot}} \\ -P_{Irot} & \frac{1}{\bar{I}_{rot}} \end{bmatrix} \quad \text{Eq. 80}$$

The LFT representation of K_{shaft} in δ_{Kshaft} is

$$K_{shaft} = \bar{K}_{shaft} + \bar{K}_{shaft} \cdot P_{Kshaft} \cdot \delta_{Kshaft} = F_u(M_{Kshaft}, \delta_{Kshaft}) \quad \text{Eq. 81}$$

Where M_{Kshaft} was identified as:

$$M_{Kshaft} = \begin{bmatrix} 0 & \bar{K}_{shaft} \\ P_{Kshaft} & \bar{K}_{shaft} \end{bmatrix} \quad \text{Eq. 82}$$

The LFT representation of B_{shaft} in δ_{Bshaft} is

$$B_{shaft} = \bar{B}_{shaft} + \bar{B}_{shaft} \cdot P_{Bshaft} \cdot \delta_{Bshaft} = F_u(M_{Bshaft}, \delta_{Bshaft}) \quad \text{Eq. 83}$$

Where M_{Kshaft} was identified as:

$$M_{Bshaft} = \begin{bmatrix} 0 & \bar{B}_{shaft} \\ P_{Bshaft} & \bar{B}_{shaft} \end{bmatrix} \quad \text{Eq. 84}$$

The LFT representation of $\frac{1}{I_{gen}}$ in δ_{Igen}

$$\frac{1}{I_{gen}} = \frac{1}{\bar{I}_{gen}} - \frac{P_{Igen}}{\bar{I}_{gen}} \cdot \delta_{Igen} \cdot (\bar{I}_{gen} + P_{Igen} \cdot \delta_{Igen})^{-1} = F_u(M_{Igen}, \delta_{Igen}) \quad \text{Eq. 85}$$

Where M_{Igen} was identified as:

$$M_{Igen} = \begin{bmatrix} -P_{Igen} & \frac{1}{\bar{I}_{gen}} \\ -P_{Igen} & \frac{1}{\bar{I}_{gen}} \end{bmatrix} \quad \text{Eq. 86}$$

The LFT representation of G_{eff} in δ_{Geff} is

$$G_{eff} = \bar{G}_{eff} + \bar{G}_{eff} \cdot P_{Geff} \cdot \delta_{Geff} = F_u(M_{Geff}, \delta_{Geff}) \quad \text{Eq. 87}$$

Where M_{Rot} was identified as:

$$M_{Geff} = \begin{bmatrix} 0 & \bar{G}_{eff} \\ P_{Geff} & \bar{G}_{eff} \end{bmatrix} \quad \text{Eq. 88}$$

The LFT representation of a in δ_a is

$$a = \bar{a} + \bar{a} \cdot P_a \cdot \delta_a = F_u(M_a, \delta_a) \quad \text{Eq. 89}$$

Where M_a was identified as:

$$M_a = \begin{bmatrix} 0 & \bar{a} \\ P_a & \bar{a} \end{bmatrix} \quad \text{Eq. 90}$$

The LFT representation of b in δ_b is

$$b = \bar{b} + \bar{b} \cdot P_b \cdot \delta_b = F_u(M_b, \delta_b) \quad \text{Eq. 91}$$

Where M_b was identified as:

$$M_b = \begin{bmatrix} 0 & \bar{b} \\ P_b & \bar{b} \end{bmatrix} \quad \text{Eq. 92}$$

The LFT representation of c in δ_c is

$$c = \bar{c} + \bar{c} \cdot P_c \cdot \delta_c = F_u(M_c, \delta_c) \quad \text{Eq. 93}$$

Where M_c was identified as:

$$M_c = \begin{bmatrix} 0 & \bar{c} \\ P_c & \bar{c} \end{bmatrix} \quad \text{Eq. 94}$$

2.4.2. Summary of the linearized model with uncertainties

The identified uncertainties are added to linearized model and the following equations are obtained:

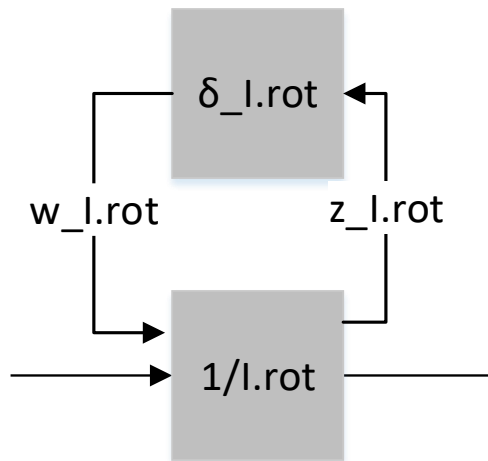


Diagram. 9. Block diagram of the rotor inertia with uncertainty

$$\begin{bmatrix} z_{Irot} \\ \dot{\Omega} \end{bmatrix} = \begin{bmatrix} -P_{Irot} & \frac{1}{I_{rot}} \\ -P_{Irot} & \frac{1}{I_{rot}} \end{bmatrix} \cdot \begin{bmatrix} w_{Irot} \\ M_{rot} - V \end{bmatrix} \quad \text{Eq. 95}$$

By solving the above equation system, we obtain the following 2 equations:

$$\dot{\Omega} = -P_{Irot} \cdot w_{Irot} + \frac{1}{I_{rot}} \cdot (M_{rot} - V) \quad \text{Eq. 96}$$

$$z_{Irot} = -P_{Irot} \cdot u_{Irot} + \frac{1}{I_{rot}} \cdot (M_{rot} - V) \quad \text{Eq. 97}$$

Where

$$w_{Irot} = \delta_{Irot} \cdot z_{Irot} \quad \text{Eq. 98}$$

$$V = M_{shaft} + V_{Bshaft} \quad \text{Eq. 99}$$

(equation obtained from the Block diagram 2)

$$M_{rot} = Va + Vb + Vc \quad \text{Eq. 100}$$

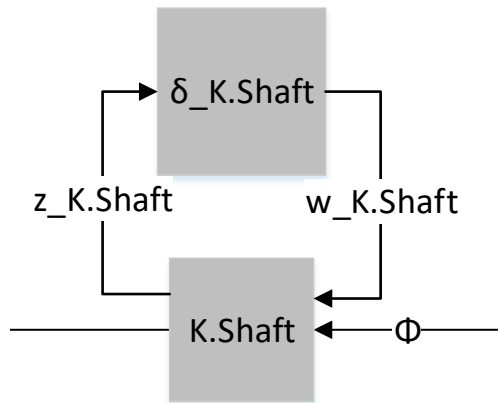


Diagram. 10. Block diagram of the main shaft spring constant with uncertainty

$$\begin{bmatrix} z_{Kshaft} \\ M_{shaft} \end{bmatrix} = \begin{bmatrix} 0 & \bar{K}_{shaft} \\ P_{Kshaft} & \bar{K}_{shaft} \end{bmatrix} \cdot \begin{bmatrix} w_{Kshaft} \\ \Phi \end{bmatrix} \quad \text{Eq. 101}$$

By solving the above equation system, we obtain the following 2 equations:

$$z_{Kshaft} = \bar{K}_{shaft} \cdot \Phi \quad \text{Eq. 102}$$

$$M_{shaft} = P_{Kshaft} \cdot w_{Kshaft} + \bar{K}_{shaft} \cdot \Phi \quad \text{Eq. 103}$$

where

$$w_{Kshaft} = \delta_{Kshaft} \cdot z_{Kshaft} \quad \text{Eq. 104}$$

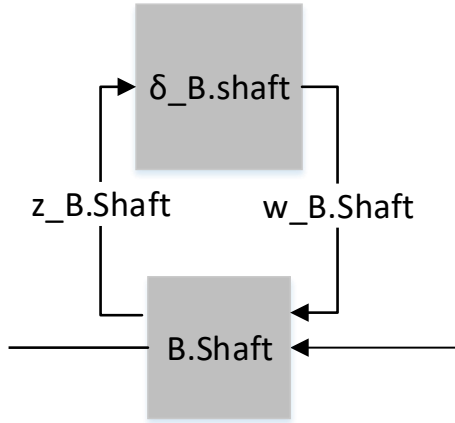


Diagram. 11. Block diagram of the main shaft viscous friction with uncertainty

$$\begin{bmatrix} Z_{Bshaft} \\ V_{Bshaft} \end{bmatrix} = \begin{bmatrix} 0 & \bar{B}_{shaft} \\ P_{Bshaft} & \bar{B}_{shaft} \end{bmatrix} \cdot \begin{bmatrix} w_{Bshaft} \\ \dot{\phi} \end{bmatrix} \quad \text{Eq. 105}$$

By solving the above equation system, we obtain the following 2 equations:

$$Z_{Bshaft} = \bar{B}_{shaft} \cdot \dot{\phi} \quad \text{Eq. 106}$$

$$V_{Bshaft} = P_{Bshaft} \cdot w_{Bshaft} + \bar{B}_{shaft} \cdot \dot{\phi} \quad \text{Eq. 107}$$

where

$$w_{Bshaft} = \delta_{Bshaft} \cdot Z_{Bshaft} \quad \text{Eq. 108}$$

$$\begin{bmatrix} Z_{Igen} \\ \dot{\omega} \end{bmatrix} = \begin{bmatrix} -P_{Igen} & \frac{1}{I_{gen}} \\ -P_{Igen} & \frac{1}{I_{gen}} \end{bmatrix} \cdot \begin{bmatrix} w_{Igen} \\ V_{N1} - M_{gen} \end{bmatrix} \quad \text{Eq. 109}$$

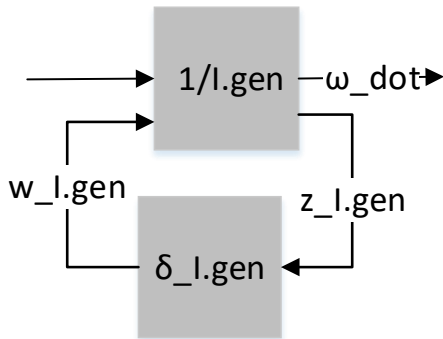


Diagram. 12. Block diagram of the generator inertia with uncertainty

By solving the equation system eq. 109, we obtain the following 2 equations:

$$Z_{Igen} = -P_{Igen} \cdot w_{Igen} + \frac{1}{I_{gen}} \cdot (V_{N1} - M_{gen}) \quad \text{Eq. 110}$$

$$\dot{\omega} = -P_{Igen} \cdot w_{Igen} + \frac{1}{I_{gen}} \cdot (V_{N1} - M_{gen}) \quad \text{Eq. 111}$$

Where

$$w_{Igen} = \delta_{Igen} \cdot Z_{Igen} \quad \text{Eq. 112}$$

From block diagram 2, it can be seen that:

$$\dot{\phi} = \Omega - \frac{1}{N} \cdot \omega \quad \text{Eq. 113}$$

$$V_{N1} = \frac{1}{N} \cdot (M_{shaft} + V_{Bshaft}) \quad \text{Eq. 114}$$

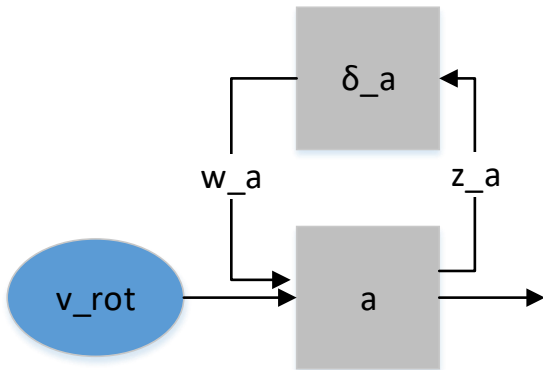


Diagram. 13. Block diagram of the Mrot's vrot coefficient with uncertainty

$$\begin{bmatrix} Z_a \\ V_a \end{bmatrix} = \begin{bmatrix} 0 & \bar{a} \\ P_a & \bar{a} \end{bmatrix} \cdot \begin{bmatrix} w_a \\ v_{rot} \end{bmatrix} \quad \text{Eq. 115}$$

By solving the above equation system, we obtain the following 2 equations:

$$Z_a = \bar{a} \cdot v_{rot} \quad \text{Eq. 116}$$

$$V_a = P_a \cdot w_a + \bar{a} \cdot v_{rot} \quad \text{Eq. 117}$$

Where

$$w_a = \delta_a \cdot Z_a \quad \text{Eq. 118}$$

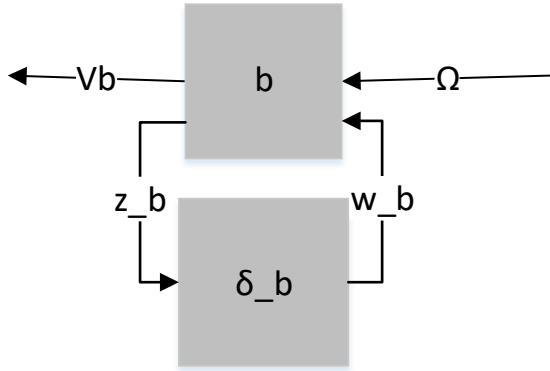


Diagram. 14. Block diagram of the Mrot's Ω coefficient with uncertainty

$$\begin{bmatrix} z_b \\ V_b \end{bmatrix} = \begin{bmatrix} 0 & \bar{b} \\ P_b & \bar{b} \end{bmatrix} \cdot \begin{bmatrix} w_b \\ \Omega \end{bmatrix} \quad \text{Eq. 119}$$

By solving the above equation system, we obtain the following 2 equations:

$$z_b = \bar{b} \cdot \Omega \quad \text{Eq. 120}$$

$$V_b = P_b \cdot w_b + \bar{b} \cdot \Omega \quad \text{Eq. 121}$$

Where

$$w_b = \delta_b \cdot z_b \quad \text{Eq. 122}$$

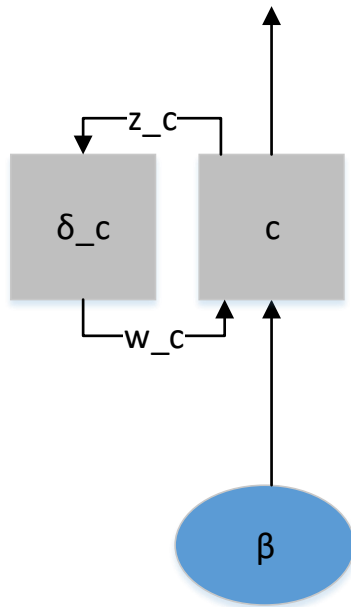


Diagram. 15. Block diagram of the Mrot's β coefficient with uncertainty

$$\begin{bmatrix} z_c \\ V_c \end{bmatrix} = \begin{bmatrix} 0 & \bar{c} \\ P_c & \bar{c} \end{bmatrix} \cdot \begin{bmatrix} w_c \\ \beta \end{bmatrix} \quad \text{Eq. 123}$$

By solving the above equation system, we obtain the following 2 equations:

$$z_c = \bar{c} \cdot \beta \quad \text{Eq. 124}$$

$$V_c = P_c \cdot w_c + \bar{c} \cdot \beta \quad \text{Eq. 125}$$

Where

$$w_c = \delta_c \cdot z_c \quad \text{Eq. 126}$$

$$\ddot{\beta} = \frac{\text{Pitch}_{delay} \cdot K \cdot B_{ref} - \text{Pitch}_{delay} \cdot K \cdot B_{meas} - \dot{\beta}}{\tau_{pitch}} \quad \text{Eq. 127}$$



Integrating the equations eq. 92 – eq. 127 into the linearized model and simplifying all the resulting equations, the following system of equations is obtained:

$$\begin{aligned} \dot{\Omega} = & -P_{Irot} \cdot w_{Irot} + \frac{1}{\bar{I}_{Irot}} \cdot P_a \cdot w_a + \frac{1}{\bar{I}_{Irot}} \cdot \bar{a} \cdot v_{rot} + \frac{1}{\bar{I}_{Irot}} \cdot P_b \cdot w_b + \frac{1}{\bar{I}_{Irot}} \cdot \bar{b} \cdot \Omega + \frac{1}{\bar{I}_{Irot}} \cdot P_c \cdot w_c + \frac{1}{\bar{I}_{Irot}} \cdot \\ & \bar{c} \cdot \beta - \frac{1}{\bar{I}_{Irot}} \cdot P_{Kshaft} \cdot w_{Kshaft} - \frac{1}{\bar{I}_{Irot}} \cdot \bar{K}_{shaft} \cdot \Phi - \frac{1}{\bar{I}_{Irot}} \cdot P_{Bshaft} \cdot w_{Bshaft} - \frac{1}{\bar{I}_{Irot}} \cdot \bar{B}_{shaft} \cdot \Omega + \\ & \frac{1}{\bar{I}_{Irot}} \cdot \bar{B}_{shaft} \cdot \frac{1}{N} \cdot \omega \end{aligned} \quad \text{Eq. 128}$$

$$\begin{aligned} z_{Irot} = & -P_{Irot} \cdot w_{Irot} + \frac{1}{\bar{I}_{Irot}} \cdot P_a \cdot w_a + \frac{1}{\bar{I}_{Irot}} \cdot \bar{a} \cdot v_{rot} + \frac{1}{\bar{I}_{Irot}} \cdot P_b \cdot w_b + \frac{1}{\bar{I}_{Irot}} \cdot \bar{b} \cdot \Omega + \frac{1}{\bar{I}_{Irot}} \cdot P_c \cdot w_c + \\ & \frac{1}{\bar{I}_{Irot}} \cdot \bar{c} \cdot \beta - \frac{1}{\bar{I}_{Irot}} \cdot P_{Kshaft} \cdot w_{Kshaft} - \frac{1}{\bar{I}_{Irot}} \cdot \bar{K}_{shaft} \cdot \Phi - \frac{1}{\bar{I}_{Irot}} \cdot P_{Bshaft} \cdot w_{Bshaft} - \frac{1}{\bar{I}_{Irot}} \cdot \bar{B}_{shaft} \cdot \\ & \Omega + \frac{1}{\bar{I}_{Irot}} \cdot \bar{B}_{shaft} \cdot \frac{1}{N} \cdot \omega \end{aligned} \quad \text{Eq. 129}$$

$$z_{Kshaft} = \bar{K}_{shaft} \cdot \Phi \quad \text{Eq. 130}$$

$$z_{Bshaft} = \bar{B}_{shaft} \cdot \Omega - \bar{B}_{shaft} \cdot \frac{1}{N} \cdot \omega \quad \text{Eq. 131}$$

$$\begin{aligned} z_{Igen} = & -P_{Igen} \cdot w_{Igen} + \frac{1}{\bar{I}_{gen}} \cdot \frac{1}{N} \cdot P_{Kshaft} \cdot w_{Kshaft} + \frac{1}{\bar{I}_{gen}} \cdot \frac{1}{N} \cdot \bar{K}_{shaft} \cdot \Phi + \frac{1}{\bar{I}_{gen}} \cdot \frac{1}{N} \cdot P_{Bshaft} \cdot \\ w_{Bshaft} & + \frac{1}{\bar{I}_{gen}} \cdot \frac{1}{N} \cdot \bar{B}_{shaft} \cdot \Omega - \frac{1}{\bar{I}_{gen}} \cdot \frac{1}{N} \cdot \bar{B}_{shaft} \cdot \frac{1}{N} \cdot \omega - \frac{1}{\bar{I}_{gen}} \cdot M_{gen} \end{aligned} \quad \text{Eq. 132}$$

$$\begin{aligned} \dot{\omega} = & -P_{Igen} \cdot w_{Igen} + \frac{1}{\bar{I}_{gen}} \cdot \frac{1}{N} \cdot P_{Kshaft} \cdot w_{Kshaft} + \frac{1}{\bar{I}_{gen}} \cdot \frac{1}{N} \cdot \bar{K}_{shaft} \cdot \Phi + \frac{1}{\bar{I}_{gen}} \cdot \frac{1}{N} \cdot P_{Bshaft} \cdot w_{Bshaft} + \\ & \frac{1}{\bar{I}_{gen}} \cdot \frac{1}{N} \cdot \bar{B}_{shaft} \cdot \Omega - \frac{1}{\bar{I}_{gen}} \cdot \frac{1}{N} \cdot \bar{B}_{shaft} \cdot \frac{1}{N} \cdot \omega - \frac{1}{\bar{I}_{gen}} \cdot M_{gen} \end{aligned} \quad \text{Eq. 133}$$

$$\dot{\Phi} = \Omega - \frac{1}{N_2} \cdot \omega \quad \text{Eq. 134}$$

$$z_a = \bar{a} \cdot v_{rot} \quad \text{Eq. 135}$$

$$z_b = \bar{b} \cdot \Omega \quad \text{Eq. 136}$$

$$z_c = \bar{c} \cdot \beta \quad \text{Eq. 137}$$

$$V_{a1} = \bar{a1} \cdot \omega \quad \text{Eq. 138}$$

$$P_{outnet} = \bar{G}_{eff} \cdot \bar{a2} \cdot M_{gen} + \bar{G}_{eff} \cdot \bar{b2} \cdot \omega \quad \text{Eq. 139}$$

$$\dot{M}_{gen} = \frac{1}{\tau_{gen}} \cdot \bar{a1} \cdot \omega - \frac{1}{\tau_{gen}} \cdot M_{gen} \quad \text{Eq. 140}$$

The diagram below represents the graphical representation of the linearized model with uncertainties where the constant blocks in diagram 2, have been replaced by block diagrams in depicted in figure:

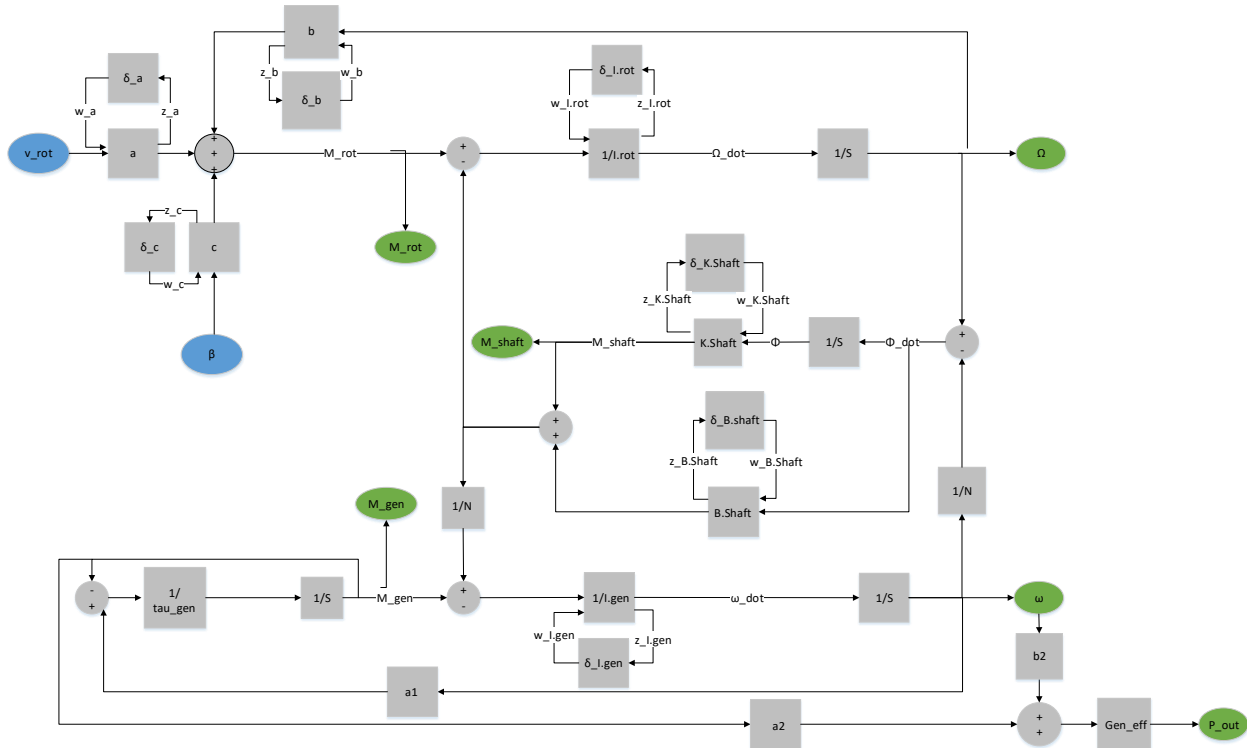


Diagram. 16. Block diagram of the linearized model with uncertainties

2.4.3. State-space linearized model with uncertainties

Before writing the above equations into state space representation, the state vector x with 4 states, the perturbations input vector w with 7 inputs, the input vector u with 2 inputs, the perturbations output vector z with 7 outputs and the output vector y with 2 outputs are defined as below:

$$x = \begin{bmatrix} x_1 \\ x_2 \\ x_3 \\ x_4 \end{bmatrix} = \begin{bmatrix} \Omega \\ \omega \\ \Phi \\ M_{gen} \end{bmatrix} \quad
 w = \begin{bmatrix} W_{Irot} \\ W_{Kshaft} \\ W_{Bshaft} \\ W_{Igen} \\ W_a \\ W_b \\ W_c \end{bmatrix} \quad
 u = \begin{bmatrix} v_{rot} \\ \beta \end{bmatrix} \quad
 z = \begin{bmatrix} Z_{Irot} \\ Z_k \\ Z_B \\ Z_{Igen} \\ Z_a \\ Z_b \\ Z_c \end{bmatrix} \quad
 y = \begin{bmatrix} \omega \\ P_{outnet} \end{bmatrix}$$

The linearized model is described by the following state-space model with 9 outputs, 9 inputs, and 4 states.:

$$\begin{cases} \dot{x} = A \cdot x + B_w \cdot w + B_u \cdot u \\ z = C_w \cdot x + D_{zw} \cdot w + D_{zu} \cdot u \\ y = C_y \cdot x + D_{yw} \cdot w + D_{yu} \cdot u \end{cases} \quad \text{Eq. 141}$$

$$\begin{cases} \dot{x} \\ z \\ y \end{cases} = \begin{bmatrix} A & B_w & B_u \\ C_w & D_{zw} & D_{zu} \\ C_y & D_{yw} & D_{yu} \end{bmatrix} \cdot \begin{bmatrix} x \\ w \\ u \end{bmatrix} \quad \text{Eq. 142}$$

For the above equation, the states matrix A is identified as:

$$A = \begin{bmatrix} \frac{1}{\bar{I}_{rot}} \cdot \bar{b} - \frac{1}{\bar{I}_{rot}} \cdot \bar{B}_{shaft} & \frac{1}{\bar{I}_{rot}} \cdot \bar{B}_{shaft} \cdot \frac{1}{\bar{N}} & -\frac{1}{\bar{I}_{rot}} \cdot \bar{K}_{shaft} & 0 \\ \frac{1}{\bar{I}_{gen}} \cdot \frac{1}{\bar{N}} \cdot \bar{B}_{shaft} & -\frac{1}{\bar{I}_{gen}} \cdot \frac{1}{\bar{N}^2} \cdot \bar{B}_{shaft} & \frac{1}{\bar{I}_{gen}} \cdot \frac{1}{\bar{N}} \cdot \bar{K}_{shaft} & -\frac{1}{\bar{I}_{gen}} \\ 1 & -\frac{1}{\bar{N}} & 0 & 0 \\ 0 & \frac{1}{\tau_{gen}} \cdot \bar{a}1 & 0 & -\frac{1}{\tau_{gen}} \end{bmatrix} \quad \text{Eq. 143}$$

For equation eq. 142 the perturbations input matrix Bw, is identified as:

$$B_w = \begin{bmatrix} -P_{Irot} & -\frac{1}{\bar{I}_{rot}} \cdot P_{Kshaft} - \frac{1}{\bar{I}_{rot}} \cdot P_{Bshaft} & 0 & \frac{1}{\bar{I}_{rot}} \cdot P_a \frac{1}{\bar{I}_{rot}} \cdot P_b \frac{1}{\bar{I}_{rot}} \cdot P_c \\ 0 & \frac{1}{\bar{I}_{gen}} \cdot \frac{1}{\bar{N}} \cdot P_{Kshaft} \frac{1}{\bar{I}_{gen}} \cdot \frac{1}{\bar{N}} \cdot P_{Bshaft} & -P_{Igen} & 0 \\ 0 & 0 & 0 & 0 \\ 0 & 0 & 0 & 0 \end{bmatrix} \quad \text{Eq. 144}$$

For equation eq. 142 the input matrix Bu, is identified as:

$$B_u = \begin{bmatrix} \frac{1}{\bar{I}_{rot}} \cdot \bar{a} \frac{1}{\bar{I}_{rot}} \cdot \bar{c} \\ 0 \\ 0 \\ 0 \end{bmatrix} \quad \text{Eq. 145}$$

The state-space's perturbations output matrix related to states, Cw is identified as:

$$C_w = \begin{bmatrix} \frac{1}{\bar{I}_{rot}} \cdot \bar{b} - \frac{1}{\bar{I}_{rot}} \cdot \bar{B}_{shaft} & \frac{1}{\bar{I}_{rot}} \cdot \bar{B}_{shaft} \cdot \frac{1}{\bar{N}} & -\frac{1}{\bar{I}_{rot}} \cdot \bar{K}_{shaft} & 0 \\ 0 & 0 & \bar{K}_{shaft} & 0 \\ \bar{B}_{shaft} & -\bar{B}_{shaft} \cdot \frac{1}{\bar{N}} & 0 & -\frac{1}{\bar{I}_{gen}} \\ \frac{1}{\bar{I}_{gen}} \cdot \frac{1}{\bar{N}} \cdot \bar{B}_{shaft} & -\frac{1}{\bar{I}_{gen}} \cdot \bar{B}_{shaft} \cdot \frac{1}{\bar{N}^2} \frac{1}{\bar{I}_{gen}} \cdot \frac{1}{\bar{N}} \cdot \bar{K}_{shaft} & 0 & 0 \\ 0 & 0 & 0 & 0 \\ \bar{b} & 0 & 0 & 0 \\ 0 & 0 & 0 & 0 \end{bmatrix} \quad \text{Eq. 146}$$

The state-space's output matrix related to states, Cy is identified as:

$$C_y = \begin{bmatrix} 0 & 1 & 0 & 0 \\ 0 & G_{eff} & b20 & G_{eff} \cdot \bar{a}2 \end{bmatrix} \quad \text{Eq. 147}$$

The state-space's perturbations output matrix related directed to perturbations inputs, D_{zw} is identified as:

$$D_{zw} = \begin{bmatrix} -P_{Irot} & -\frac{1}{\bar{I}_{rot}} \cdot P_{Kshaft} & -\frac{1}{\bar{I}_{rot}} \cdot P_{Bshaft} & 0 & \frac{1}{\bar{I}_{rot}} \cdot P_a \frac{1}{\bar{I}_{rot}} \cdot P_b \frac{1}{\bar{I}_{rot}} \cdot P_c \\ 0 & 0 & 0 & 0 & 0 \\ 0 & 0 & 0 & 0 & 0 \\ 0 & \frac{1}{\bar{I}_{gen}} \cdot \frac{1}{\bar{N}} \cdot P_{Kshaft} & \frac{1}{\bar{I}_{gen}} \cdot \frac{1}{\bar{N}} \cdot P_{Bshaft} & -P_{Igen} & 0 \\ 0 & 0 & 0 & 0 & 0 \\ 0 & 0 & 0 & 0 & 0 \\ 0 & 0 & 0 & 0 & 0 \end{bmatrix} \quad \text{Eq. 148}$$

The state-space's perturbations output matrix related directed to inputs, D_{zu} is identified as:

$$D_{zu} = \begin{bmatrix} \frac{1}{\bar{I}_{rot}} \cdot \bar{a} \frac{1}{\bar{I}_{rot}} \cdot \bar{c} \\ 0 & 0 \\ 0 & 0 \\ 0 & 0 \\ \bar{a} & 0 \\ 0 & 0 \\ 0 & \bar{c} \end{bmatrix} \quad \text{Eq. 149}$$

The state-space's output matrix related directed to perturbations inputs, D_{yw} is identified as:

$$D_{yw} = \begin{bmatrix} 0000000 \\ 0000000 \end{bmatrix} \quad \text{Eq. 150}$$

The state-space's output matrix related directed to inputs, D_{yu} is identified as:

$$D_{yu} = \begin{bmatrix} 00 \\ 00 \end{bmatrix} \quad \text{Eq. 151}$$

The following transfer function represents the transfer function from the pitch angle β to generator angular velocity ω :

$$TF2_{\beta\omega_{gen}} = \frac{-3.152 \cdot s^2 - 471.6 \cdot s - 4400}{s^4 + 11.71 \cdot s^3 + 208.1 \cdot s^2 + 2023 \cdot s + 349.4} \quad \text{Eq. 152}$$

In the next figure, it can be seen the bode diagram of the linear model transfer function with uncertainties from the pitch angle β to generator angular velocity ω :

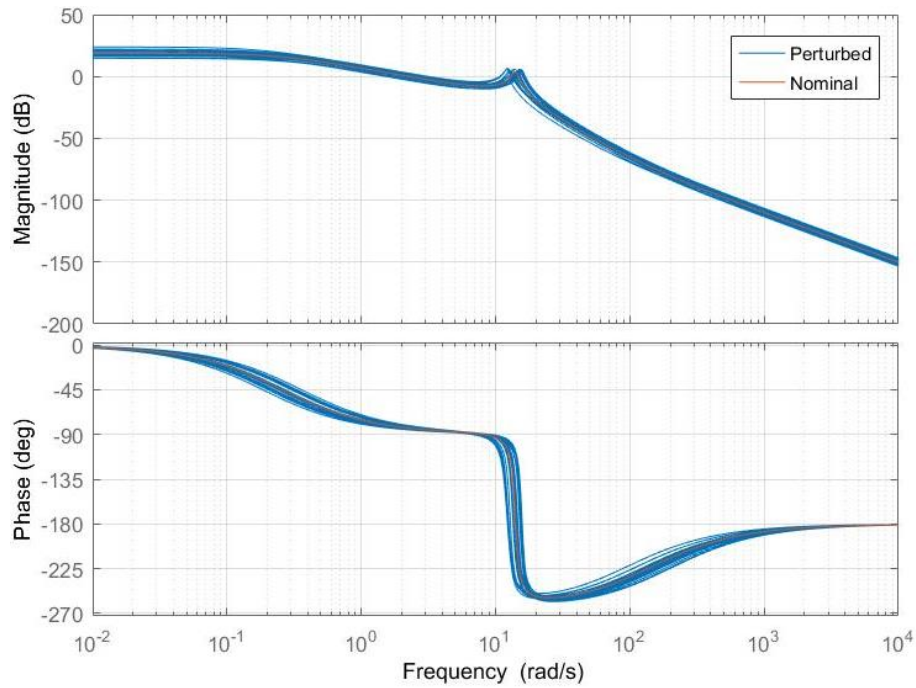


Diagram. 17. Bode diagram of the open loop with uncertainties: pitch angle to generator angular velocity relation

From above figure, for the nominal plant, it can be seen that the gain margin is -3.63 dB at 14.1 [rad/s] and the phase margin is -37.4 deg at 14.8 [rad/s].

Below it can be seen the pole-zero map of the linear model transfer function with uncertainties from the pitch angle β to generator angular velocity ω :

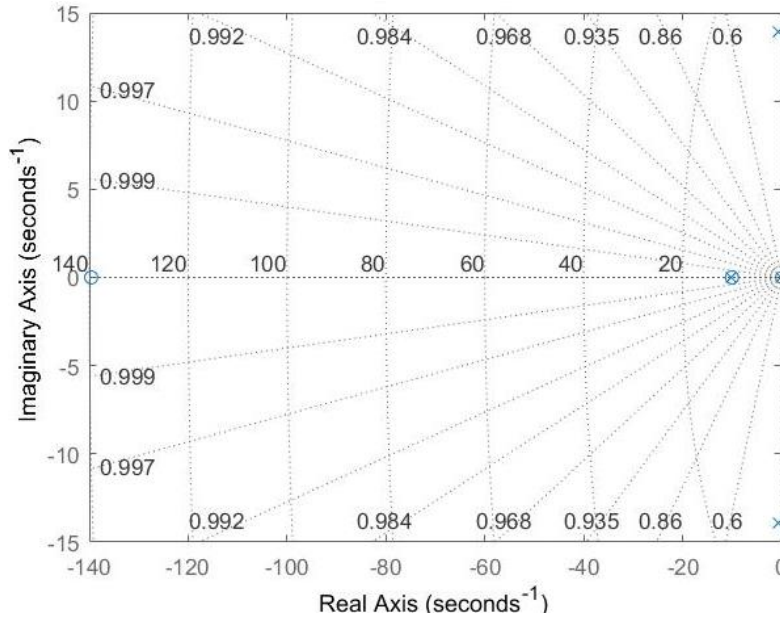


Diagram. 18. Pole-zero map of the open loop with uncertainties: pitch angle to generator angular velocity relation



Poles:	From the diagram 21, it	Also in the diagram	Zeros:
-0.6243 +13.8855i	can be seen that the all	21, the zero of the	-139.6037
-0.6243 -13.8855i	the poles are in Left Half	system can be	-10.0000
-10.2821	Plane (LHP) showing that	identified	
-0.1759	the model is stable		

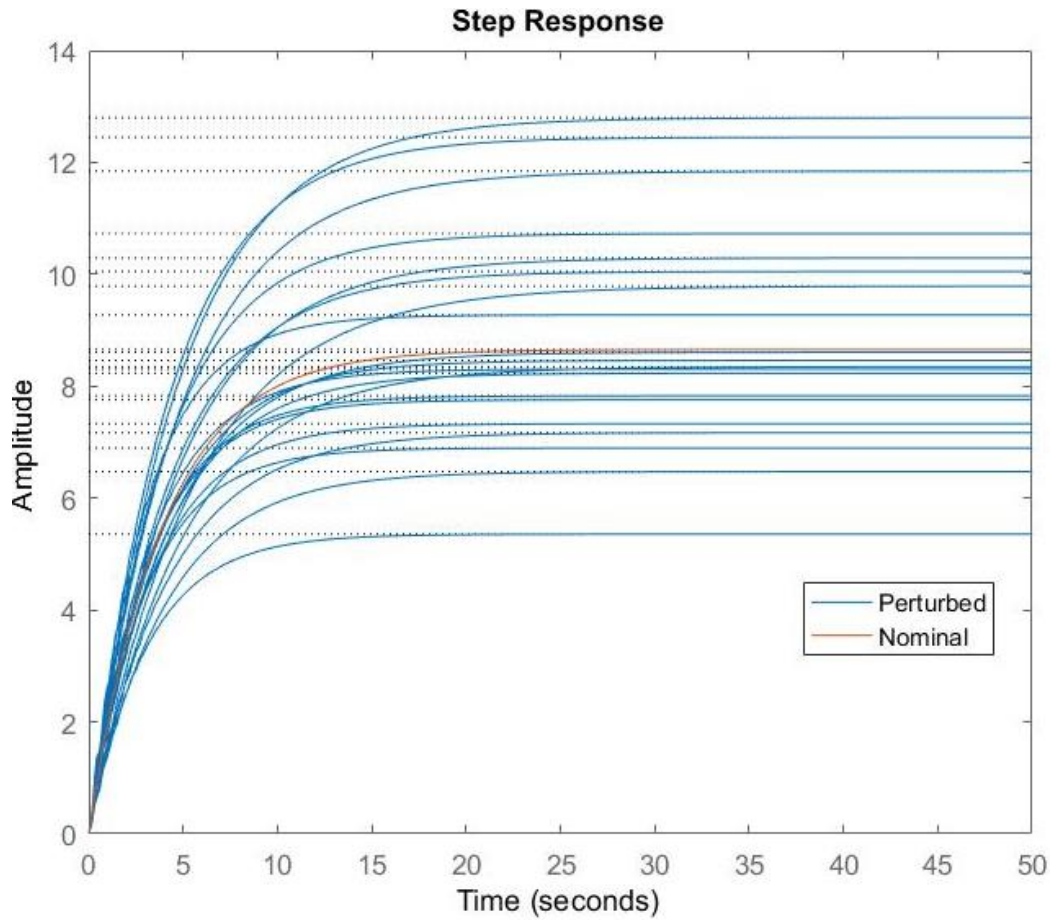


Diagram. 19. Step response of the open loop with uncertainties: pitch angle to generator angular velocity relation

The following transfer function represents the transfer function from the pitch angle β to output power P_{out} :

$$TF1_{\beta P_{out}} = \frac{-1.275e05 \cdot s^2 - 1.78e07 \cdot s + 77.43}{s^4 + 11.71 \cdot s^3 + 208.1 \cdot s^2 + 2023 \cdot s + 349.4} \quad \text{Eq. 153}$$

In the figure below it can be seen the bode diagram of the linear model with uncertainties transfer function from the pitch angle β to output power P_{out} :

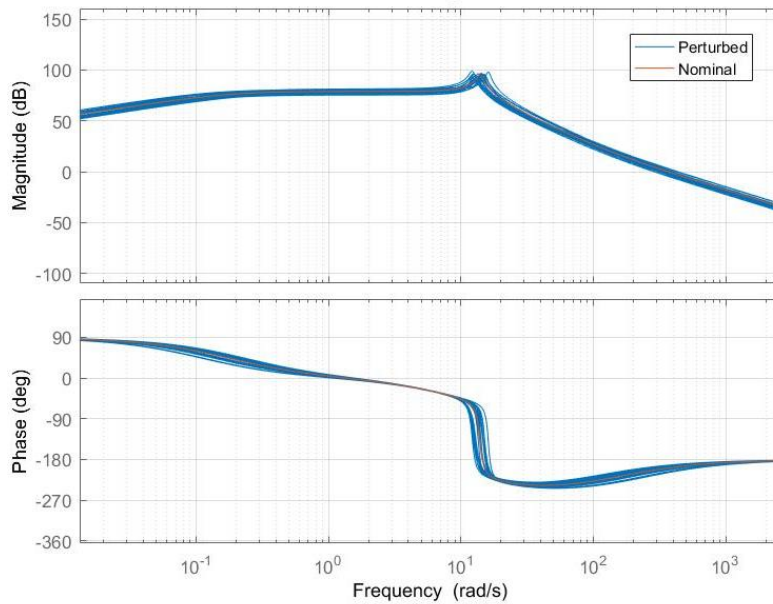


Diagram. 20. Bode diagram of the open loop with uncertainties: pitch angle to output power relation

From above figure, it can be seen that the gain margin is -92.3 dB at 14.5 [rad/s] and the minimum phase margin is 18.9 deg at 370[rad/s].

Below it can be seen the pole-zero map of the linear model with uncertainties transfer function from the pitch angle β to output power P_{out} :

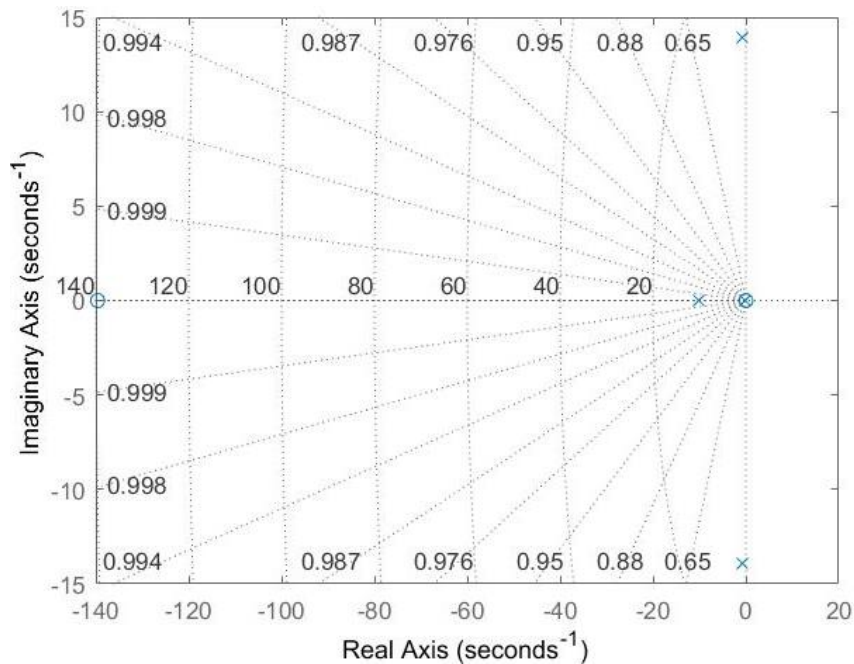


Diagram. 21. Pole-zero map of the open loop with uncertainties: pitch angle to output power relation



<p>Poles: -0.6243 +13.8855i -0.6243 -13.8855i -10.2821 -0.1759</p>	<p>From the above diagram, it can be seen that the all the poles are in Left Half Plane (LHP) showing that the model is stable</p>	<p>Also in the above figure, the zero of the system can be identified</p>	<p>Zeros: -139.6037 0.0000</p>
--	--	---	--

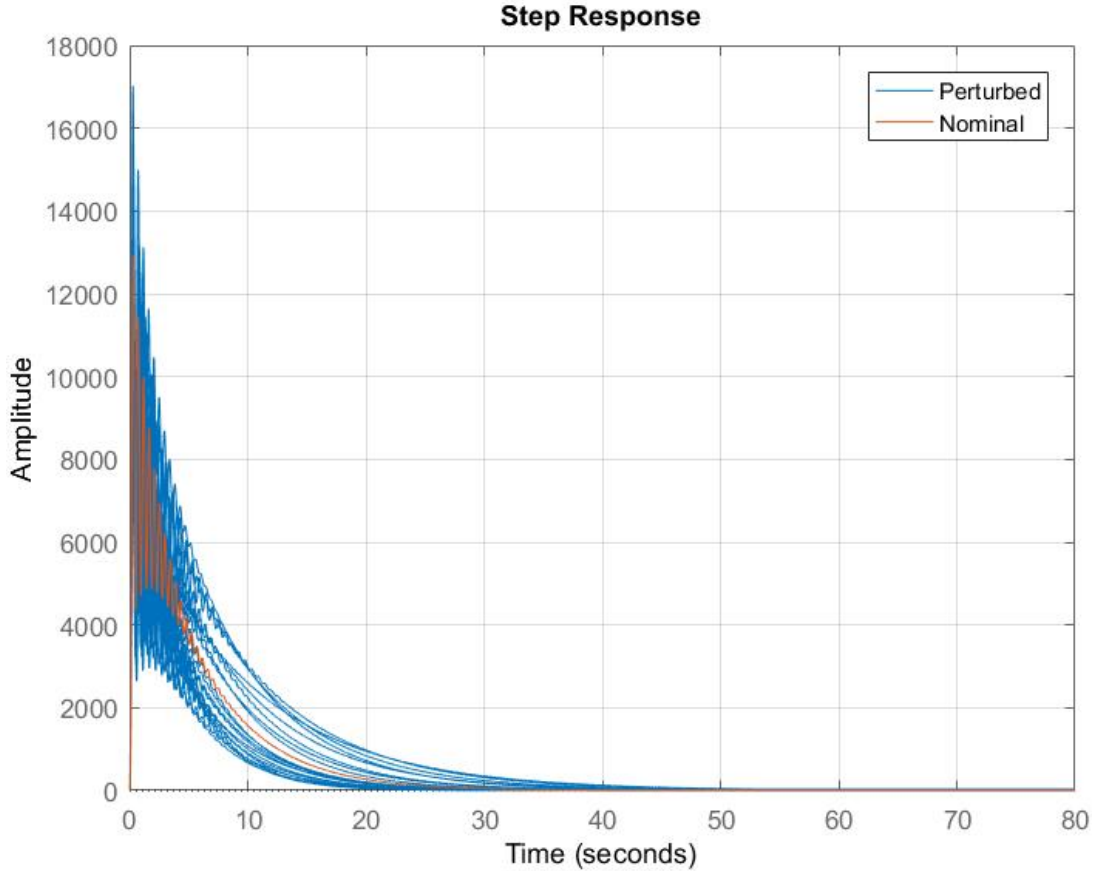


Diagram. 22. Step response of the open loop with uncertainties: pitch angle to output power relation

By substituting equations eq... in the uncertainty variation from eq... the following equations are obtained

$$(I_{rot} \cdot (1 - P_{I.rot})) \leq I_{rot} \leq (I_{rot} \cdot (1 + P_{I.rot})) \quad \text{Eq. 154}$$

$$(K_{Shaft} \cdot (1 - P_{K.Shaft})) \leq K_{Shaft} \leq (K_{Shaft} \cdot (1 + P_{K.Shaft})) \quad \text{Eq. 155}$$

$$(B_{Shaft} \cdot (1 - P_{B.Shaft})) \leq B_{Shaft} \leq (B_{Shaft} \cdot (1 + P_{B.Shaft})) \quad \text{Eq. 156}$$

$$(I_{gen} \cdot (1 - P_{I.gen})) \leq I_{gen} \leq (I_{gen} \cdot (1 + P_{I.gen})) \quad \text{Eq. 157}$$

$$(a \cdot (1 - P_a)) \leq a \leq (a \cdot (1 + P_a)) \quad \text{Eq. 158}$$

$$(b \cdot (1 - P_b)) \leq b \leq (b \cdot (1 + P_b)) \quad \text{Eq. 159}$$

$$(c \cdot (1 - P_c)) \leq c \leq (c \cdot (1 + P_c)) \quad \text{Eq. 160}$$

Let G denote the input/output dynamics of the linearized system with uncertainties, which takes into account the uncertainty of parameters as shown in Figure 8.5. G has 9 inputs ($w_{I.rot}$, $w_{K.shaft}$, $w_{B.shaft}$, $w_{I.gen}$, w_a , w_b , w_c , v_{rot} , β), 9 outputs ($z_{I.rot}$, $z_{K.shaft}$, $z_{B.shaft}$, $z_{I.gen}$, z_a , z_b , z_c , ω , P_{out}) and 4 states (Ω , ω , Φ and M_{gen}).

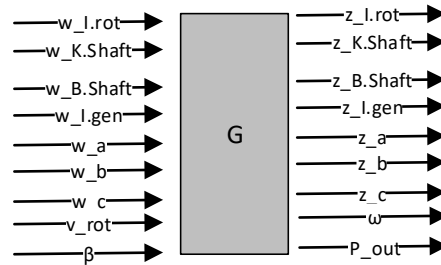


Diagram. 23. Input/output block diagram of the linearized model with uncertainties

The uncertain response of the nonlinear system can be described by an upper LFT representation:

$$Y = F_u(G, \Delta) \cdot u \tag{Eq. 161}$$

with diagonal uncertainty matrix $\Delta = \text{diag}(\delta_{Irot}, \delta_{Kshaft}, \delta_{Bshaft}, \delta_{Igen}, \delta_{Geff}, \delta_a, \delta_b, \delta_c)$ as shown in the equation ... Note that the unknown matrix Δ is a diagonal matrix with a fixed structure and is called the uncertainty matrix. It could, in general.

$$w = \Delta \cdot z \tag{Eq. 162}$$

$$\begin{bmatrix} w_{Irot} \\ w_{Kshaft} \\ w_{Bshaft} \\ w_{Igen} \\ w_a \\ w_b \\ w_c \end{bmatrix} = \begin{bmatrix} \delta_{Irot} & 0 & 0 & 0 & 0 & 0 & 0 \\ 0 & \delta_{Kshaft} & 0 & 0 & 0 & 0 & 0 \\ 0 & 0 & \delta_{Bshaft} & 0 & 0 & 0 & 0 \\ 0 & 0 & 0 & \delta_{Igen} & 0 & 0 & 0 \\ 0 & 0 & 0 & 0 & \delta_a & 0 & 0 \\ 0 & 0 & 0 & 0 & 0 & \delta_b & 0 \\ 0 & 0 & 0 & 0 & 0 & 0 & \delta_c \end{bmatrix} \cdot \begin{bmatrix} z_{Irot} \\ z_{Kshaft} \\ z_{Bshaft} \\ z_{Igen} \\ z_a \\ z_b \\ z_c \end{bmatrix} \tag{Eq. 163}$$

In the diagram below, it can be seen the LFT representation of the linearized model with uncertainties

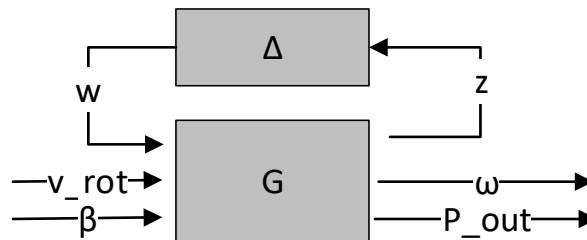


Diagram. 24. LFT representation of the linearized model with uncertainties

The above diagram can be simplified by unifying the inputs and outputs:

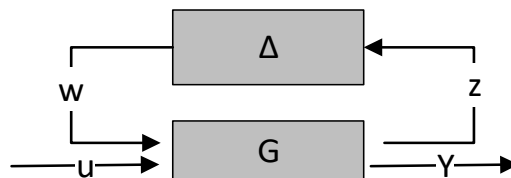
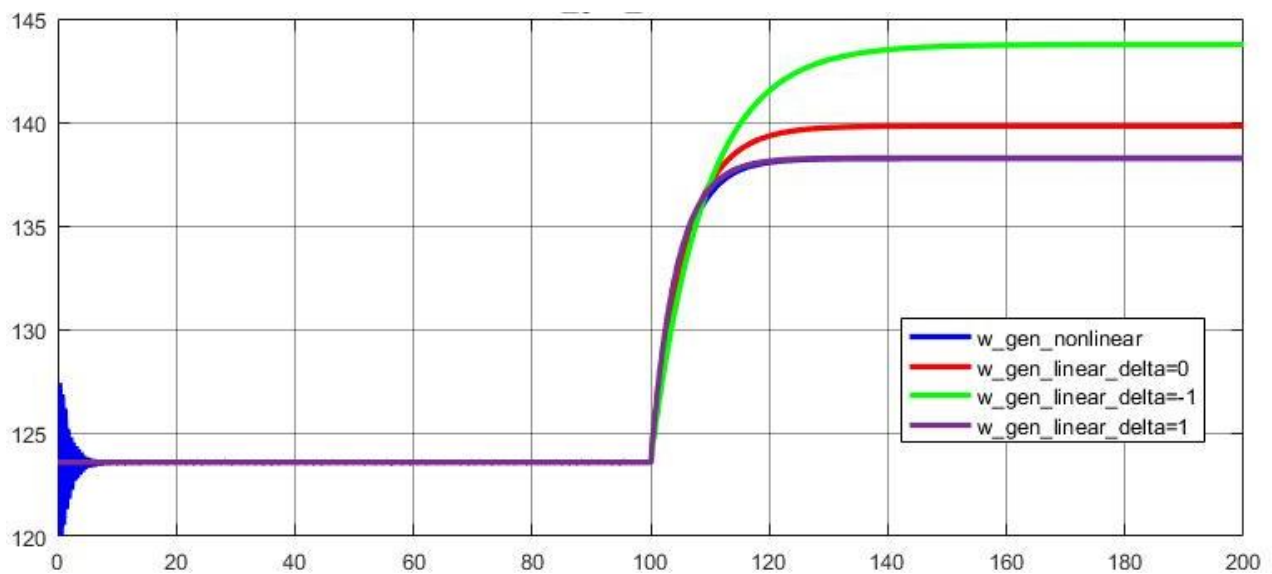


Diagram. 25. Simplified LFT representation of the linearized model with uncertainties

2.4.4. Linearized model with uncertainties vs. Linearized model vs. Nonlinear model

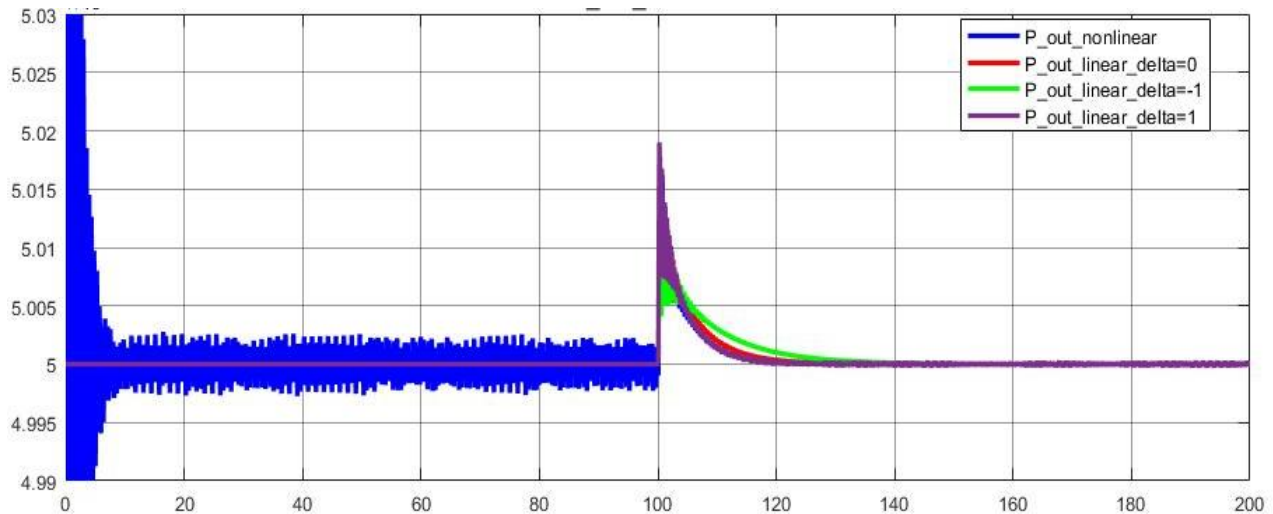
In the figure below it can be seen the comparison between the generator angular velocity ω obtained from the nonlinear model and the one obtained from the linearized model with different uncertainties ($\Delta=\text{diag}(0)$, $\Delta=\text{diag}(-1)$, $\Delta=\text{diag}(1)$):



Graph 10. Generator angular velocity response of the nonlinear vs. linearized model with uncertainties

From the above graph, it can be seen that the generator angular velocity ω linearized model with uncertainties $\Delta=\text{diag}(0)$, behave exactly like the linearized model without uncertainties (error $_{\Delta 1}=-1.574$ [rad/s]). The linearized model with uncertainties $\Delta=\text{diag}(-1)$ deviates the most from the nonlinear model (error $_{\Delta 2}=-5.503$ [rad/s]). The linearized model with uncertainties $\Delta=\text{diag}(1)$ responds the closest to the nonlinear model (error $_{\Delta 3}=-0.03$ [rad/s]):

In the figure below it can be seen the comparison between the output power P_{out} obtained from the nonlinear model and the one obtained from the linearized model with uncertainties ($\Delta=\text{diag}(0)$, $\Delta=\text{diag}(-1)$, $\Delta=\text{diag}(1)$):



Graph 11. Output power response of the nonlinear vs. linearized model with uncertainties

From the above graph, it can be seen that the output power P_{out} of the linearized model with uncertainties $\Delta=\text{diag}(0)$, dynamically behaves quite close to the nonlinear model and when it stabilizes deviates a bit from the nonlinear model ($\text{error}_{\Delta 4}=0.11$ [kW]). The linearized model with uncertainties $\Delta=\text{diag}(-1)$ dynamically behaves the worst compared to the nonlinear model, but when stabilizes deviates the least from the nonlinear model ($\text{error}_{\Delta 5}=0.029$ [kW]). The linearized model with uncertainties $\Delta=\text{diag}(1)$ dynamically behaves the closest compared to the nonlinear model, but when stabilizes deviates the most to the nonlinear model ($\text{error}_{\Delta 6}=74.32$ [kW]).

3. Robust controller for wind turbine

In this chapter, uncertainty modelling, design and implementation of the controller takes place. Uncertainty parameters are represented by block diagrams and then formulated into the matrix form for the controller design by using Linear Fractional Transformations (LFT's). The uncertainties have been defined as a multiplicative uncertainty. The weight of the uncertainties was defined in percentages, so that each uncertain parameter will be in a defined range of uncertainty. Then the uncertain state space model transformed into a suitable form for H infinity control design purposes [18].

3.1. Uncertainty model for robust controller

For designing the robust controller, the linearized MIMO (multiple input – multiple output) model with uncertainties is reduced to linearized SISO (single input single output) model with uncertainties.

For doing so, the equations eq. 139 – eq.140 are discarded (just the eq. 128 – eq. 138 are kept), and the equation eq. 138 is reduced to the following equation:

$$\dot{M}_{gen} = -\frac{1}{\tau_{gen}} \cdot M_{gen} \quad \text{Eq. 164}$$

Before writing the above equations into state space representation, the state vector x with 4 states, the input vector u with 2 inputs, where actually the first input (v_{rot}) acts as a disturbance because is not a controllable input, and the output vector y with one output, are defined as below:

$$x = \begin{bmatrix} x_1 \\ x_2 \\ x_3 \\ x_4 \end{bmatrix} = \begin{bmatrix} \Omega \\ \omega \\ \Phi \\ M_{gen} \end{bmatrix} \quad w = \begin{bmatrix} W_{Irot} \\ W_{Kshaft} \\ W_{Bshaft} \\ W_{Igen} \\ W_a \\ W_b \\ W_c \end{bmatrix} \quad u = \begin{bmatrix} v_{rot} \\ \beta \end{bmatrix} \quad z = \begin{bmatrix} Z_{Irot} \\ Z_k \\ Z_B \\ Z_{Igen} \\ Z_a \\ Z_b \\ Z_c \end{bmatrix} \quad y = [\omega]$$

The linearized model is described by the following state-space model with 8 outputs, 9 inputs, and 4 states.:

$$\begin{cases} \dot{x} = A \cdot x + B_w \cdot w + B_u \cdot u \\ z = C_w \cdot x + D_{zw} \cdot w + D_{zu} \cdot u \\ y = C_y \cdot x + D_{yw} \cdot w + D_{yu} \cdot u \end{cases} \quad \text{Eq. 165}$$

$$\begin{cases} \dot{x} \\ z \\ y \end{cases} = \begin{bmatrix} A & B_w & B_u \\ C_w & D_{zw} & D_{zu} \\ C_y & D_{yw} & D_{yu} \end{bmatrix} \cdot \begin{bmatrix} x \\ w \\ u \end{bmatrix} \quad \text{Eq. 166}$$

For the equations (eq. 165 and eq. 166) the states matrix A is identified as:

$$A = \begin{bmatrix} \frac{1}{\bar{I}_{rot}} \cdot \bar{b} - \frac{1}{\bar{I}_{rot}} \cdot \bar{B}_{shaft} & \frac{1}{\bar{I}_{rot}} \cdot \bar{B}_{shaft} \cdot \frac{1}{N} & -\frac{1}{\bar{I}_{rot}} \cdot \bar{K}_{shaft} & 0 \\ \frac{1}{\bar{I}_{gen}} \cdot \frac{1}{N} \cdot \bar{B}_{shaft} & -\frac{1}{\bar{I}_{gen}} \cdot \frac{1}{N^2} \cdot \bar{B}_{shaft} & \frac{1}{\bar{I}_{gen}} \cdot \frac{1}{N} \cdot \bar{K}_{shaft} & -\frac{1}{\bar{I}_{gen}} \\ 1 & -\frac{1}{N} & 0 & 0 \\ 0 & 0 & 0 & -\frac{1}{\tau_{gen}} \end{bmatrix} \quad \text{Eq. 167}$$

The state-space's output matrix related to states, Cy is identified as:

$$C_y = [0 \ 1 \ 0 \ 0] \quad \text{Eq. 168}$$

The state-space's output matrix related directed to perturbations inputs, Dyw is identified as:

$$D_{yw} = [0 \ 0 \ 0 \ 0 \ 0 \ 0] \quad \text{Eq. 169}$$

The state-space's output matrix related directed to inputs, Dyu is identified as:

$$D_{yu} = [0 \ 0] \quad \text{Eq. 170}$$

The perturbations input matrix Bw, the input matrix Bu, the perturbations output matrix related to states Cw, perturbations output matrix related directed to perturbations inputs Dzw, and the perturbations output matrix related directed to inputs, Dzu are the same as the one is identified in [section 2.3.8. Linearized model with uncertainties vs. Linearized model vs. Nonlinear model!](#)

The uncertain response of the nonlinear system can be described by the same upper LFT representation as in eq. 78 – eq. 94: with the same diagonal uncertainty matrix Δ as in the eq. 163

In the diagram 26, which represents also the upper LFT representation for the uncertainty model for the robust controller, the pitch angle β can be also represented by the input u, and the output power P_{out} can be represented by the output Y as in the figure below:

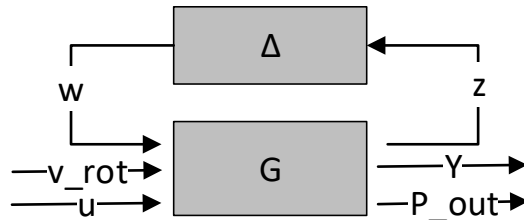


Diagram. 26. Simplified LFT representation of the linearized model with uncertainties for robust controller

3.2. H-inf Robust Controller

H[∞] based robust control first proposed by G. Zames, which deals with model uncertainties, external disturbances and addresses both the performance and stability criterion of a control system (sensitivity minimization) [19]. H[∞] robust control synthesis is a way to guarantee robustness and good performance, which provides high disturbance rejection and satisfies stability for different operating

conditions. There are several ways to design the H infinity controller and it has been used to address many theoretical and practical problems. Due to its widely acceptance controller can be designed by using loop shaping technique since the performance requisites can be associated in the design stage as performance weights.[20] By weighing the signals in various loops in a way determined by design specifications, the plant can be augmented to produce satisfying closed loop transfer function tradeoffs. In this report, H-infinity-optimal controller obtained by using Robust control toolbox of MATLAB software.

To ensure good performance and robustness of closed loop system following criterions must be satisfied

1. Stability criterions

The roots of characteristic equation $1 + G(s)K(s) = 0$ must be in the left half of the s plane.

2. Performance Criterion

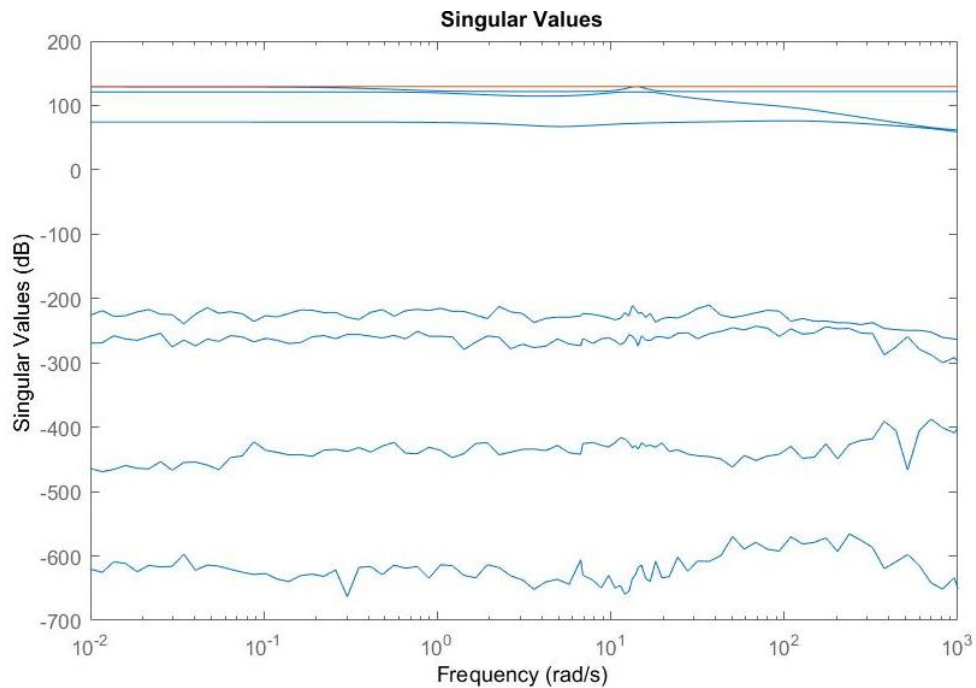
The sensitivity function $S(s) = (1 + G(s)K(s))^{-1}$ must be small when there is large disturbance and set point change, for all frequencies.

3. Robustness criterion

Stability and performance should also be maintained for the plant models which are close to the nominal model. These perturbed plant models are either created by modelling errors or disturbance, so the controller should also be able to satisfy the necessary conditions to these perturbed plant models besides nominal plant model. H^∞ norm of a transfer function, F is its maximum value of the complete spectrum which represented as

$$\|F(j\omega)\|_\infty = \sup \sigma(F(j\omega))$$

where the σ is the largest singular value of a transfer function



Graph 12. Singular values for h-infinity controller

3.3. Control Plan & Implementation

The main purpose is to synthesize the controller so that the H^∞ norm of the plant will remain between certain limits. The formulation of robust control problem is as follows

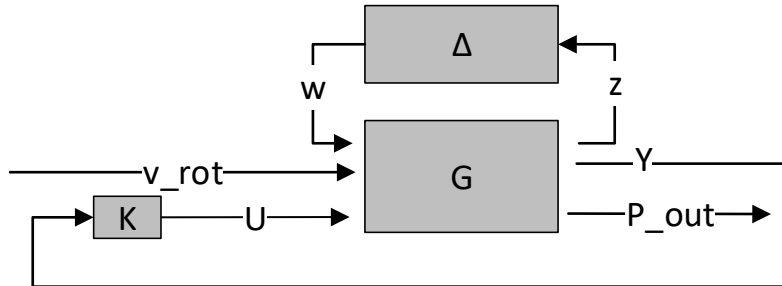


Diagram. 27. LFT representation of the linearized model with uncertainties with H infinity controller

w is the vector of all disturbance signals;

z is the cost signal consisting of all errors;

y is the vector consisting of measurement variables;

u is the vector of all control variables.

H^∞ control synthesis divides the control problem into 2 sections which the two transfer functions deal with stability and performance separately. The sensitivity function S and the complementary sensitivity function T which required for the synthesis are

$$S = \frac{1}{1+GK} \quad \text{Eq. 171 Sensitivity function is the ratio of output to the disturbance of a system}$$

$$T = \frac{GK}{1+GK} \quad \text{Eq. 172 Complementary sensitivity function is the ratio of output to input}$$

Controller K must generate a signal which cancels the effect of w on z by minimizing the norm w to z. This can be achieved by limiting the values of $\sigma(S)$ and $\sigma(T)$.

The LTI plant model was implemented in MATLAB to compute a stabilizing H-infinite optimal controller K by using “hinfsyn” command. The obtained controller is LTI/SS and has the same number of states as the plant model. The plant transformed into the form where the inputs to B_u are the control inputs and outputs of C_y are the measurements provided to the controller. The inputs to B_w are the disturbances and the outputs of C_w are the errors which must be kept small.

$$\begin{bmatrix} A & B_w & B_u \\ C_w & D_{zw} & D_{zu} \\ C_y & D_{yw} & D_{yu} \end{bmatrix}$$

For the function “hinfsyn” the number of control inputs and the number of output measurements provided to the controller must be defined. So, the NCON, the number of outputs of the controller and NMEAS, the number of measurements provided to the controller must be defined. To be able to provide these information, the matrix must be changed before using hinfsyn function, in the form that the column size of the B_u is one and the row size of the C_y is one. So that we have only one measurement provided to the controller and one output from the controller. After the implementation of the synthesis, the

optimal LTI controller, K , of the plant, LTI closed loop system Ty_1u_1 , and the optimal H_∞ cost GAM are computed. GAM is the $\|Ty_1u_1\|_\infty$, which is the infinity norm of the obtained closed loop system. The obtained LTI closed loop system is the linear fractional transformation of the plant model and the controller. A singular-value plot was used to verify that $\|Ty_1u_1\|_\infty \triangleq \sup \sigma_{max}(Ty_1u_1(jw)) < \gamma$

In the next figure, it can be seen the bode diagram of loop gain with uncertainties from the pitch angle β to generator angular velocity ω :

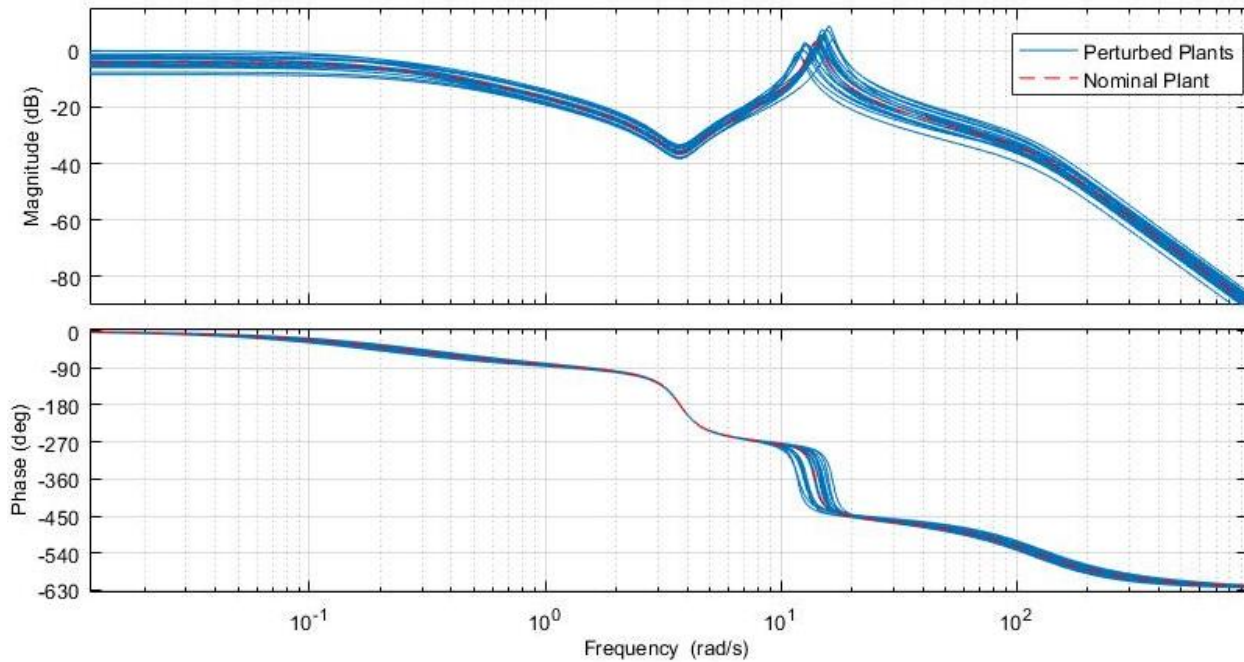


Diagram. 28. Bode diagram of the loop gain with uncertainties

From above figure, it can be seen that the gain margin is 36.2 dB at 3.73 [rad/s] and the minimum phase margin is 129 deg at 14.9 [rad/s].



Below it can be seen the pole-zero map of the loop gain with uncertainties transfer function from the pitch angle β to generator angular velocity ω :

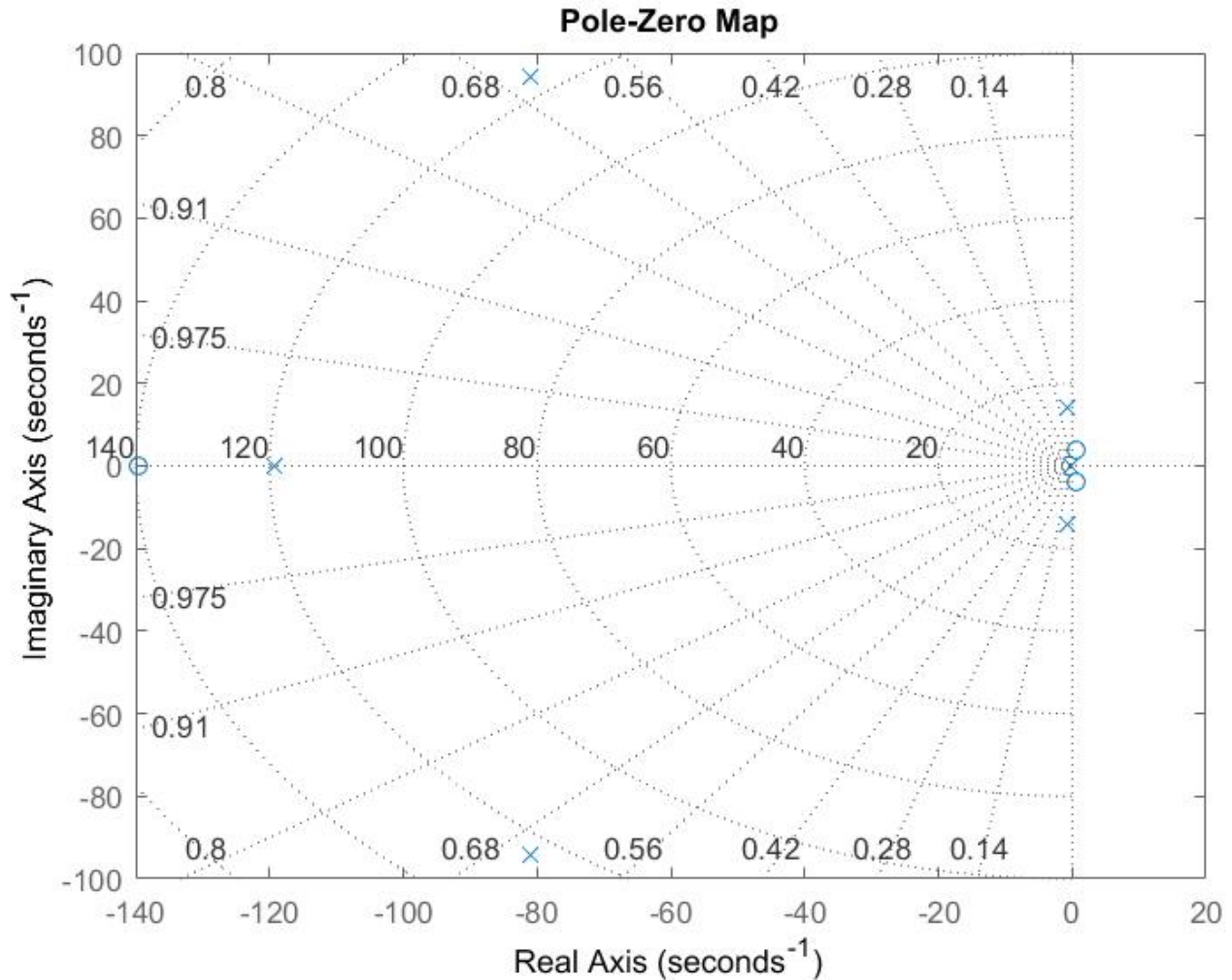


Diagram. 29. Pole-zero map of the loop gain with uncertainties: pitch angle to output power relation

Poles:

- 80.97 + 94.10i
- 80.97 - 94.10i
- 19.23
- 00.26
- 00.72 + 14.02i
- 00.72 - 14.02i
- 10.00
- 10.00

From the diagram 21, it can be seen that the all the poles are in Left Half Plane (LHP) showing that the model is stable

Also in diagram 21, the zero of the system can be identified

Zeros:

- 139.60
- 0.62 + 3.68i
- 0.62 - 3.68i
- 10.00
- 10.00

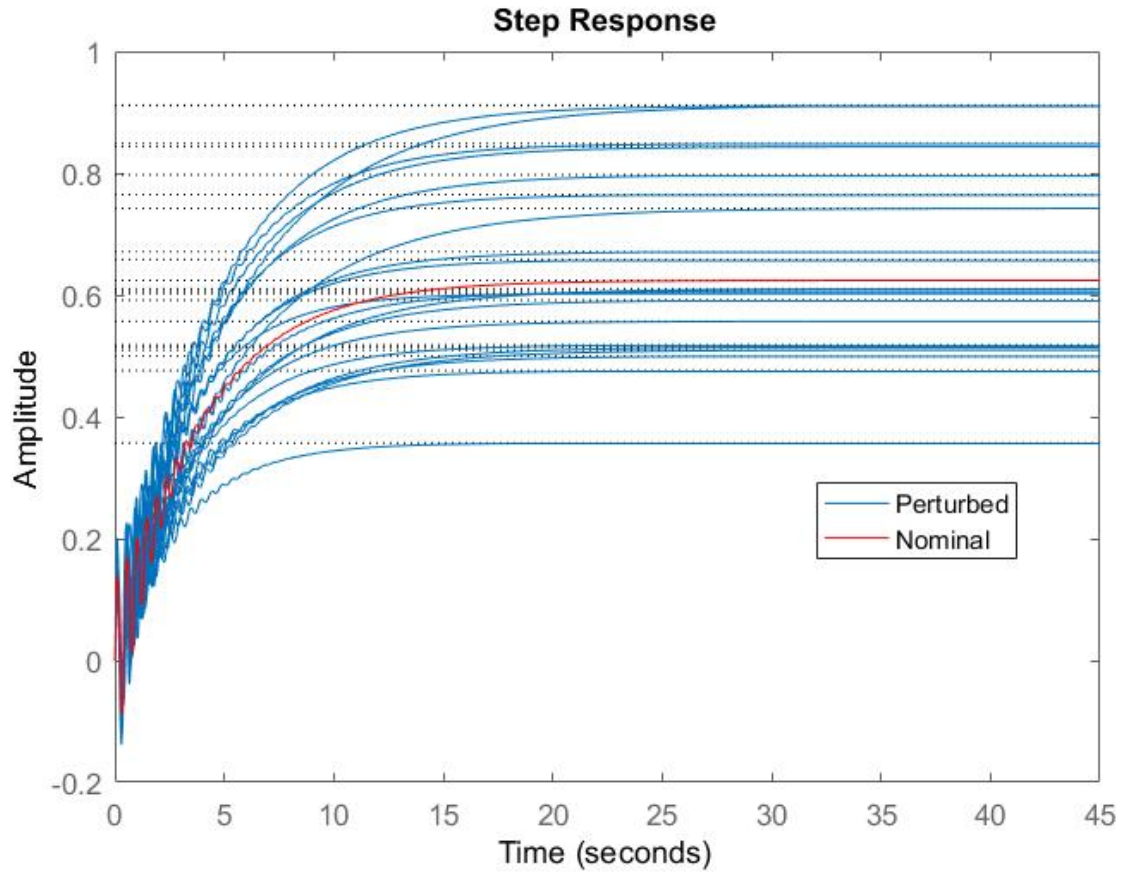
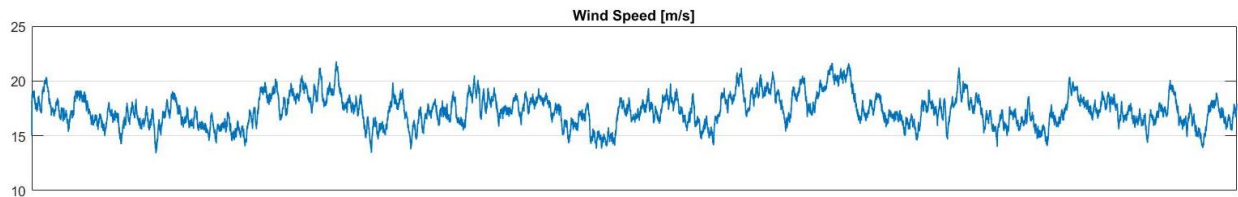


Diagram. 30. Step Response of the Loop gain with uncertainties



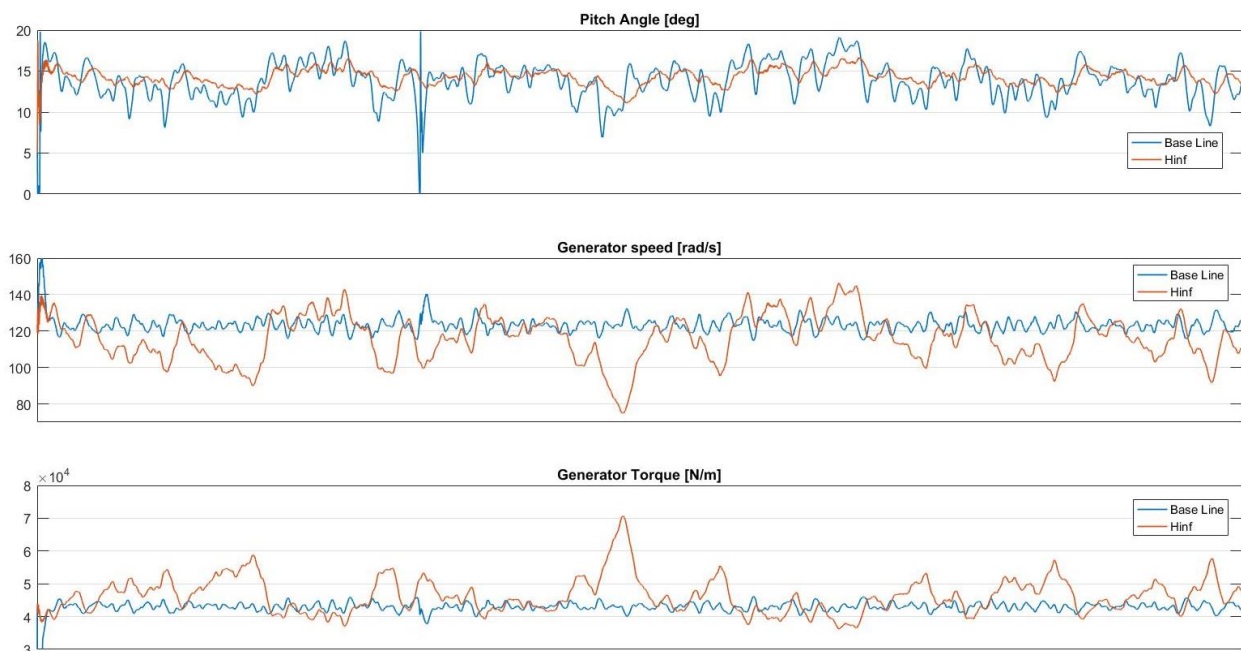
3.4. Results

In this section, the results with the baseline controller and the H-infinity controller are presented. The control system, which was designed by using linear-model, was tested on non-linear NREL 5MW Simulink model. The pitch angle, generator speed, generator torque, power output, tower moment and blade moments are compared with the same wind speed. Modeling and controlling the wind turbine, was conducted in Simulink. Simulation results for the NREL 5MW wind turbine with different controllers are as follows,



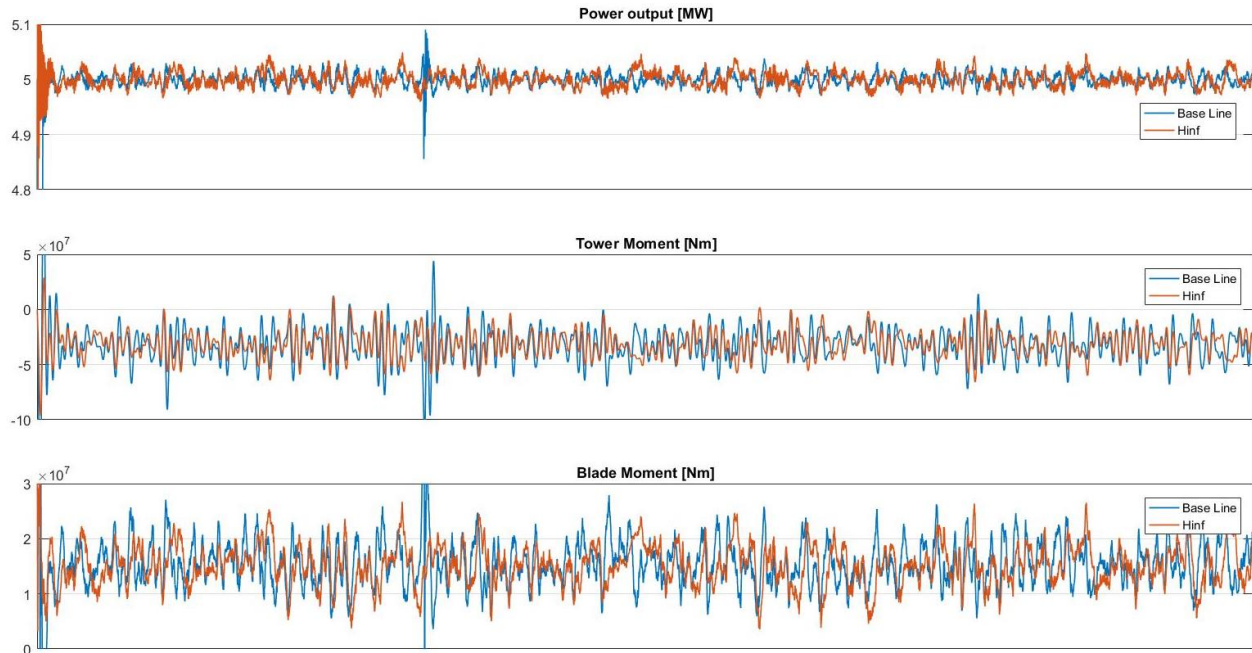
Graph 13. Wind speed(m/s)

The wind speed is the time series which fluctuates between around 14 to 22 m/s and the simulations for both controllers took place under same data of the wind speed.



Graph 14. H-infinity results, pitch angle, generator speed and generator torque

The simulations demonstrate that, the pitch angle of the H-infinity controller does not variate as much as the baseline controller. Nevertheless, results with H-infinity controller causes higher fluctuations in generator speed and higher torque variations in generator, where the generator speed and torque of the baseline controller are more stable with smaller fluctuations.



Graph 15. Simulation results power output, tower and blade moments

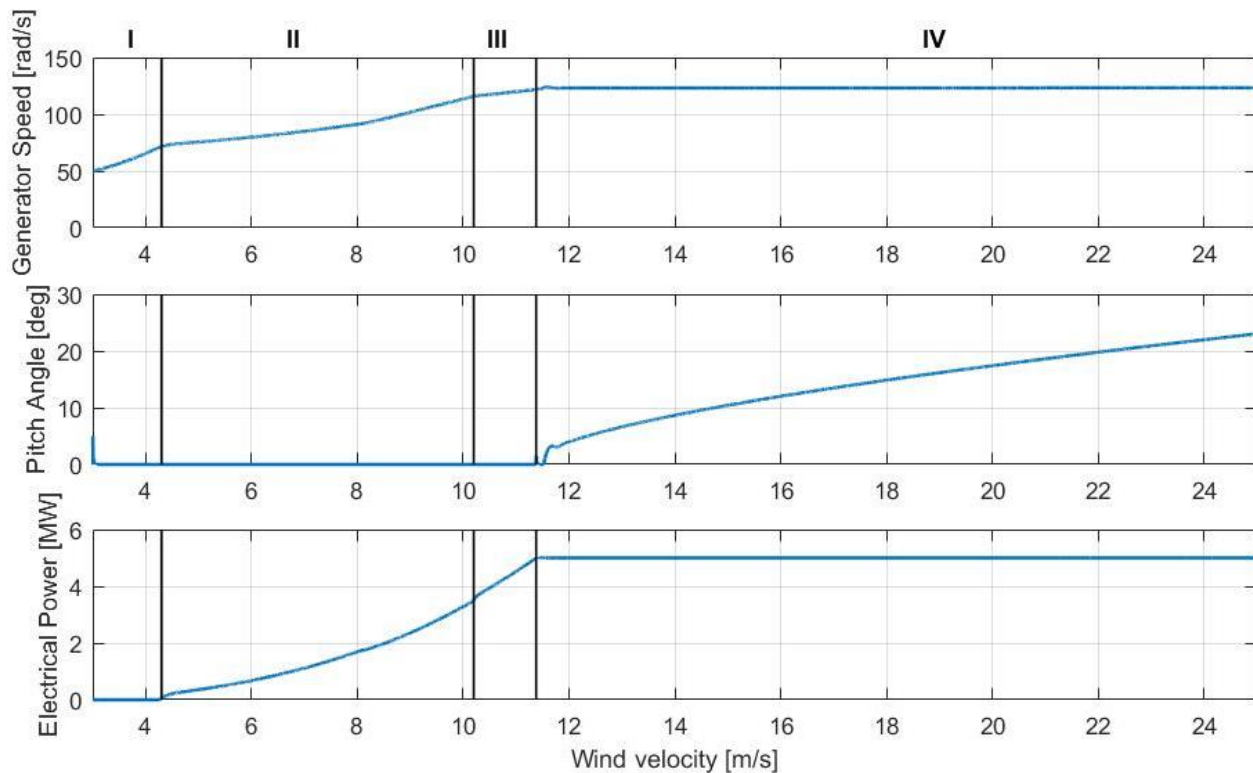
The output power is constant around 5 MW with small changes for both controller. There is not a significant difference on output power between baseline controller and the H-infinity controller, whereas the moment on the tower is slightly less with the H-infinity controller. So, with the above-rated speeds, the H-infinity controller partially mitigates the moment on the tower. Moreover, the moments on the blades are also decreased. Although it is not very significant in graphs, the load mitigation calculated in the next sections and the difference of loads are presented.

4. Power boosting mode

In this chapter, the wind turbine is defined as a control object including the discussion regarding the optimal equilibrium points and defining the operating modes of the wind turbine with and without the power boosting mode.

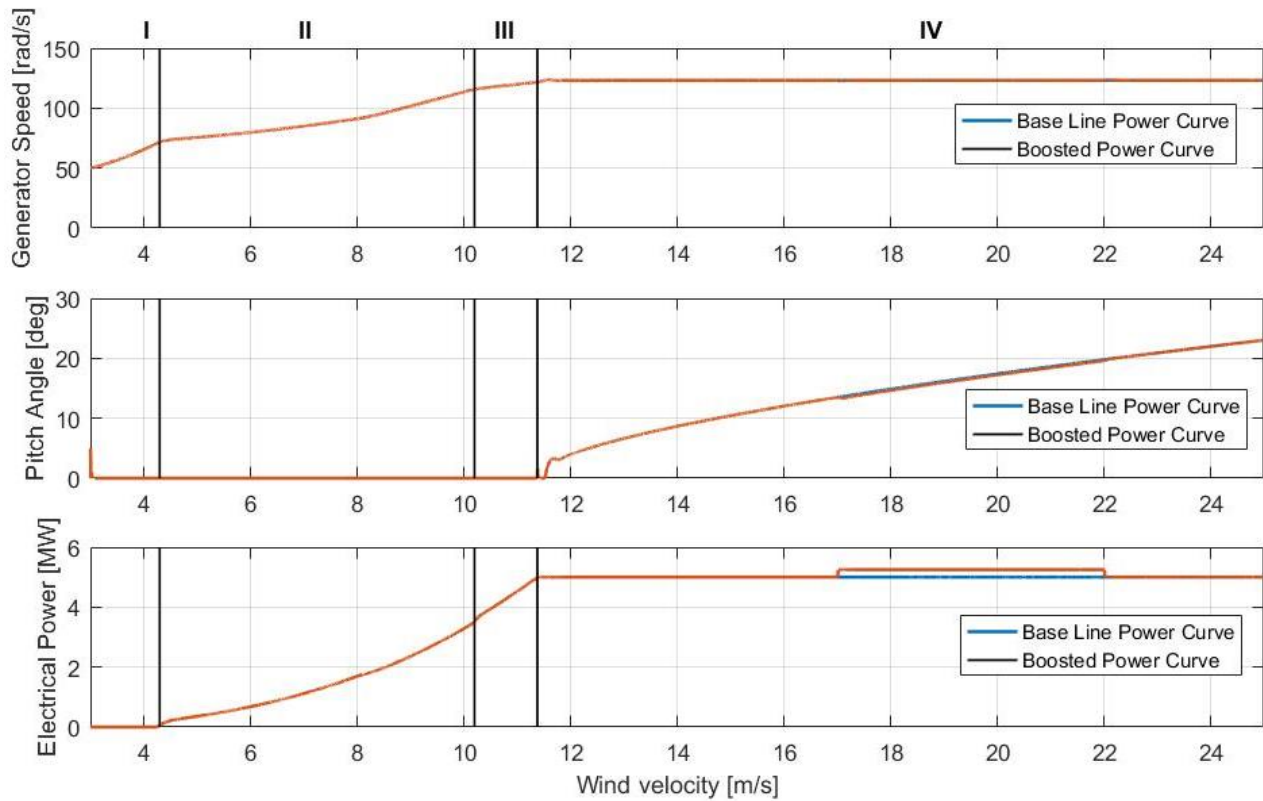
From the wind turbine model described in [chapter 2. Wind Turbine modelling](#) it can be seen that described dynamic system has three inputs: the wind speed v , pitch angle reference signal β_{ref} , and power reference P_{ref} . From those inputs the first one, the wind speed v , represents the disturbance while the last two inputs, the pitch angle reference signal β_{ref} and the power reference P_{ref} are controllable inputs. The primary outputs of the system are set to be the generator speed ω and the produced power P .

In the following figure, it can be seen the power curve of the NREL 5 MW wind turbine operating without the power boosting mode.



Graph 16. 5 MW NREL wind turbine generator speed, pitch angle, electrical power

The wind turbine power boost mode is an operating mode of the wind turbine which increases the power production of a wind turbine by increasing the wind turbine's nominal power output by up to 5% [12]. The wind turbine's nominal power output can be increase through the direct increase of the rotor torque (indirect increase of the generator torque) when certain operating conditions like wind speed is within certain limits.



Graph 17. 5 MW NREL boosted wind turbine generator speed, pitch angle, electrical power

As depicted in figure, the power is expected to increase in the above rated wind speeds with the power booster mode. The logic was designed, which switch between H-infinity controller and the boost H-infinity controller between desired wind speeds. The wind limits for the boosting mode are determined between 15 and 22 m/s. Between these wind speeds the system is controlled by the boosting mode. In this region, the power reference is changed to 5.25 MW and the controller is switched to the boosting controller which is designed for this region. By using this mode, the power production is increased which also results in increasing the loads. The results of the H-infinity controllers with and without the boosting mode is analyzed and compared with the baseline controller.

5. Robust controller for wind turbine power booster

This chapter presents the uncertainty modelling, design and implementation of the h-infinity robust controller of the wind turbine including the power booster mode and the comparison with the uncertainty modelling, design and implementation of the h-infinity robust controller for the standard operation of the wind turbine [18].

5.1. Operating and linearization points for wind turbine power booster controller

The linearization for the wind turbine power booster model was done using the same procedure as for the standard linearized wind turbine mathematical model. The only difference between the 2 models consists in different operating and linearization points.

5.1.1. Tip speed ratio linearization for power booster

Same as for the linearization of the model for the wind turbine robust controller, the first equation which is linearized for the wind turbine power booster robust is the tip speed ratio ($\lambda = \frac{R \cdot \Omega}{v_{rot}}$). The wind speed at the rotor v_{rot0} , rotor angular velocity Ω_0 and the tip speed ratio λ_0 at a wind speed in front of the rotor of 18 [m/s] were identified to be very similar to the ones for the linearized model for the robust controller without the power booster:

$$\Omega_0 = 1.274$$

$$v_{rot0} = 17.981$$

$$\lambda_0 = 4.463$$

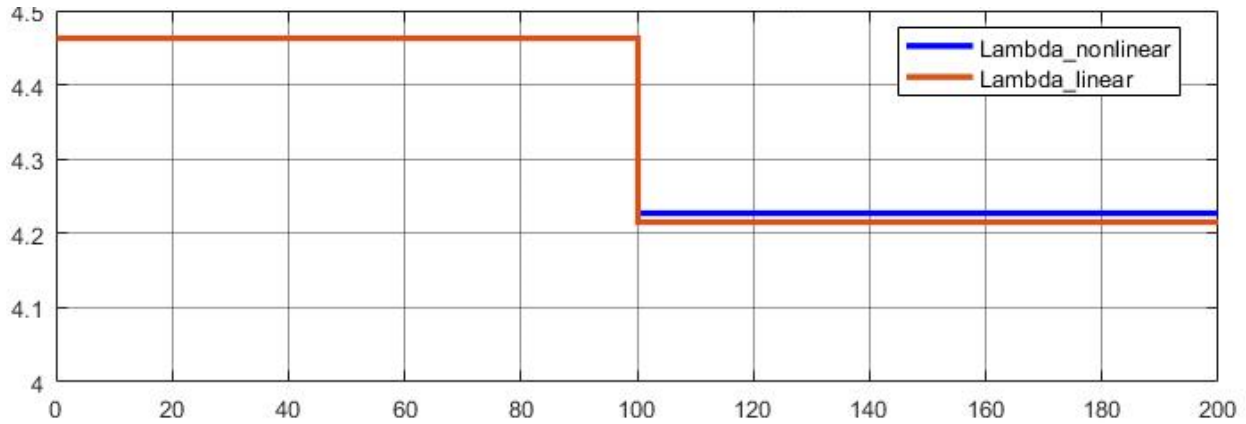
Same as in the linearization of the tip speed ratio for the model of the robust controller without the power booster, in the linearization of the tip speed ratio for the model of the robust controller with the power booster, the Taylor expansion approximation was used.

The slopes of the angular velocity and wind speed at rotor which contributes to the change in tip speed ratio were identified to be the same as in the linearized model for the robust controller without the power booster:

$$\left. \frac{\partial \lambda}{\partial \Omega} \right|_{(\Omega_0, v_{rot0})} = \frac{R}{v_{rot0}} = 3.504 \quad \text{Eq. 173}$$

$$\left. \frac{\partial \lambda}{\partial v_{rot}} \right|_{(\Omega_0, v_{rot0})} = -\frac{R \cdot \Omega_0}{v_{rot0}^2} = -0.248 \quad \text{Eq. 174}$$

The next graph represents the comparison between the nonlinear and linearized equations of the tip speed ratio:



Graph 18. Tip speed ratio nonlinear vs. linearized power booster equation

From the above graph, it can be seen that the linearized tip speed ratio of the model for the power booster controller behaves exactly the same as the one of the model for the controller without the power booster: there is a small difference between the outputs of the nonlinear and linear equations due to the error ($e_{\lambda, PB}=0.0131$) occurred using the Taylor series approximation for linearizing the equation.

5.1.2. Power coefficient linearization for power booster

The nonlinear equation for linearizing the power coefficient was the same as the one in subchapter 2.3.2. [Power coefficient linearization](#). By using the wind speed at the rotor v_{rot0} , the pitch angle β_0 , the tip speed ratio λ_0 and the at a wind speed in front of the rotor of 18 [m/s], and the equation (eq.24) to calculate the power coefficient C_{p0} at the same linearization speed:

$$v_{R0} = 17.981 \quad \beta_0 = 14.578 \quad \lambda_0 = 4.464 \quad C_{p0} = 0.125$$

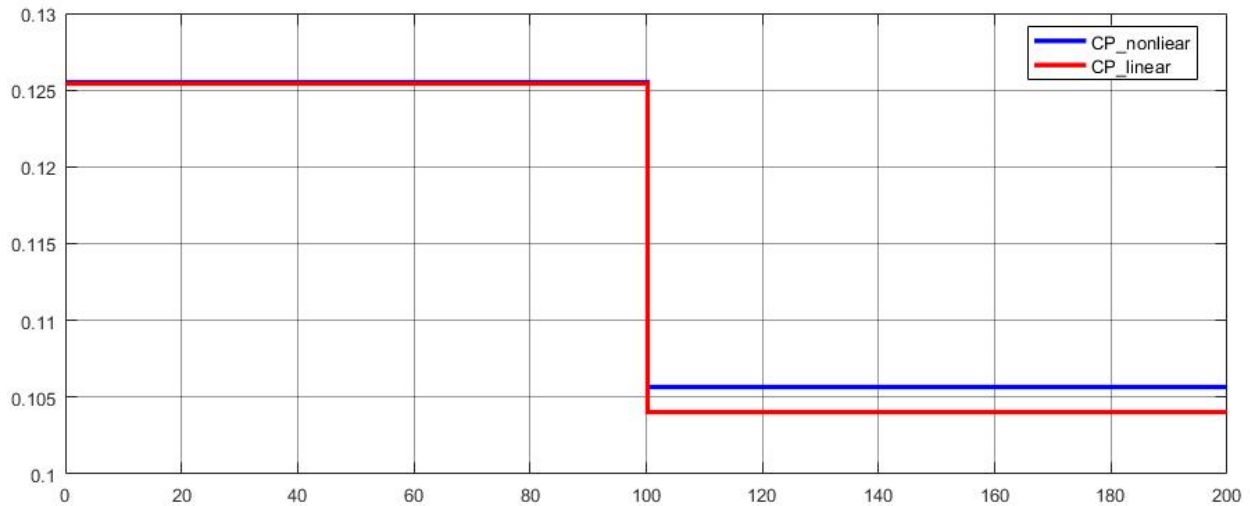
Same as in the linearization of the power coefficient for the model of the robust controller without the power booster, in the linearization of the power coefficient for the model of the robust controller with the power booster, the Taylor expansion approximation was used.

The slopes of the pitch angle and tips speed which contributes to the change in power coefficient were identified to be the same as in the linearized model for the robust controller without the power booster:

$$\left. \frac{\partial C_P}{\partial \beta} \right|_{(\beta_0, \lambda_0)} = -0.027 \quad \text{Eq. 175}$$

$$\left. \frac{\partial C_P}{\partial \lambda} \right|_{(\beta_0, \lambda_0)} = -0.059 \quad \text{Eq. 176}$$

The following graph represents the comparison between the look up table and linear equations of the power coefficient:



Graph 19. CP look up table vs. linearized power booster equation

From the above graph, it can be seen that the linearized power coefficient of the model for the power booster controller behaves similar to the one of the model for the controller without the power booster: there is small difference between the outputs of the nonlinear and linear equations due to the error ($e_{CP.PB}=0.001617$) occurred using the Taylor series approximation for linearizing the equation.

5.1.3. Rotor torque linearization for power booster

Same as for the linearization of the model for the wind turbine robust controller, the next equation which is linearized, is the rotor torque (eq. 4). The first step in executing the linearization is by using the wind speed at the rotor v_{rot0} , rotor angular velocity Ω_0 and the power coefficient C_{p0} at a wind speed in front of the rotor of 18 [m/s] and using the equation (eq. 4) from the nonlinear model to calculate the M_{rot0} at the same linearization point:

$$v_{R_0} = 18$$

$$v_{rot0} = 17.981$$

$$C_{p0} = 0.125$$

$$\Omega_0 = 1.274$$

$$M_{rot0} = 4.365e + 6$$

Same as in the linearization of the rotor torque for the model of the robust controller without the power booster, in the linearization of the power coefficient for the model of the robust controller with the power booster, the Taylor expansion approximation was used.

The change in rotor torque M_{rot} in respect to wind speed at rotor v_{rot} is derived from the Eq. 36

$$a_{PB} = \left. \frac{\partial M_{rot}}{\partial v_{rot}} \right|_{(v_{rot0}, \Omega_0, \beta_0)} = 1.237e + 06 \quad \text{Eq. 177}$$

The change in rotor torque M_{rot} in respect to rotor angular velocity Ω is derived from the Eq. 37

$$b_{PB} = \left. \frac{\partial M_{rot}}{\partial \Omega} \right|_{(v_{rot0}, \Omega_0, \beta_0)} = -1.06e + 07 \quad \text{Eq. 178}$$

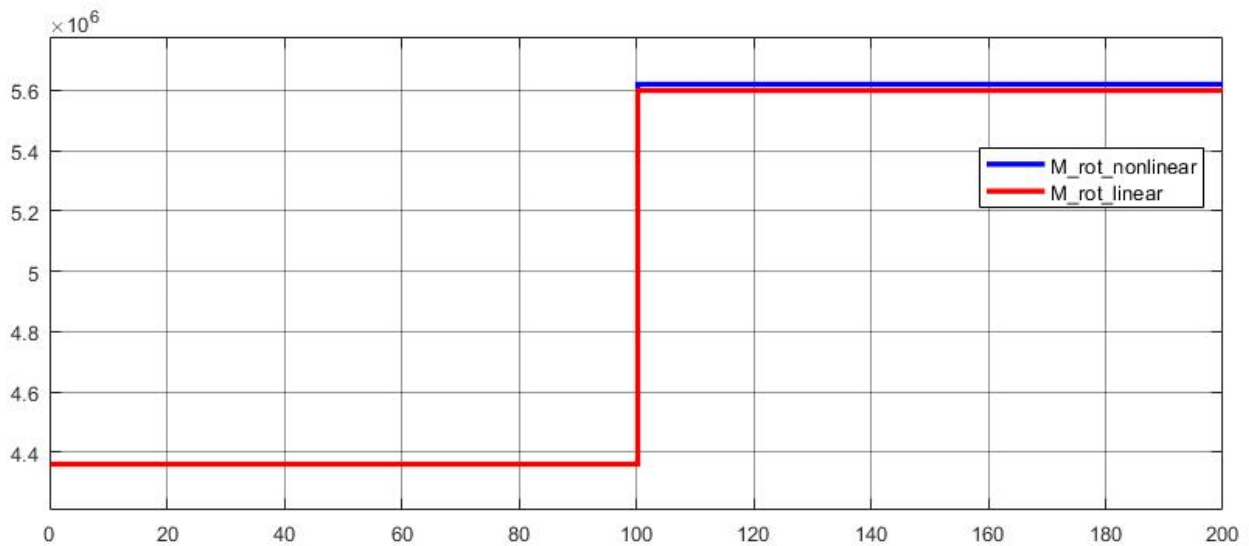
The change in rotor torque M_{rot} in respect to pitch angle β is derived from the Eq.38

$$c_{PB} = \left. \frac{\partial M_{rot}}{\partial \beta} \right|_{(v_{rot0}, \Omega_0, \beta_0)} = -9.312e + 05 \quad \text{Eq. 179}$$

Simplifying Eq. 35 with the above coefficients (Eq. 176-177) the new equation becomes:

$$\Delta M_{rot} = a \cdot \Delta v_{rot} + b \cdot \Delta \Omega + c \cdot \Delta \beta \quad \text{Eq. 180}$$

The following graph represents the comparison between the nonlinear and linear equations of the rotor torque:



Graph 20. Rotor torque nonlinear vs. linearized power booster equation

From the above graph, it can be seen that the linearized rotor torque of the model for the power booster controller behaves similar to the one of the model for the controller without the power booster: there is small difference between the outputs of the nonlinear and linear equations due to the error ($e_{M_{rot,PB}}=1.944e+4$) occurred using the Taylor series approximation for linearizing the equation.

5.1.4. Rotor torque reference linearization for power booster

Same as for the linearization of the linearized model, the next equation which is linearized in the power booster model, is the rotor torque (eq. 11). The first step in executing the linearization is by using the wind

speed at the rotor v_{rot0} , generator angular velocity ω_0 and the power reference P_{ref0} at a wind speed in front of the rotor of 18 [m/s] and using the equation (eq. 11) from the nonlinear model to calculate the generator torque reference M_{genref} at the same linearization point.

$$v_{R0} = 17.981$$

$$P_{ref0} = 5.561e + 06$$

$$\omega_0 = 123.586$$

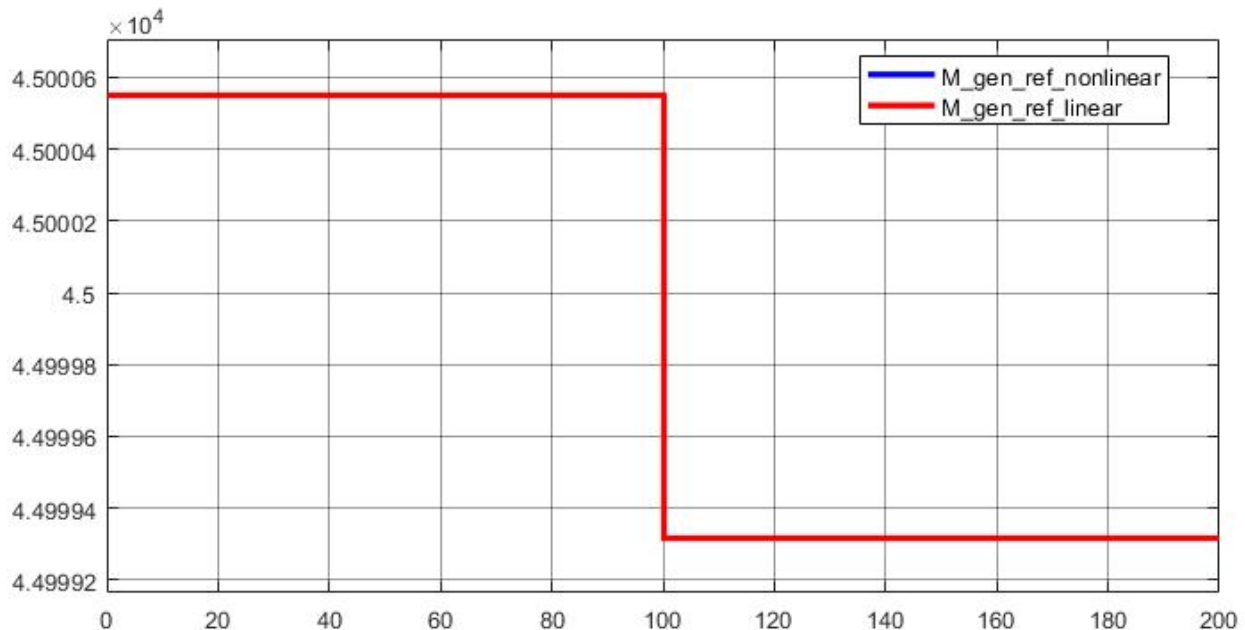
$$M_{genref0} = 4.5e + 04$$

Same as in the linearization of the rotor torque reference for the linearized model, in the linearization of the rotor torque reference the linearized power booster model, the Taylor expansion approximation was used.

The slopes of power reference and generator angular velocity which contributes to the change in generator torque reference are calculated:

$$\Delta M_{genref} = a_1 \cdot \Delta \omega \quad \text{Where } a_1 = -364.123 \quad \text{Eq. 181}$$

In the following graph, it can be seen the accuracy of the linearization:



Graph 21. Rotor torque reference nonlinear vs. linearized power booster equation

5.1.5. Gross output power linearization for power booster

Same as for the linearization of the linearized model, the next equation which is linearized in the power booster model, is the gross output power (eq. 9). The first step in executing the linearization is by using the wind speed at the rotor v_{rot0} , generator angular velocity ω_0 and the generator torque M_{gen0} at a wind

speed in front of the rotor of 18 [m/s] and using the equation (eq. 9) from the nonlinear model to calculate the gross output power $P_{out.gross}$ at the same linearization point.

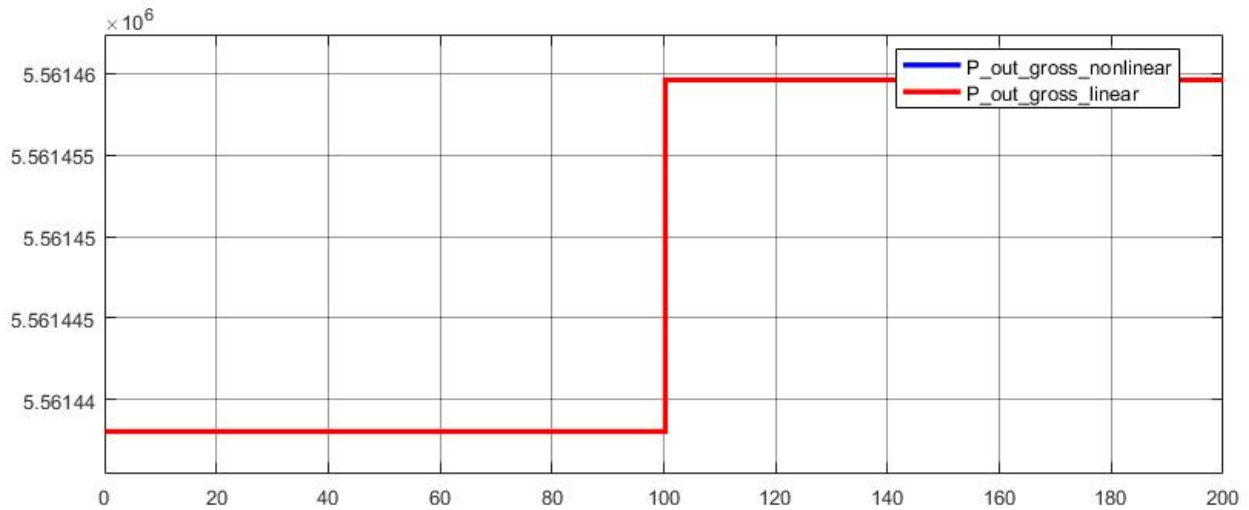
$$v_{R_0} = 18 \quad \omega_0 = 123.586 \quad M_{gen_0} = 4.5e + 04 \quad P_{out.gross} = 5.561e + 06$$

Same as in the linearization of the gross output power for the linearized model, in the linearization of the gross output power the linearized power booster model, the Taylor expansion approximation was used.

The slopes of the generator torque and generator angular velocity which contributes to the change in gross output power are calculated:

$$a_2 = \left. \frac{\partial P_{out.gross}}{\partial M_{gen}} \right|_{(M_{gen_0}, \omega_0)} = 123.586 \quad \text{Eq. 182} \quad b_2 = \left. \frac{\partial P_{out.gross}}{\partial \omega} \right|_{(M_{gen_0}, \omega_0)} = 4.5e + 04 \quad \text{Eq. 183}$$

In the following graph, it can be seen the accuracy of the gross output power linearization:



Graph 22. Gross output power nonlinear vs. linearized power booster equation

5.1.6. Summary of the power booster linearized model

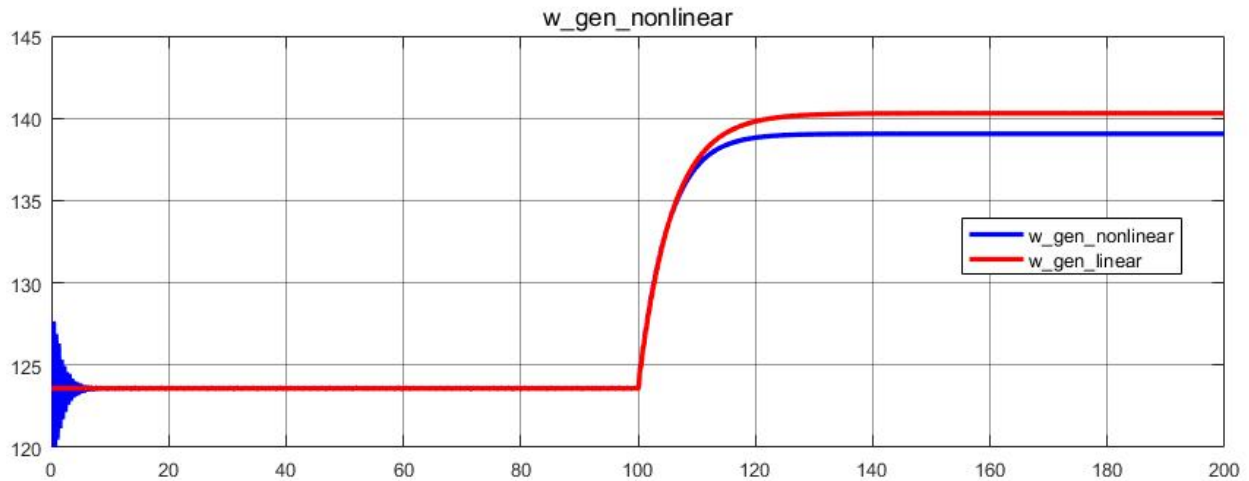
The linearized model of the power booster mode consists in the same equations and has the same graphical representation (block diagram) as the linearized model from section [2.3.6 Summary of the linearized model](#) updated with the coefficients calculated above.

5.1.7. State-space for power booster linearized model

The state-space model of the power booster mode consists in the same state-space model with 2 outputs, 2 inputs, and 4 states state vector x with as the state-space model from section [2.3.6 State-space model](#).

5.1.8. Linearized power booster model vs. nonlinear power booster model

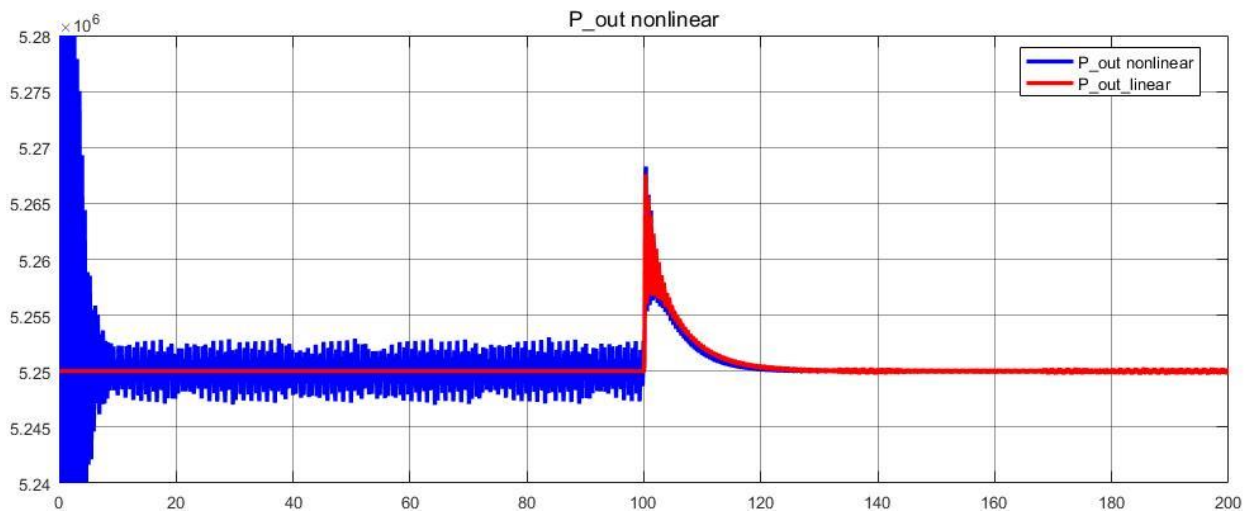
In the figure below it can be seen the comparison between the generator angular velocity ω obtained from the nonlinear power booster model and the one obtained from the linearized power booster model:



Graph 23. Generator angular velocity response of the nonlinear vs. linearized power booster models

From the above graph, it can be seen that there is an acceptable difference between the outputs of the nonlinear and linearized power booster models due to the errors ($e_{\omega_{gen.PB}}=-1.574$) occurred using the Taylor series approximation for linearizing the nonlinear equations.

In the figure below it can be seen the comparison between the output power P_{out} obtained from the nonlinear power booster model and the one obtained from the linearized power booster model:



Graph 24. Output power response of the nonlinear vs. linearized power booster models

From the above graph, it can be seen the high accuracy between the nonlinear and linearized power booster models output power ($e_{P_{out.PB}}=252.7$ [kW]).

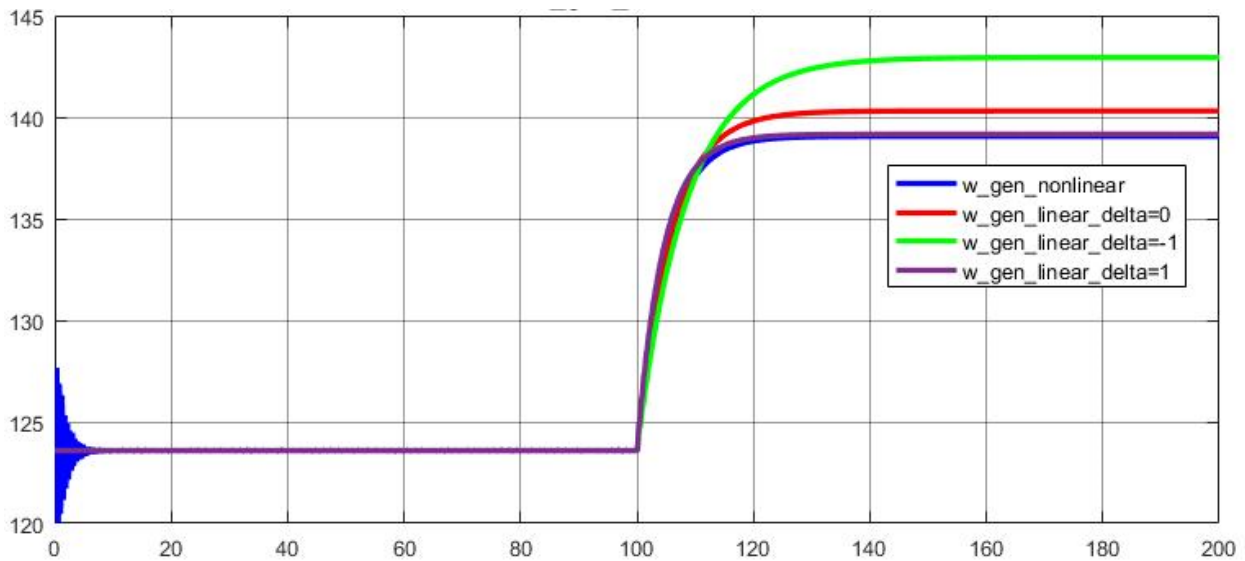
5.2. Uncertainty model for wind turbine power booster robust controller

The uncertainty model for wind turbine booster robust controller represents the same model, with almost the same nominal values except the values presented below, the same uncertainties and perturbations from the nominal values as the one in subchapter 2.3 Linearized model with uncertainties:

$\overline{a_{PB}} = 1.237e + 06$	M_{rot} 's v_{rot} coefficient	$\overline{a_{1PB}} = -364.123$	M_{genref} 's ω coefficient
$\overline{b_{PB}} = -1.06e + 07$	M_{rot} 's Ω coefficient	$\overline{a_{2PB}} = 123.586$	$P_{outgross}$'s M_{gen} coefficient
$\overline{c_{PB}} = -9.312e + 05$	M_{rot} 's β coefficient	$\overline{b_{2PB}} = 4.5e + 04$	$P_{outgross}$'s ω coefficient

For designing the power booster robust controller, the reduced and linearized SISO model with uncertainties from subchapter 3.1 Uncertainty model for robust controller is update with the coefficients and linearization points presented above.

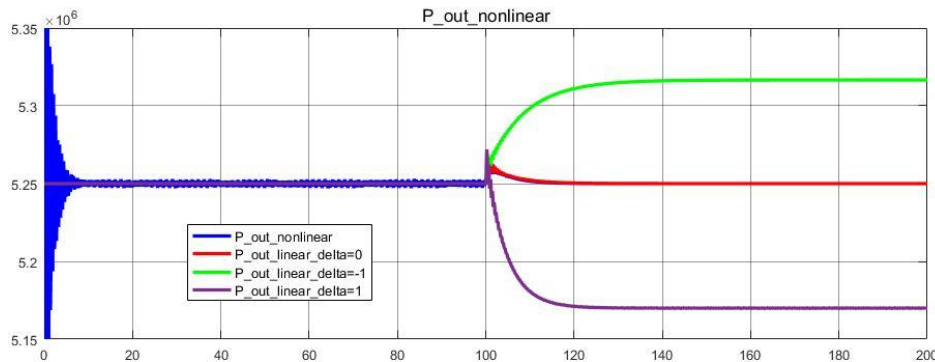
In the figure below it can be seen the comparison between the generator angular velocity ω obtained from the nonlinear model and the one obtained from the linearized power booster model with different uncertainties ($\Delta=diag(0)$, $\Delta=diag(-1)$, $\Delta=diag(1)$):



Graph 25. Generator angular velocity response of the nonlinear power booster model vs. linearized power booster model with uncertainties

From the above graph, it can be seen that the generator angular velocity ω of the linearized power booster model with uncertainties $\Delta=diag(0)$, behave exactly like the linearized power booster model without uncertainties (error $_{\Delta 7} = -1.245$ [rad/s]). The linearized model with uncertainties $\Delta=diag(-1)$ deviates the most from the nonlinear model (error $_{\Delta 8} = -3.885$ [rad/s]). The linearized model with uncertainties $\Delta=diag(1)$ responds the closest to the nonlinear model (error $_{\Delta 9} = -0.1056$ [rad/s]).

In the figure below it can be seen the comparison between the output power P_{out} obtained from the nonlinear power booster model and the one obtained from the linearized power booster model with uncertainties ($\Delta = \text{diag}(0)$, $\Delta = \text{diag}(-1)$, $\Delta = \text{diag}(1)$):



Graph 26. Graph 18. Output power response of the nonlinear power booster model vs. linearized power booster model with uncertainties

From the above graph, it can be seen that the output power P_{out} of the linearized power booster model with uncertainties $\Delta = \text{diag}(0)$, dynamically behaves quite close to the nonlinear power booster model and when it stabilizes, deviates the least from the nonlinear model ($\text{error}_{\Delta 10} = 0.1153$ [kW]). The linearized model with uncertainties $\Delta = \text{diag}(-1)$ dynamically behaves the very different compared to the nonlinear model and when stabilizes there is a difference of $\text{error}_{\Delta 11} = -6.66e+4$ [kW] from the nonlinear power booster model. The linearized model with uncertainties $\Delta = \text{diag}(1)$ dynamically behaves very different compared to the nonlinear model and when stabilizes the difference from the nonlinear power booster model is $\text{error}_{\Delta 12} = 7.967e+4$ [kW].

In the next figure, it can be seen the bode diagram of the power boosters open loop with uncertainties compare to the standard open loop with uncertainties:

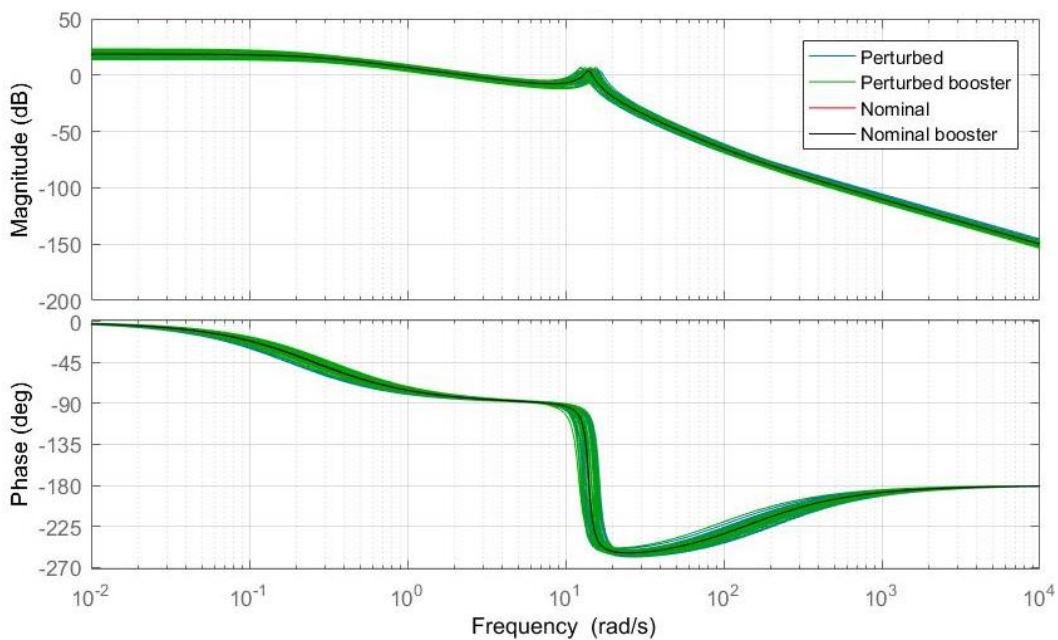


Diagram. 31. Bode diagram of the power booster Open-loop

From diagram 31, by taking a closer look just at the bode diagram of the power booster nominal open loop, it can be seen that the gain margin is -3.63 dB at 14.1 [rad/s]. The phase margin is -37.3 deg at 14.8 [rad/s].

Below it can be seen the pole zero map of the power boosters open loop with uncertainties compare to the standard open loop with uncertainties:

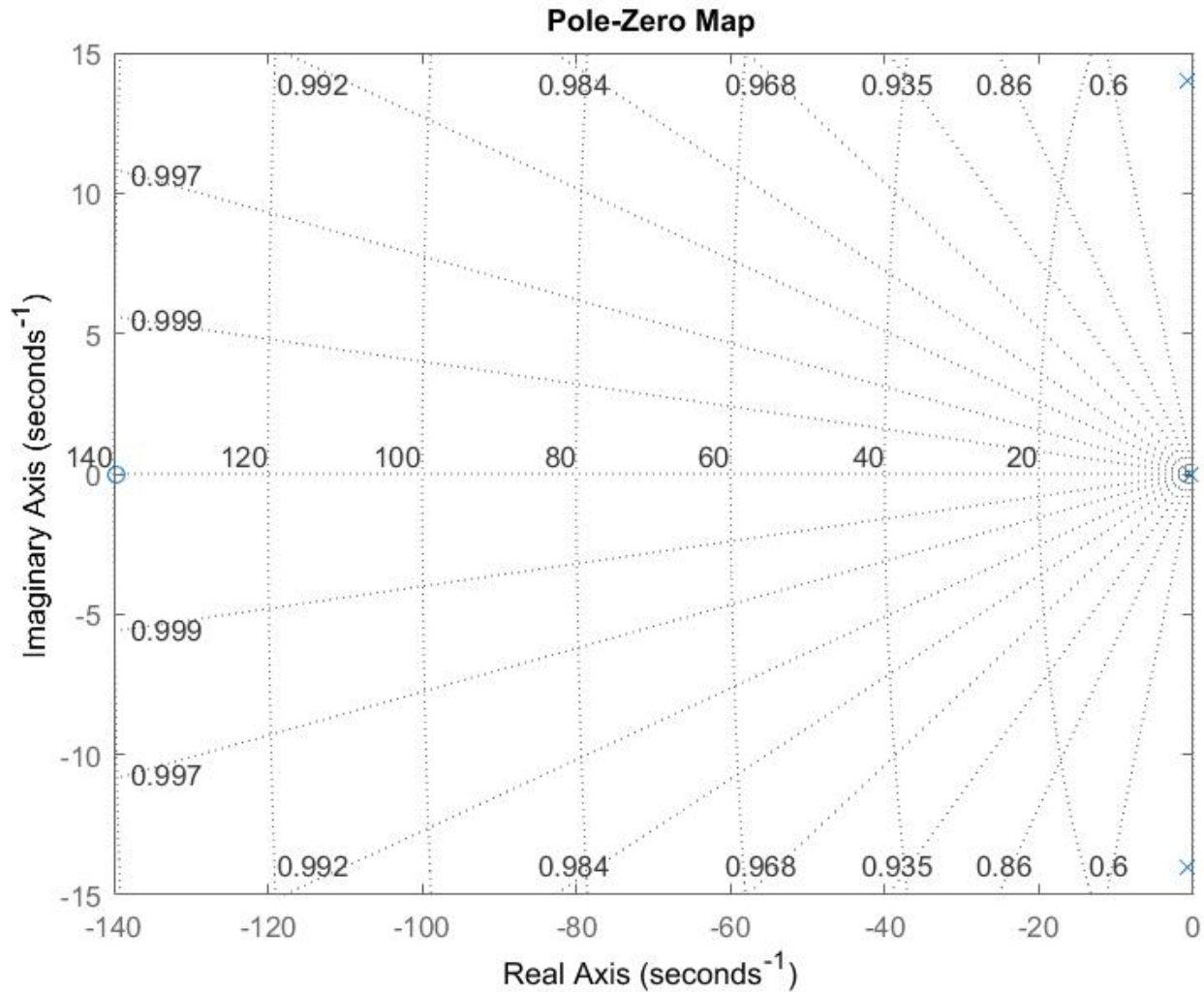


Diagram. 32. Pole-zero map of the power booster open loop with uncertainties: pitch angle to output power relation

Poles: -0.2620 -0.7246 +14.0211i -0.7246 -14.0211i -10.0000	From the above diagram, it can be seen that the all the poles are in Left Half Plane (LHP) showing that the model is stable	Also in the above figure, the zero of the system can be identified	Zeros: -139.6037 0.0000
--	---	--	--------------------------------------

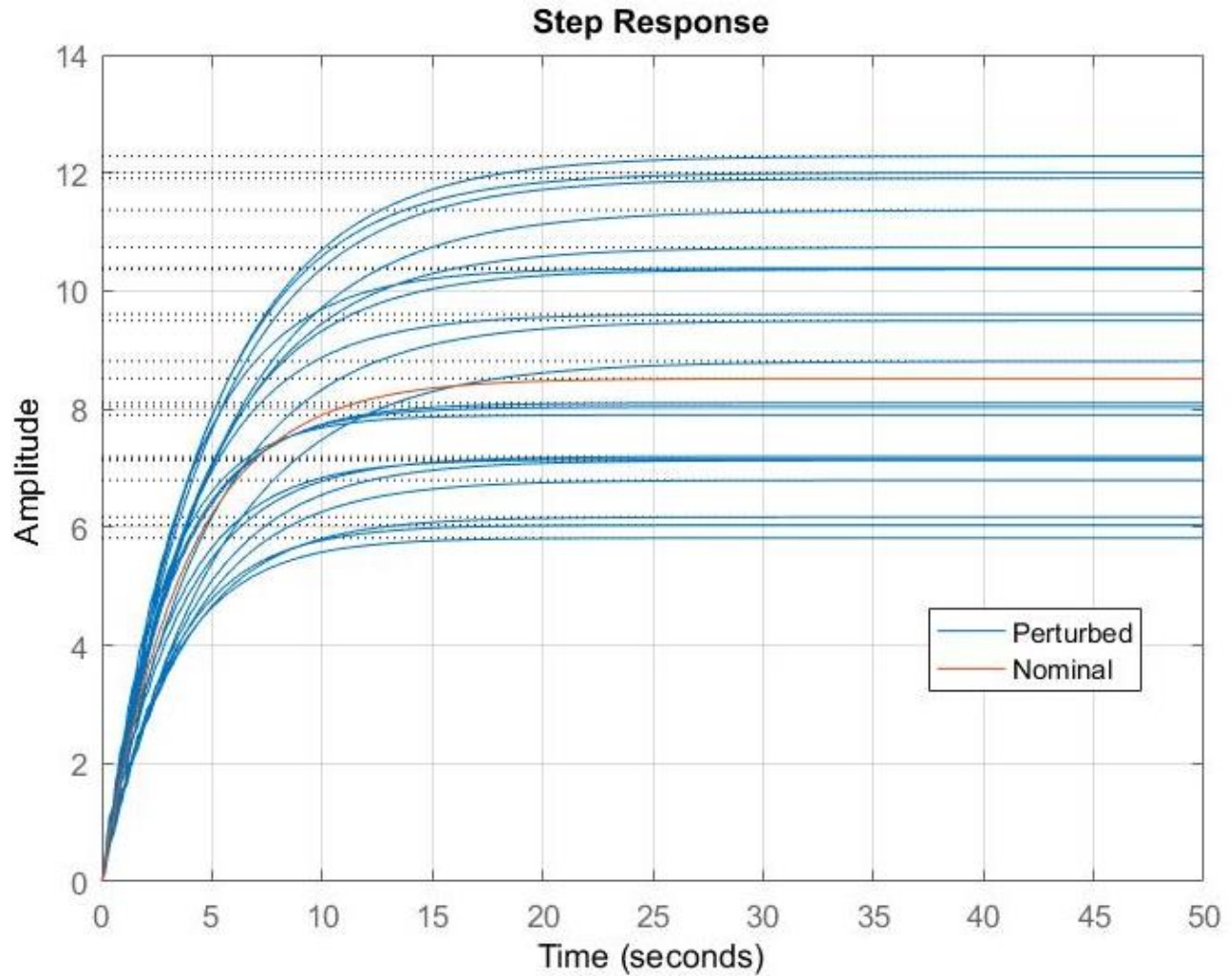


Diagram. 33. Step Response of the power booster open loop with uncertainties

In the above diagram, it can be seen the responses of the power booster and its perturbation open loop responses.

5.3. Power booster logic

In the next figure (Diagram. 31), it can be seen the power booster logic which sets the pitch angle reference (Pitch_ref in Diagram. 31) and power reference (Power_ref in Diagram. 31) based on the change in wind speed changes (v_{rot} in Diagram. 31):

1. If the v_{rot} changes from a value lower than 17 m/s to another value lower than 17 m/s:
 - a. The pitch angle is set to the pitch angle provided by the h-infinity robust controller;
 - b. The power reference is set to 5.297 MW;
2. If the v_{rot} changes from a value lower than 17 m/s to a value higher than 17 m/s, but still lower than 21 m/s:
 - a. The pitch angle is set to the pitch angle provided by the h-infinity robust controller with power booster
 - b. The power reference is set to 5.561 MW;
3. If the v_{rot} changes from a value lower than 21 m/s (but still higher than 15 m/s) to a value higher than 21 m/s:
 - a. The pitch angle is set to the pitch angle provided by the h-infinity robust controller;
 - b. The power reference is set to 5.297 MW
4. If the v_{rot} changes from a value higher than 22 m/s to a value lower than 22 m/s (but still higher than 15 m/s):
 - a. The pitch angle is set to the pitch angle provided by the h-infinity robust controller with power booster
 - b. The power reference is set to 5.561 MW;

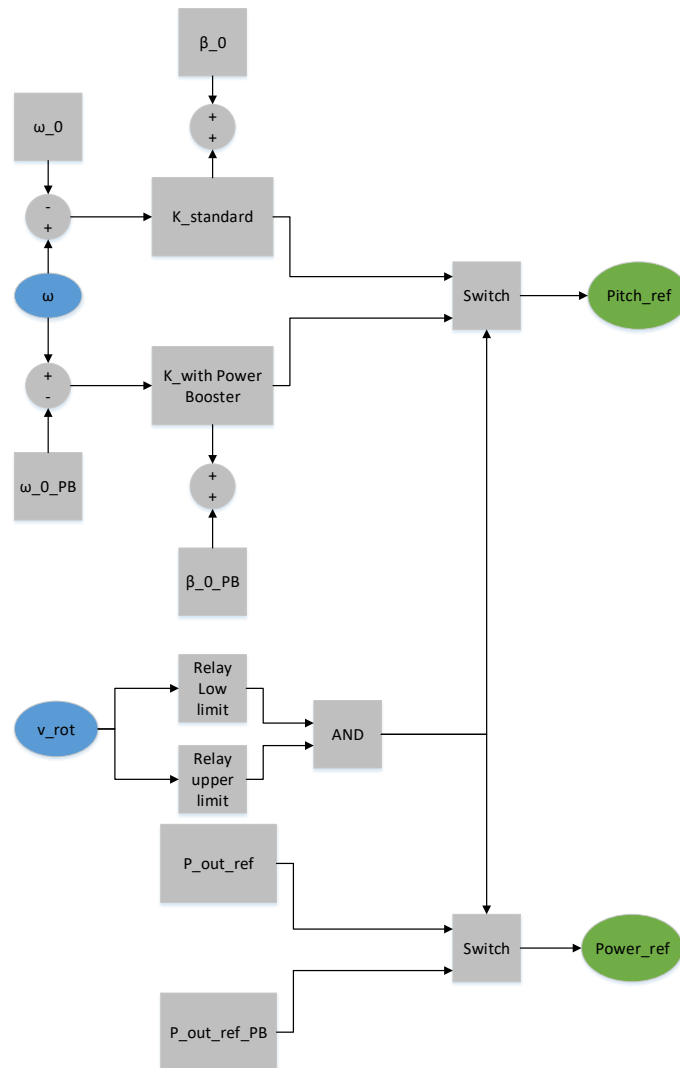


Diagram. 34. Logic to switch from standard h-infinity controller to h-infinity power booster controller

5. If the v_{rot} changes from a value higher than 15 m/s to a value lower than 15 m/s
 - a. The pitch angle is set to the pitch angle provided by the h-infinity robust controller;
 - b. The power reference is set to 5.297 MW

In the next figure, it can be seen the bode diagram of the power boosters h-infinity robust controller loop gain with uncertainties compare to the standard h-infinity robust controller loop gain with uncertainties:

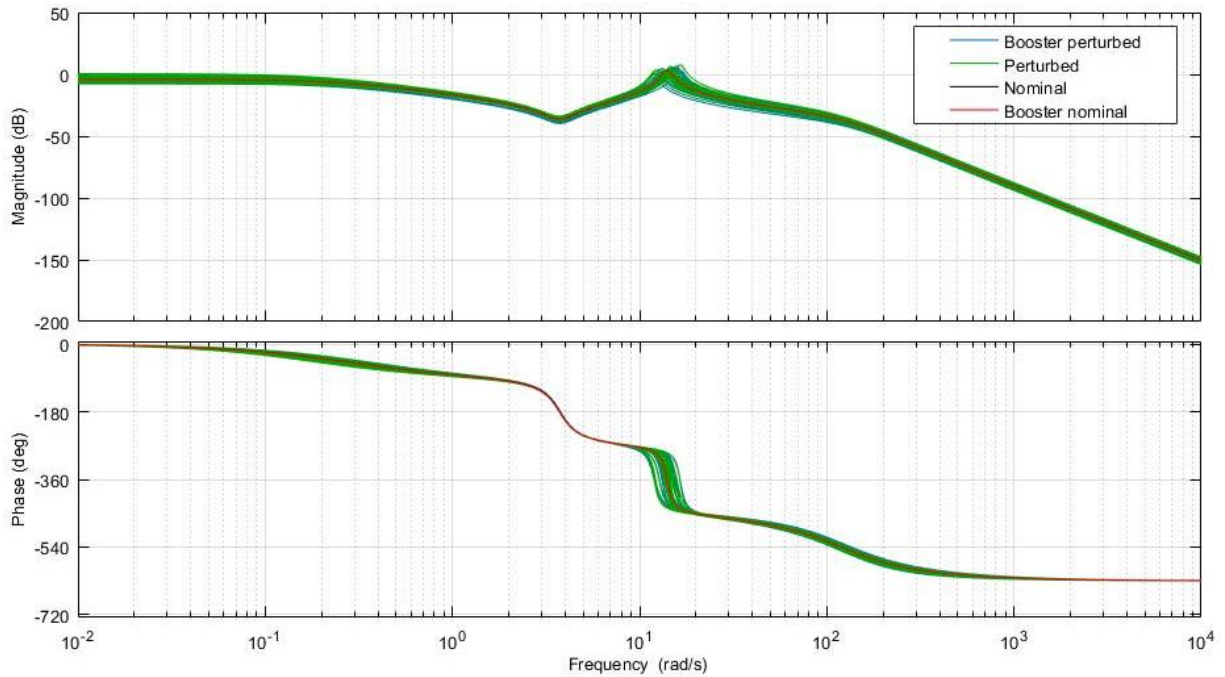


Diagram. 35. Bode diagram of the power booster controller loop gain

From above diagram, by taking a closer look just at the bode diagram of the power booster nominal open loop, it can be seen that the gain margin is slightly different than the standard nominal loop gain, 36.2 dB at 3.76 [rad/s]. The phase margin is 129 deg at 14.9 [rad/s] (almost the same as the standard nominal loop gain).

Below it can be seen the pole zero map of the power boosters loop gain with uncertainties compare to the standard loop gain with uncertainties:

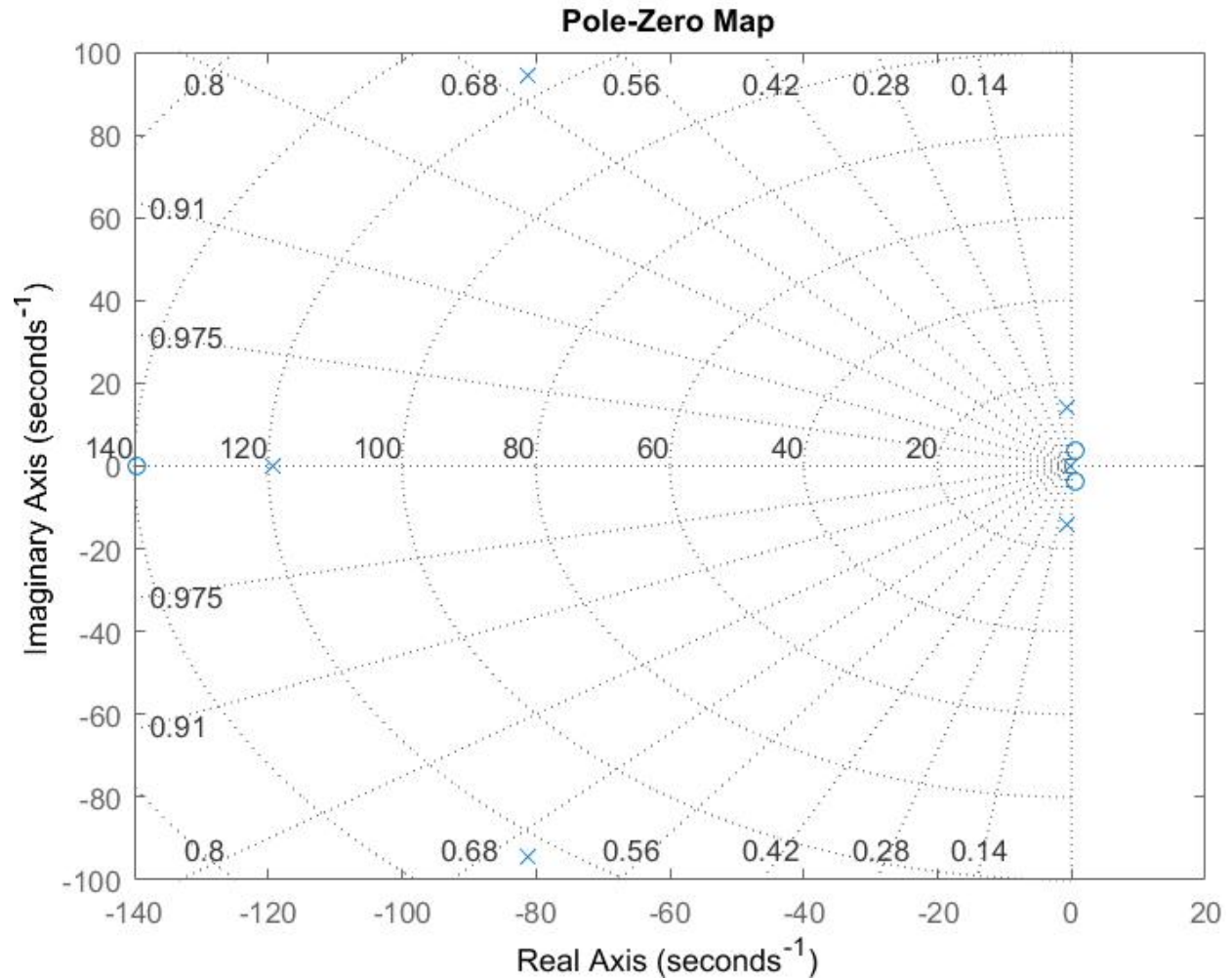


Diagram. 36. Pole zero map of the power booster controller loop gain

Poles:

- 81.12 + 94.28i
- 81.12 - 94.28i
- 119.29
- 0.26
- 0.72 + 14.02i
- 0.72 - 14.02i
- 10
- 10

From the above diagram, it can be seen that the all the poles are in Left Half Plane (LHP) showing that the model is stable

Also in the above figure, the zero of the system can be identified

Zeros:

- 139.60
- 0.62 + 3.71i
- 0.62 - 3.71i
- 10
- 10

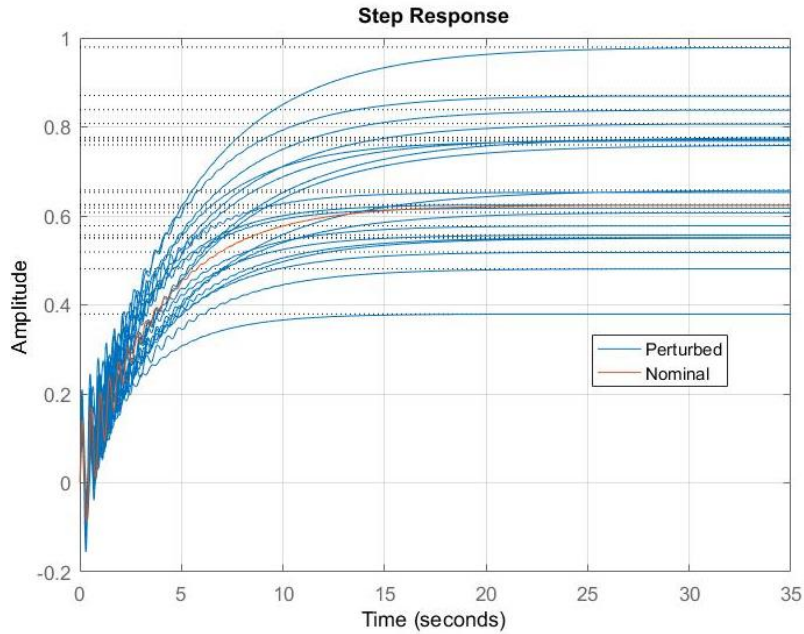
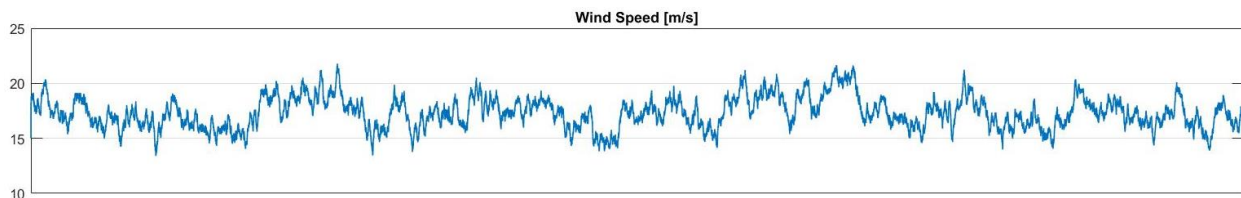


Diagram. 37. Step Response of the power booster loop gain with uncertainties

In the above diagram, it can be seen the responses of the power booster and its perturbation loop gain responses.

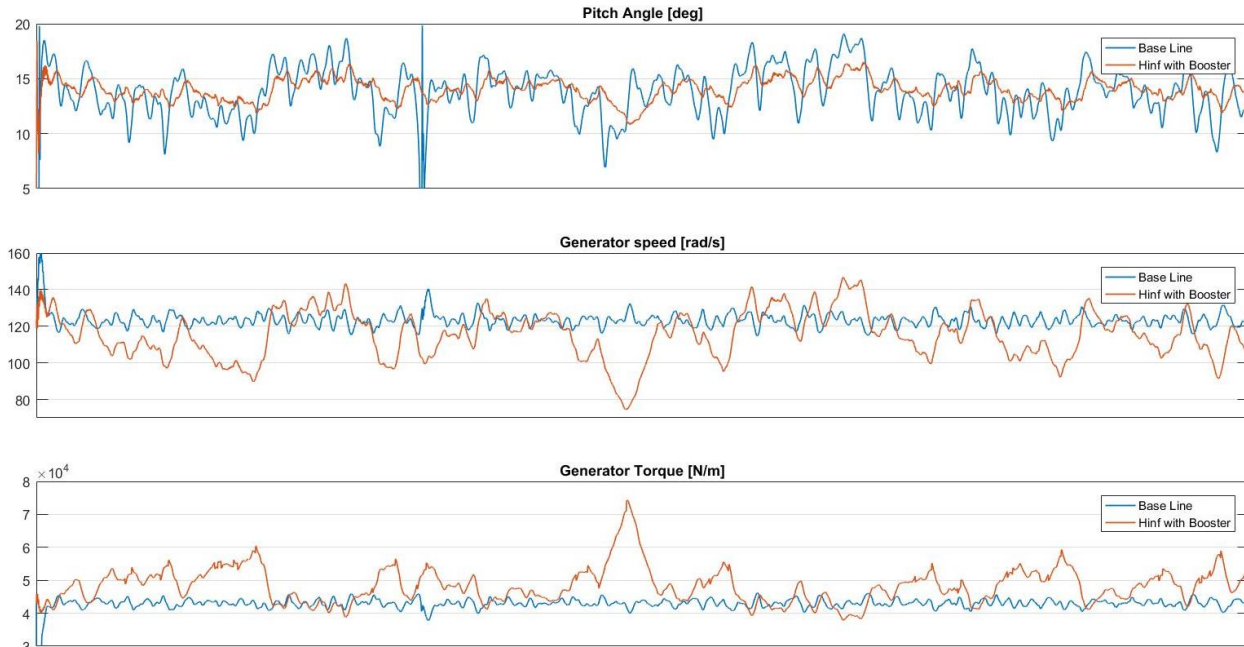
5.4. Results

In this section, the results with the baseline controller and the H-infinity boost-controller are presented. The pitch angle, generator speed, generator torque, power output, tower moment and blade moments are compared. The wind turbine model and control are simulated in Simulink. Simulation results for the NREL 5MW wind turbine with different controller are as follows,

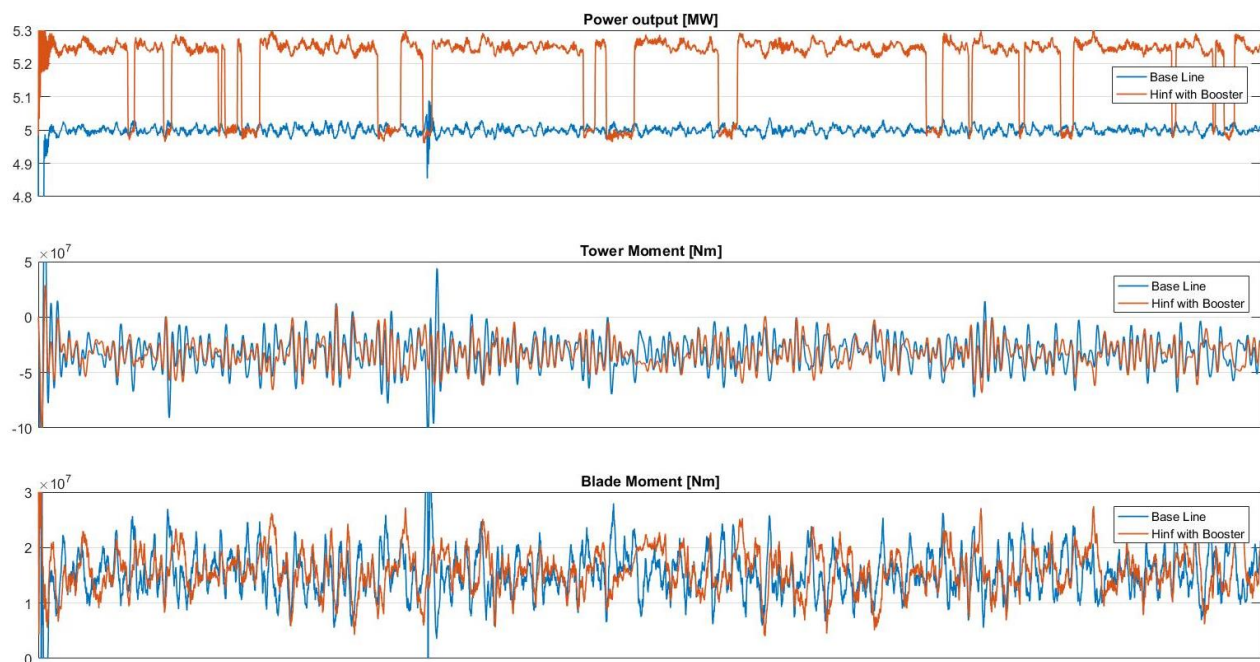


Graph 27. Wind speed(m/s)

The simulation results of the H-infinity boost controller are similar to the H-infinity controller and in some regions where the power is boosted, insignificant differences appear. It can be seen that, the pitch angle of the H-infinity boost controller is less varying than the pitch angle of the baseline controller, but like the normal H-infinity controller, the generator speed varies more. The generator torque increases between the wind speeds 15 and 22 m/s, which shows a significant difference with the generator torque of the baseline controller. It is also obvious that at the wind speeds where the generator speed decreases the torque increases.



Graph 28. H-infinity with booster results, pitch angle, generator speed and generator torque



Graph 29. H-infinity with booster results, power output, tower and blade moments

The graphs show that the boost mode increases the power output to 5.25 MW in the regions where the wind speed lays between 15 and 22 m/s. Surprisingly, although the power increased, the tower and blade moments of the boost H-infinity controller are still smaller than the baseline controller.

6. Fatigue Analysis

In order to evaluate the performance of the robust controller with and without the power booster regarding the blades and tower increase in loads, the equivalent damages exerted on the blades and tower during the entire simulated period, called DELs (damage equivalent loads), were calculated.

Tower bottom DELs were calculated based on the standard deviation of the bending moment as in the following formula [21]:

$$DEL_{tow} = (8 \cdot m_{t0})^{0.5} \cdot \left[\Gamma \left(\frac{2+m_t}{2} \right) \right]^{\frac{1}{m_t}} \quad \text{Eq. 184}$$

Where:
 m_{t0} - zeroth spectral moment of quantity used;
 Γ - gamma function;
 m_t - is the inverse slope of the S-N-curve;

For steel, the S-N-curve does have inverse slopes of $m=3$ and $m=5$. As a typical value $m=4$ can be used;

$(m_{t0})^{0.5}$ is the standard deviation of the tower bending moment.

The tower bending moments from graph. 15 and graph. 32 simulated by controlling the wind turbine with three different controllers: gain scheduled PI controller (base line), h-infinity controller for standard operation and h-infinity robust controller with power booster, were approximated in DELs with help of Eq. 184:

$$DEL_{tow.BL} = 5.963e + 07$$

$$DEL_{tow.Hinf} = 4.001e + 07$$

$$DEL_{tow.PB} = 4.050e + 07$$

The above results confirms the visual comparison from graphs 14 and 30 which states that the robust controller reduces the tower fatigue loads compared to scheduled PI controller, and adding a power booster to h-infinity controller increases the fatigue loads just 1.2% the fatigue loads.

Note that the above equation (eq. 184) is just a simple approximation based on the standard deviation of the tower bending moment used just for comparison and is not a dynamic simulation. For more accurate results, dynamic analysis using FEM (finite element method) software is recommended.

The DELs for the blades were calculated similar as the DELs for the tower bottom:

$$DEL_{blades} = (8 \cdot m_{b0})^{0.5} \cdot \left[\Gamma \left(\frac{2+m_b}{2} \right) \right]^{\frac{1}{m_b}} \quad \text{Eq. 185}$$

Where:
 m_{b0} - zeroth spectral moment of quantity used;
 Γ - gamma function;
 m_b - is the inverse slope of the S-N-curve;

For fiberglass, the S-N-curve does have inverse slopes of $m=8$ and $m=12$ [22]. As a typical value $m=10$ can be used;

$(m_{b0})^{0.5}$ is the standard deviation of the blades bending moment.

The DELs for the blades were calculated similar as the DELs for the tower bottom:

The blades bending moments from graph. 15 and graph. 32 simulated by controlling the wind turbine with three different controllers: gain scheduled PI controller (base line), h-infinity controller for standard operation and h-infinity robust controller with power booster, were approximated similar to in DELs (similar to tower DELs) with help of Eq. 185:

$$DEL_{blade.BL} = 2.464e + 07$$

$$DEL_{blade.Hinf} = 1.752e + 07$$

$$DEL_{blade.PB} = 1.771e + 07$$

The above results confirms the visual comparison from graphs 14 and 30 which states that the robust controller reduces the blade fatigue loads compared to scheduled PI controller, and adding a power booster to h-infinity controller increases the blade fatigue loads just 1.07% the fatigue loads.

Note:

1. The same deflections with the same accelerations and velocities occurs at the same time for all the three blades
2. That the above equation (eq. 184) is just a simple approximation based on the standard deviation of the blade bending moment used just for comparison and is not a dynamic simulation. For more accurate results, dynamic analysis using FEM (finite element method) software is recommended.

7. Further Developments and discussions

To improve the reliability of the system some changes can be made. During the analysis of the h-infinity robust controller, was observed that the performance and stability of the loop gain was better in the region closer to the linearization point. Due to this, more points can be linearized through the operating region, for covering larger operating area with better performance.

The obtained optimal controller can be implemented by using H-infinity loop shaping or H-infinity mixed-sensitivity synthesis method for robust control design where the weighting functions are defined and it might be easier to achieve good closed-loop properties such as robustness and high bandwidth. For the boost controller design, the wind turbine tower oscillations fore-aft can be included in control design for the load mitigation on tower and blades. Moreover, the individual pitch controller can be added so that the pitch angle of each blade can be controlled separately so that the loads can be mitigated significantly in turbulence conditions.

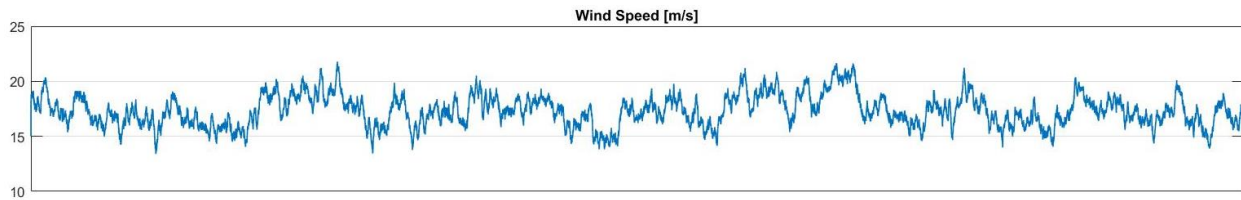
Due to the reason that the current h-infinity controller was designed just for region IV, similar h-infinity controller should be designed for the other regions.

In fatigue analysis, the damage equivalent loads are simple approximations based on the standard deviations of the tower and blades bending moment. For better fatigue loads comparison, rainflow-counting method can be used where the arbitrary waveform converted into equivalent stress ranges, but for even better fatigue loads estimations a dynamic analysis using FEM (finite element method) software is recommended.



8. Conclusion

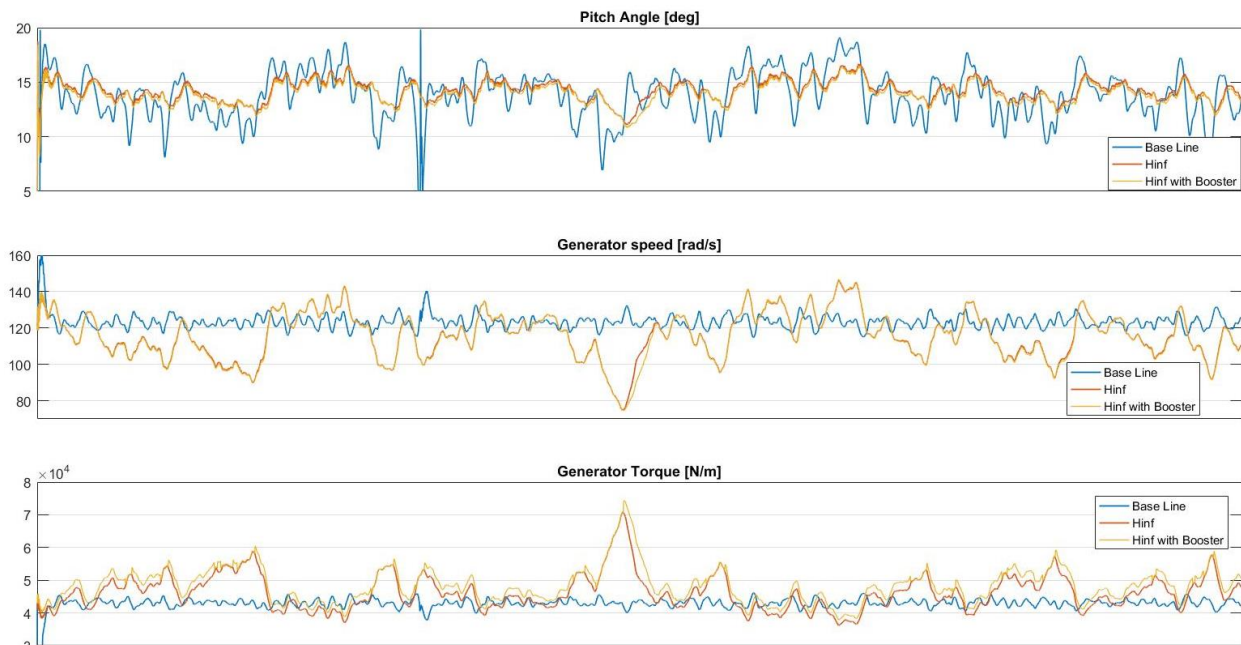
Finally, by using the nonlinear mathematical model, the response and performance of the h-infinity robust controller with and without the power booster was compared with the response and performance of the gain scheduled PI controller (base line) to the same wind speed variation.



Graph 30. Wind speed(m/s)

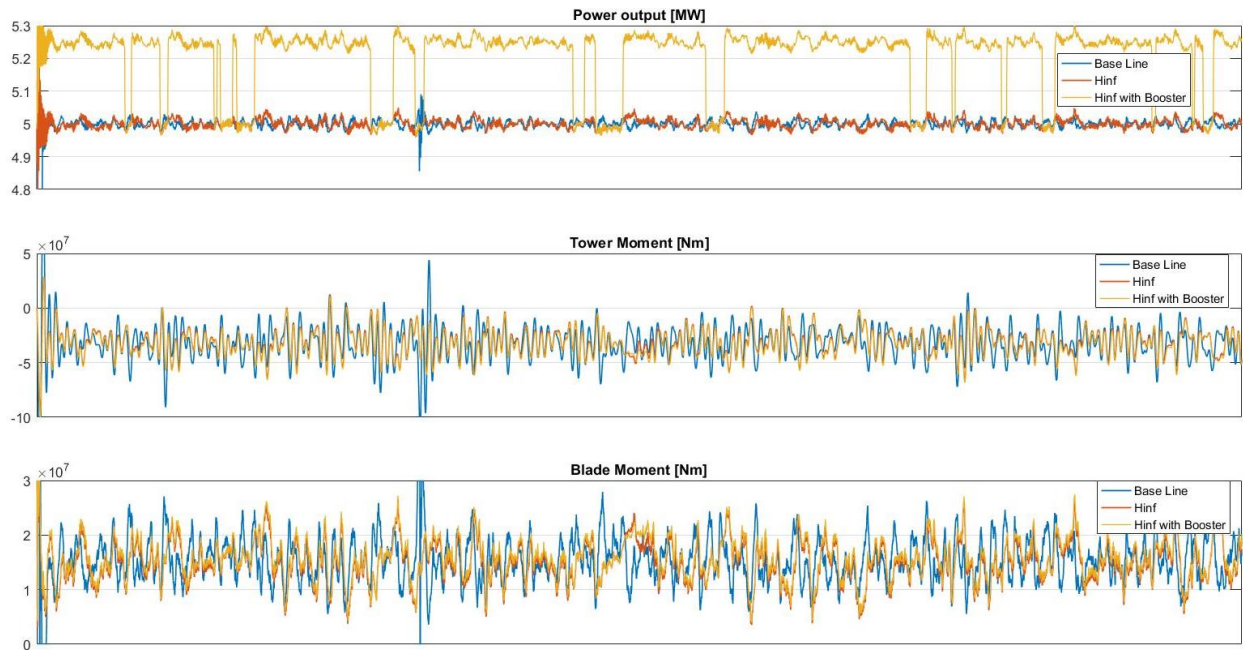
By comparing the controllers output, the pitch angle, it can be seen that the pitch angle of the baseline controller variates more than the other controllers and there is not a significant difference in pitch angle between boost and normal H-infinite controllers.

Unlikely, to the controllers pitch angle variations, as it was expected, the generator speed of the baseline controller variates less than the other controllers, but the insignificant difference between booster and normal H-infinite controller is still kept. The similarity in the response of the pitch angles and generator speeds of both h-infinity robust controllers can be explain by the same linearization and operation points associated with pitch angle and generator speed. From the graphs, it can be also seen that the generator speeds of the two H-infinity robust controllers are decreasing in higher speeds whereas the generator speed and torque stays constant at high speeds.



Graph 31. Base line, H-infinity robust controller with and without booster results, pitch angle, generator speed and generator torque

Similar to the generator speed responses, the generator torque of the baseline controller varies less than the other controllers, but on the other hand, the insignificant difference between boost and normal H-infinite controllers becomes more clearly. This fact can be explained by a significant difference between linearization and operation points associated with the generator torque. Also, the generator torque of the two H-infinity robust controllers increases dramatically where the generator speed decreases.



Graph 32. Base line, H-infinity robust controller with and without booster results, power output, tower and blade moments

By analyzing the output power response of the different controllers, the H-infinity robust controller with power booster, boosts the power from 5 MW to 5.25 MW when the defined conditions (the wind speed lays between 15 and 22 m/s) are meet.

The graphs with the tower and blade moments were also confirmed by the fatigue analysis with the DELs calculated based on the standard deviation of the bending moments which states that the robust controller reduces the tower and blade fatigue loads compared to schaduled PI controller. By analysing the graphs and confirmed by the DELs analysis it is can be concluded that by adding a power booster to h-infinity controller increases the tower fatigue loads just 1.2% and the blades fatigue loads just 1.07%.

Reference

- [1] A. . Fallis, “Global Wind Statistics 2015. GWEC,” *J. Chem. Inf. Model.*, vol. 53, no. 9, pp. 1689–1699, 2015.
- [2] Ewea, “Wind in power - 2015 European statistics,” *2015 Eur. Stat.*, vol. 2016, no. February 13, p. The European Wind Energy Association, 2016.
- [3] Agora, “Energy Transition in the Power Sector in Europe: State of Affairs in 2015,” 2016.
- [4] “Elproduktion-i-Danmark @ www.energinet.dk.” .
- [5] “2020-energy-strategy @ ec.europa.eu.” .
- [6] U. Jassmann, S. Dickler, J. Zierath, M. Hakenberg, and D. Abel, “Model Predictive Wind Turbine Control With Move-Blocking Strategy For Load Alleviation and Power Leveling.”
- [7] H. Liu, Y. Wang, Q. Tang, and X. Yuan, “Individual Pitch Control Strategy of Wind Turbine To Reduce Load Fluctuations and Torque Ripples,” no. 2.
- [8] R. Ungurán and M. Kühn, “A comparison of individual pitch and trailing edge flap control for structural load mitigation of a wind turbine,” *SmartBlades Conf.*, pp. 2307–2313, 2016.
- [9] N. K. P. Damien Castaignet¹, Thanasis Barlas², Thomas Buhl² and C. B. and T. K. Jens Jakob Wedel-Heinen¹, Niels A. Olesen¹, “Full-scale test of trailing edge flaps on a Vestas V27 wind turbine: active load reduction and system identification,” *Wind Energy*, vol. 17, no. January 2013, pp. 549–564, 2014.
- [10] Z. J. Chen, K. A. Stol, and B. R. Mace, “Wind turbine blade optimisation with individual pitch and trailing edge flap control,” *Renew. Energy*, vol. 103, pp. 750–765, 2017.
- [11] “power boost function power boost function Siemens – Powered by Partnership,” p. 2015, 2015.
- [12] P. Description, “Siemens power boost function.”
- [13] J. Grunnet, M. Soltani, and T. Knudsen, “Aeolus toolbox for dynamics wind farm model, simulation and control,” *Eur. Wind Energy ...*, p. 10, 2010.
- [14] K. Hammerum, P. Brath, and N. K. Poulsen, “A fatigue approach to wind turbine control,” *J. Phys. Conf. Ser.*, vol. 75, no. Copyright 2008, The Institution of Engineering and Technology, p. 12081, 2007.
- [15] O. W. Collaborative, “OFFSHORE WIND TECHNOLOGY OVERVIEW Long Island - New York City,” 2009.
- [16] R. C. Design, *Robust Control Design with MATLAB* ®. .
- [17] M. J. Grimble and M. A. Johnson, *Advanced Textbooks in Control and Signal*. .
- [18] S. M. N. Soltani, R. Izadi-zamanabadi, and J. Stoustrup, “Parametric Fault Estimation Based on H_{∞} Optimization in A Satellite Launch Vehicle,” pp. 727–732, 2008.
- [19] G. Zames, “Feedback and Optimal Sensitivity: Model Reference Transformations, Multiplicative Seminorms, and Approximate Inverses,” *IEEE Trans. Automat. Contr.*, vol. 26, no. 2, pp. 301–320, 1981.
- [20] A. Bansal and V. Sharma, “Design and Analysis of Robust H-infinity Controller,” *Control Theory Informatics*, vol. 3, no. 2, pp. 7–14, 2013.
- [21] M. Seidel, “Wave induced fatigue loads: Insights from frequency domain calculations,” *Stahlbau*, vol. 83, no. 8, pp. 535–541, 2014.
- [22] J. F. Mandell, R. M. Reed, D. D. Samborsky, and C. Hall, “Fatigue of Fiberglass Wind Turbine Blade Materials,” no. August, 1992.

